

# Adhesion and dispersion dynamics of marine bacteria on a solid substrate

---

Gujinović, Luka

Doctoral thesis / Doktorski rad

2024

*Degree Grantor / Ustanova koja je dodijelila akademski / stručni stupanj:* **University of Split, Faculty of Science / Sveučilište u Splitu, Prirodoslovno-matematički fakultet**

*Permanent link / Trajna poveznica:* <https://um.nsk.hr/um:nbn:hr:166:648948>

*Rights / Prava:* [In copyright](#)/[Zaštićeno autorskim pravom.](#)

*Download date / Datum preuzimanja:* **2024-11-26**

*Repository / Repozitorij:*

[Repository of Faculty of Science](#)





FACULTY OF SCIENCE

Doctoral Study of Biophysics

Doctoral thesis

**Adhesion and dispersion dynamics of marine bacteria  
on a solid substrate**

Luka Gujinović

Split, 2024.



PRIRODOSLOVNO-MATEMATIČKI FAKULTET

Doktorski studij Biofizika

Doktorski rad

**Dinamika adhezije i raspršenja morske bakterije na  
čvrstom supstratu**

Luka Gujinović

Split, 2024.

University of Split, Faculty of Science  
Department of Physics, Doctoral Study of Biophysics

**Adhesion and dispersion dynamics of marine bacteria on a solid substrate**

The PhD thesis authored by Luka Gujinović was conducted under the supervision of Full Professor Dražen Zanchi, Ph. D. and co-supervision of Assistant Professor Ivica Šamanić, Ph. D. This research was undertaken as a necessary requirement to obtain the PhD title.

Achieved academic title: PhD Natural sciences, field of Physics.

Members of the Expert Board for Assessment and Defending of Doctoral Thesis:

1. Full Professor Ante Bilušić, PhD, Faculty of Science, Split, chairman

\_\_\_\_\_

2. Research Director Nelly Henry, PhD, Laboratoire Jean Perrin, CNRS/Sorbonne Université, member

\_\_\_\_\_

3. Associate Professor Marija Raguž, PhD, Faculty of Medicine, Split, member

\_\_\_\_\_

hereby confirm that the PhD thesis has been defended on the date: \_\_\_\_\_.

Doctoral Study Head:  
Associate Professor Damir Kovačić, PhD

\_\_\_\_\_

DEAN:  
Full Professor Mile Dželalija, PhD

\_\_\_\_\_



Sveučilište u Splitu, Prirodoslovno-matematički fakultet  
Odjel za fiziku, Doktorski studij Biofizika

## **Dinamika adhezije i raspršenja morske bakterije na čvrstom supstratu**

Doktorski rad autora Luke Gujinovića kao dio obaveza potrebnih da se dobije doktorat znanosti, izrađen pod mentorstvom prof. dr. sc. Dražena Zanchija i komentorstvom doc. dr. sc. Ivice Šamanića.

Dobiveni akademski naziv i stupanj: doktor znanosti u području prirodnih znanosti (znanstveno polje fizika).

Povjerenstvo za ocjenu i obranu doktorskog rada u sastavu:

1. prof. dr. sc. Ante Bilušić, Prirodoslovno matematički fakultet u Splitu, predsjednik

---

2. dr. sc. Nelly Henry, Research Director, Laboratoire Jean Perrin, CNRS/Sorbonne Université, član

---

3. izv. prof. dr. sc. Marija Raguž, Medicinski fakultet u Splitu, član

---

potvrđuje da je doktorska disertacija uspješno obranjena dana: \_\_\_\_\_.

Voditelj doktorskog studija:  
izv. prof. dr. sc. Damir Kovačić

---

DEKAN:  
prof. dr.sc. Mile Dželalija

---

## BASIC DOCUMENTATION CARD

---

University of Split  
Faculty of Science

Ph.D. thesis

### **Adhesion and dispersion dynamics of marine bacteria on a solid substrate**

**Luka Gujinović**

Thesis performed at the Matter and Complex Systems Laboratory at the University Paris Cité, Faculty of Science at the University of Split and the Institute of Oceanography and Fisheries

#### **Abstract**

The marine bacterium *Vibrio gigantis* was isolated from Kaštela Bay from wild early-phase biofilm and cultivated. The results showed that *Vibrio gigantis* can be used as an appropriate and versatile model species for adhesion dynamics and biofilm evolution research. NGS analysis confirmed the highest relative abundance of this species inside biofilm samples. Its predicted genetic potential confirmed the activity in surface adhesion, cell motility and quorum sensing – a bacterial communication for collective behaviour. The adhesion dynamics was successfully quantified in a newly designed experimental setup. Real-time adhesion was also quantified in two different geometries, a barrel-like container and a microchannel, showing a spontaneous nutrient, and oxygen-dependent adhesion, with a sudden and irreversible detachment. Proceeding with the colony evolution experiments under a constant resource supply, the colonies first grew exponentially and eventually dispersed from the surface. Dispersion was simultaneous and collective, leaving filamentous-form bacteria on the bottom. It was shown to be triggered at a certain substrate coverage, indicating the importance of the adhered bacteria concentration for a collective response to unfavourable conditions. The progression of this collective dispersion phenomenon was studied by measuring its dependence on the position along a microfluidic PDMS channel under controlled longitudinal laminar flux. In particular, simultaneous monitoring of two different positions in the channel allowed a direct observation of dispersion delay. Furthermore, 2D monitoring revealed both transversal and longitudinal time dependence of the dispersion, both presented as a front-like space-time pattern. This indicated that dispersion is indeed driven by interaction between bacteria. The fact that the dispersion dynamics is independent of colony growth pattern (clustering) rules out the contact and/or hydrodynamical nature of bacterial interaction. Thereby, it is concluded that the coordination of bacterial dispersion is of a biological nature, i.e. quorum sensing-like.

(130 pages, 88 figures, 9 tables, 93 references, 1 appendix, original in English)

**Keywords:** Adhesion dynamics, bacterial biofilm, colony evolution, dispersion dynamics, *Vibrio gigantis*.

**Thesis deposited in:** National and University Library in Zagreb, University Library in Split, Library of the Faculty of Science University of Split

**Supervisor:** Dražen Zanchi, Full professor, Ph. D.

**Co-supervisor:** Ivica Šamanić, Assistant professor, Ph. D.

#### **Committee:**

1. Ante Bilušić, Full professor, Ph. D.
2. Nelly Henry, Research director, Ph. D.
3. Marija Raguž, Associate professor, Ph. D.

**Thesis accepted:** April 24, 2024.

## Dinamika adhezije i raspršenja morske bakterije na čvrstom supstratu

Luka Gujinović

Rad je izrađen u laboratoriju za materiju i kompleksne sisteme na Paris Cité sveučilištu, Prirodoslovno matematičkom fakultetu Sveučilišta u Splitu te Institutu za oceanografiju i ribarstvo.

### Sažetak

Morska bakterija *Vibrio gigantis* izolirana je iz Kaštelanskog zaljeva iz ranofaznog prirodnog biofilma te kultivirana. Rezultati su pokazali da je *Vibrio gigantis* prikladna i prilagodljiva modelna vrsta za istraživanje adhezijske dinamike i razvoja biofilma. NGS analizom pokazana je najveća relativna prisutnost ove vrste u uzorcima biofilma. Njen predviđeni genetski potencijal potvrdio je aktivnost u površinskoj adheziji, bakterijskom gibanju i kolektivnom osjećanju (engl. quorum sensing) – bakterijskoj komunikaciji za kolektivno ponašanje. Dinamika adhezije je uspješno kvantificirana u novodizajniranom eksperimentalnom postavu. Adhezija u stvarnom vremenu je također kvantificirana u dvjema različitim geometrijama, bačvastom spremniku i mikrokanalu, koji su pokazali spontanu adheziju ovisnu o nutrijentima i kisiku, uz naglo i nepovratno odljepljivanje. Nastavljajući s eksperimentima evolucije kolonija pod stalnom opskrbom resursima, kolonije su prvo rasle eksponencijalno, ali bi se u konačnici i raspršile s površine. Raspršenje je bilo istovremeno i kolektivno pri čemu su na dnu ostale filamentne bakterije. Pokazano je da je raspršenje izazvano pri određenoj pokrivenosti supstrata, ukazujući na važnost koncentracije zalijepljenih bakterija u kontroliranom odzivu na nepovoljne uvjete. Napredovanje fenomena kolektivne disperzije je ispitano mjereći njegovu ovisnost o poziciji uzduž mikrofluidnog PDMS kanala, u kontroliranom longitudinalnom laminarnom toku. Konkretno, istovremeno praćenje dva različita položaja u kanalu omogućilo je izravno promatranje kašnjenja disperzije. Nadalje, 2D praćenje otkrilo je i transverzalnu i longitudinalnu vremensku ovisnost disperzije, prikazanu kao prostorno-vremenski uzorak u obliku fronte. To je ukazalo da je disperzija doista potaknuta interakcijom između bakterija. Činjenica da je dinamika disperzije neovisna o uzorku rasta kolonija (klasterima) isključuje kontaktnu i/ili hidrodinamičku prirodu bakterijske interakcije. Time se zaključuje da je koordinacija bakterijske disperzije biološke prirode, tj. nalik na komunikaciju quorum sensingom.

(130 stranica, 88 slika, 9 tablica, 93 literaturna navoda, 1 prilog, original na engleskom)

**Ključne riječi:** Dinamika adhezije, bakterijski biofilm, evolucija kolonija, dinamika disperzije, *Vibrio gigantis*.

**Rad je pohranjen u:** Nacionalnoj sveučilišnoj knjižnici u Zagrebu, Sveučilišnoj knjižnici u Splitu i Knjižnici Prirodoslovno-matematičkog fakulteta Sveučilišta u Splitu.

**Mentor:** prof. dr. sc. Dražen Zanchi

**Komentor:** doc. dr. sc. Ivica Šamanić

### Ocjenjivači:

1. prof. dr. sc. Ante Bilušić
2. dr. sc. Nelly Henry, research director
3. izv. prof. dr. sc. Marija Raguž

**Rad prihvaćen: 24.4.2024.**

## **Zahvale / Acknowledgements**

Prije svega zahvaljujem svojoj obitelji na strpljenju, potpori i nebrojenim slušanjima svih nastalih ideja, dojmova, poteškoća, ali i uspjeha koje su sa mnom dijelili tijekom ovog putovanja, podmećući svoja leđa kad god je bilo potrebno.

Također zahvaljujem mentoru i komentoru ovog rada na stručnom vodstvu i entuzijazmu te inovativnosti čime je osigurana kvaliteta i sveobuhvatnost rada.

Hvala i mojim kolegama na svim savjetima i podršci.

Rad posvećujem svome piletu i pilici, koje su najviše gubile u mojim dugotrajnim druženjima s bakterijama, besanim noćima i nužnim odsustvima u ključnim trenucima nastajanja naše obitelji, a imajući na umu da se ipak sve nadoknadi (usprkos zahtjevnim turbulencijama života) i ispravno posloži (kako je i davnih dana gatano iz jednog dlana djeteta, djevojčeta, žene i danas majke).

A za one koji više nisu s nama, neka se uz nas raduju budućnosti.

# Content

<b>List of Figures.....</b>	<b>I</b>
<b>List of Tables.....</b>	<b>II</b>
<b>1. Introduction.....</b>	<b>1</b>
<b>1.1. Marine biofilm and bacteria.....</b>	<b>1</b>
<b>1.2. Scientific background.....</b>	<b>3</b>
<b>1.3. Goals and Hypothesis.....</b>	<b>11</b>
<b>2. Materials and methods.....</b>	<b>14</b>
<b>2.1. Choosing the bacterial model species .....</b>	<b>14</b>
2.1.1. Isolation and identification of biofilm-forming species .....	14
2.1.2. Preliminary adhesion tendency tests.....	15
<b>2.2. NGS (Next generation sequencing) analysis.....</b>	<b>16</b>
2.2.1. DNA isolation and preparation of samples.....	16
2.2.2. 16S rRNA amplicon sequencing and data accession.....	17
2.2.3. NGS analysis and $\alpha$ - and $\beta$ -diversity calculation.....	17
<b>2.3. Prediction of metagenome functional potential.....</b>	<b>18</b>
<b>2.4. Adhesion dynamics in a bioreactor.....</b>	<b>20</b>
2.4.1. Premeasurements.....	21
2.4.2. Bioreactor experiment setup.....	21
2.4.3. Image analysis.....	22

<b>2.5. Real-time adhesion dynamics.....</b>	<b>24</b>
<b>2.5.1. Premeasurements.....</b>	<b>24</b>
<b>2.5.2. Real-time adhesion dynamics in a barrel-like container.....</b>	<b>24</b>
2.5.2.1. Experimental setup.....	24
2.5.2.2. Sample preparation.....	26
2.5.2.3. Image analysis.....	27
<b>2.5.3. Real-time adhesion dynamics in a microchannel.....</b>	<b>28</b>
2.5.3.1. Experimental setup.....	29
2.5.3.2. Sample preparation.....	29
2.5.3.3. Image analysis.....	31
<b>2.6. Real-time colony evolution.....</b>	<b>31</b>
<b>2.6.1. Real-time colony evolution in a microchannel.....</b>	<b>31</b>
2.6.1.1. Experimental setup.....	32
2.6.1.2. Sample preparation .....	33
2.6.1.3. Image analysis.....	34
<b>2.6.2. Real-time colony evolution in a PDMS microchannel.....</b>	<b>35</b>
2.6.2.1. Experimental setup.....	35
2.6.2.2. Sample preparation.....	39
2.6.2.3. Image analysis.....	40
<b>3. Results and Discussion.....</b>	<b>45</b>
<b>3.1. Choosing the bacterial model species.....</b>	<b>45</b>
3.1.1. Isolation and identification of biofilm-forming species.....	45
3.1.2. Preliminary adhesion tendency tests.....	47
<b>3.2. NGS (Next generation sequencing) analysis.....</b>	<b>49</b>

3.2.1. Sequencing depth.....	49
3.2.2. Relative abundances analysis.....	51
3.2.3. Samples diversities.....	57
<b>3.3. Prediction of metagenome functional potential.....</b>	<b>60</b>
3.3.1. Functional capacity at the genus level.....	60
3.3.2. Functional capacity at the species level.....	62
<b>3.4. Adhesion dynamics in a bioreactor.....</b>	<b>65</b>
3.4.1. Adhesion quantification.....	66
3.4.2. Aggregate analysis.....	71
<b>3.5. Real-time adhesion dynamics.....</b>	<b>74</b>
3.5.1. Growth kinetics.....	74
3.5.2. Real-time adhesion dynamics in a barrel-like container.....	76
3.5.3. Real-time adhesion dynamics in a microchannel.....	82
<b>3.6. Real-time colony evolution.....</b>	<b>88</b>
3.6.1. Real-time colony evolution in a microchannel.....	88
3.6.2. Dispersion time and conditions.....	100
3.6.3. Real-time colony evolution in a PDMS microchannel.....	106
<b>4. Conclusion.....</b>	<b>123</b>
<b>5. Appendix.....</b>	<b>125</b>
<b>6. References.....</b>	<b>132</b>

## List of Figures

**Figure 1.** A general biofilm evolution, with an extension to the aquatic environment.

**Figure 2.** Vessel hull fouling and biocorrosion.

**Figure 3.** **A)** Calculated MSD as a function of  $\tau$  time interval. **B)** Near-surface motility **C)** rheotaxis and orientation dynamics.

**Figure 4.** **A)** 3D biofilm structures of *Vibrio cholerae* **B)** Modes of escape from a developed biofilm.

**Figure 5.** A millifluidic channel with two different species, measured as confocal fluorescence intensities.

**Figure 6.** **A)** MSD dependence of time interval  $\tau$  **B)** Rectangular microfluidic channel and a bacterium **C)** Shear rate of ambient flow  $G$ .

**Figure 7.** **A)** Velocity field calculation **B)** Bottom shear stress variation across the channel width.

**Figure 8.** **A)** Velocity field at a fixed  $x$  position and at the heights of  $z = 60\mu m$  and  $z = 10\mu m$  **B)** Velocity field at the height of  $z = 1\mu m$ .

**Figure 9.** **A)** 30  $\mu m$  high microchannel **B)** PicoTwist apparatus as an inverted microscope.

**Figure 10.** Schematic view of the Styrofoam carrier with 110 inserted microscopic slides.

**Figure 11.** A simple workflow of the PICRUST algorithm.

**Figure 12.** **A)** Styrofoam carrier with 8 microscopic slides **B)** A simple schematic view of a bioreactor.

**Figure 13.** A slide, immersed into the bacterial sample with examined regions of interest.

**Figure 14.** Two fragments of images at the early and late phases of the bioreactor experiment.

**Figure 15.** A schematic view of barrel-like container experimental setup for real-time adhesion dynamics.

**Figure 16.** The bacterial sample preparation scheme for real-time adhesion dynamics in a barrel-like container

**Figure 17.** Step-by-step preparation of an image for the surface coverage percentage analysis.

**Figure 18.** A schematic view of microchannel experimental setup for real-time adhesion dynamics.

**Figure 19.** **A)** Schematic representation of a real-time colony evolution experiment **B)** Changing the initial concentrations of bacteria set at the beginning of the experiments.

**Figure 20.** A step-by-step presentation of preparing for the colony size analysis on a random image.

**Figure 21.** The side and top view of a mould used for preparing the PDMS microchannel.

**Figure 22.** **A)** PDMS, placed over the mould and microscopic slide. **B)** PDMS with mould imprint and clean microscopic slide (substrate) fixed together **C)** The formed 120  $\mu m$  high PDMS microchannel.

**Figure 23.** **A)** 3D PDMS microchannel view **B)** Regions of interest monitored in the PDMS microchannel.

**Figure 24.** Regions of interest monitored in the curved PDMS microchannel.

**Figure 25.** Image analysis of a random frame of colony evolution experiment in PDMS microchannel at 20x magnification.

**Figure 26.** Image analysis of a random frame of colony evolution experiment in PDMS microchannel at 5x magnification and the observed area division.

**Figure 27.** Image analysis of a random frame of colony evolution experiment in PDMS microchannel at 1.5x magnification and the observed area division.

**Figure 28.** Image analysis of a random frame of colony evolution experiment in PDMS microchannel at 0.75x magnification and the observed area division.

**Figure 29.** Dividing the curved PDMS microchannel into areas to observe: **A)** Width dispersion progression. **B)** Length dispersion progression.

**Figure 30.** Mostly bacterial biofilm formed in the sea environment after three days.

**Figure 31.** Different dilutions of the scraped biofilm resulted in the desired density of developed colonies.

**Figure 32.** The morphology and shape check for the monoculture number 1.



**Figure 33.** The surface of the microchannel with the adhering *V. gigantea* at the initial and the latter phase.

**Figure 34.** Percentage of covered surface as a measure of adhesion of *V. gigantea*.

**Figure 35.** The DNA material collected from the biofilm samples and the rarefaction measure of the samples.

**Figure 36.** The exact number of sequences at different taxonomic depths in the samples.

**Figure 37.** Species with the highest relative abundances among the samples.

**Figure 38.** Genera with the highest relative abundances among the samples.

**Figure 39.** A phylogenetic diversity for one seawater and three biofilm samples.

**Figure 40.** Shannon (H) and Simpson ( $\lambda$ ) diversity indices of the samples.

**Figure 41.** Weighted UniFrac distance metric between the samples.

**Figure 42.** Principal coordinate analysis (PCoA), explaining the variations between samples.

**Figure 43.** The growth kinetics of *V. gigantea*.

**Figure 44.** Adhesion dynamics in a bioreactor: A random image taken with 100x magnification objective.

**Figure 45.** Adhesion of *V. gigantea* on a microscopic slide at indicated extraction times.

**Figure 46.** Adhesion dynamics of *V. gigantea* calculated as covered surface percentage (3-hour experiment).

**Figure 47.** Adhesion dynamics of *V. gigantea* calculated as covered surface percentage (1-hour experiment).

**Figure 48.** Adhesion dynamics of *V. gigantea* in the experiments with the doubled incubation and omitted incubation.

**Figure 49.** The average number of variously-sized aggregates at time points of the three-hour experiment.

**Figure 50.** Growth kinetics of *V. gigantea* at six different temperatures and with a constantly mixed sample.

**Figure 51.** Growth kinetics of *V. gigantea* at 25°C with average and triplicate values.

**Figure 52.** Adhesion dynamics in a barrel-like container for three different mixing rates of medium mixing.

**Figure 53.** Starting and maximum coverage at two positions from the 1 mL/min mixing rate experiment.

**Figure 54.** Adding both nutrients and oxygen after bacterial detachment in a barrel-like container.

**Figure 55.** Adding both nutrients and oxygen every 30 minutes in a barrel-like container.

**Figure 56.** The maximum coverage from the experiment with changing the whole broth every 30 minutes.

**Figure 57.** Adding oxygen after bacterial detachment in a barrel-like container.

**Figure 58.** Adhesion dynamics in a microchannel: two repetitions of ejection experiment.

**Figure 59.** Maximum coverage of the ejection experiment.

**Figure 60.** Adhesion dynamics in a microchannel: three repetitions of injection experiment.

**Figure 61.** Adhesion dynamics in a microchannel: both the ejection/injection (pulling/pushing) experiments.

**Figure 62.** Adhesion dynamics both in a microchannel and a barrel-like container

**Figure 63.** Colony surface evolution with 20x magnification.

**Figure 64.** Colony evolution representation from the 20x magnification experiment.

**Figure 65.** The average colony surfaces with four simple exponential growth models of different division times.

**Figure 66.** The average colony surfaces with exponential growth models of different initial surfaces.

**Figure 67.** The ratio of average colony surface originating from four and one initial bacteria.

**Figure 68.** Colony surface evolution with 100x magnification.

**Figure 69.** The ln value of average colony surfaces with four exponential growth models.

**Figure 70.** Colony surface evolution with 100x magnification, with an accent on dispersion and behaviour afterwards.

**Figure 71.** Colony evolution representation from the 100x magnification experiment.

**Figure 72.** The filamentous form of bacteria found after dispersion in colony evolution experiments.

**Figure 73.** Colony surface evolution from the experiment with 10 initial bacteria (second repetition).

**Figure 74.** The 10 (A), 100 (B), and 5 (C) initial bacteria experiment before the dispersion and at the minimum coverage

**Figure 75.** Percentage of covered surface for different initial concentrations of bacteria.

**Figure 76.** The exact times of dispersion and the percentages of the covered substrate at the dispersion time for different initial concentrations of bacteria.

**Figure 77.** The average colony surface in time at 1/4, 2/4, and 3/4 of the barrier length in the PDMS channel.

**Figure 78.** The average colony surface at all barrier lengths in the PDMS channel.

**Figure 79.** An example of colony evolution from a 1/4 barrier length in the PDMS channel.

**Figure 80.** The exact dispersion times for different channel positions regarding the barrier length.

**Figure 81.** The adjusted dispersion times for different channel positions regarding the barrier length.

**Figure 82.** The average colony surface at 3/8 of the barrier length in the PDMS channel under increased flux.

**Figure 83.** The coverage percentage per left and right area thirds, at 3/8 of the barrier length in the PDMS channel.

**Figure 84.** The coverage percentage in the left and right channel arm, at 3/8 of the barrier length in the PDMS channel.

**Figure 85.** Curved PDMS channel: A) Covered surface at the second and third curve position B) Zoomed graphs at the second and third curve positions C) A view of the experiment and a channel.

**Figure 86.** Curved PDMS channel: A) Covered surface at the first and second curve position under a smaller magnification.

**Figure 87.** Curved PDMS channel: Covered surface for each third of the channel's width at the first and second curve positions.

**Figure 88.** Curved PDMS channel: Covered surface for each lengthwise area at the first curve position.

## List of Tables

**Table 1A.** Taxonomic identification of 16 monocultures from forward (F) and reverse (R) sequencing.

**Table 1B.** The repeated taxonomic identification for the monoculture number 1.

**Table 2.** Relative abundances of most frequent species in the samples.

**Table 3.** Relative abundances of most frequent genera in the samples.

**Table 4.** All the OTUs from the genus *Vibrio*, regardless of their species level defined or undefined.

**Table 5.** All the OTUs from genus *Vibrio* with their relative abundance in the samples.

**Table 6.** Molecular function (L3) prediction of selected genera in the samples.

**Table 7.** Molecular function (L3) prediction of selected species in samples.

**Table 8.** Gene activity (L4) prediction of selected species in samples.

**Table 9.** Lux family gene activity (L4) prediction of selected species in samples.

# 1. Introduction

## 1.1. Marine biofilm and bacteria

Bacterial biofilms are microorganism communities that are associated with their surfaces and merged in a polymer matrix [1]. They naturally consist of a larger number of species, but can also develop from a single species [2,3]. Specifically, marine bacterial biofilms are a common phenomenon that occurs below sea level on almost any immersed surface, even artificial ones [4-6]. Right from the moment the surface is immersed, the biofilm is rapidly formed and evolves [7] since it is an important survival mechanism of marine bacteria [5]. This life state is preferable for many bacteria as it offers many advantages, such as protection from harmful conditions and predators, utilization of community cooperation, nutrient exploitation, better response to toxins and antibiotics, etc. [5,8,9]. At the beginning, the individual bacterial cells attach to the surface (adhere) and form monolayers. As they divide and more bacteria adhere, multilayers develop, consisting of clusters of cells [10]. The multilayer biofilm consists not only of bacterial cells but also of an extracellular polymer matrix secreted by the bacteria [1,10,11], which is essential for biofilm development. This phase of biofilm serves as the initial phase for more complex communities, consisting of algae, bivalves, barnacles, and larvae as well [6,11,12]. A simple timeline of biofilm evolution, from individual bacteria and bacterial clusters and colonies to a more diverse latter phase, is shown in Figure 1 [13].

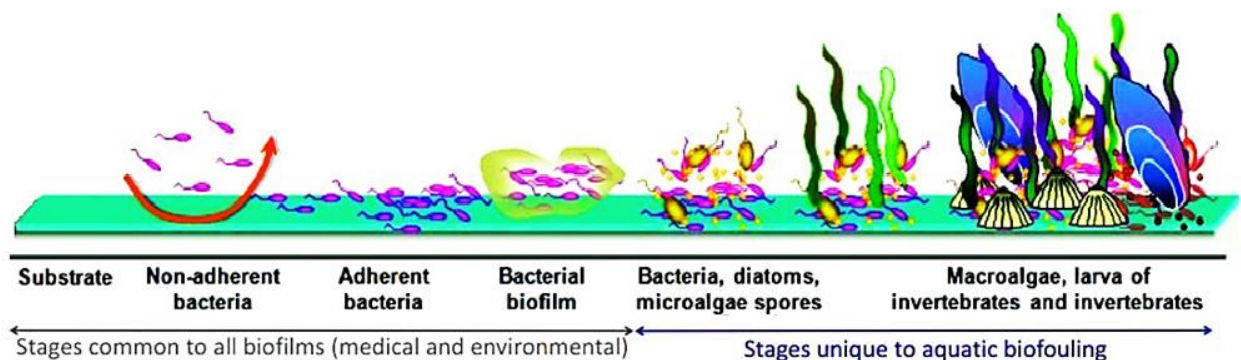


**Figure 1.** A general biofilm evolution, with an extension to the aquatic environment [13].

As stated in Figure 1, the first half of the timeline describes the stages common to all biofilms and involves only bacterial species, while the rest of it is typical only for the aquatic environment. The stages at which only the bacteria are present are the focus of this dissertation. Moreover, marine bacteria are chosen as a primary target for numerous reasons.

The development of marine bacterial biofilms, often called biofouling, causes various struggles [12,14,15]. Growing on the vessel hulls (Figure 2A [14]) and increasing vessel resistance and fuel consumption, biofouling presents a major economic issue in maritime traffic but is also a damaging factor causing biocorrosion (Figure 2B [15]). Very often non-indigenous species are transferred by vessels due to interacting and adhering to developed biofilm, creating ecological issues as well. All these problems are initiated exactly by marine bacteria, as the initial phase of biofilm formation, making them a tempting research subject.

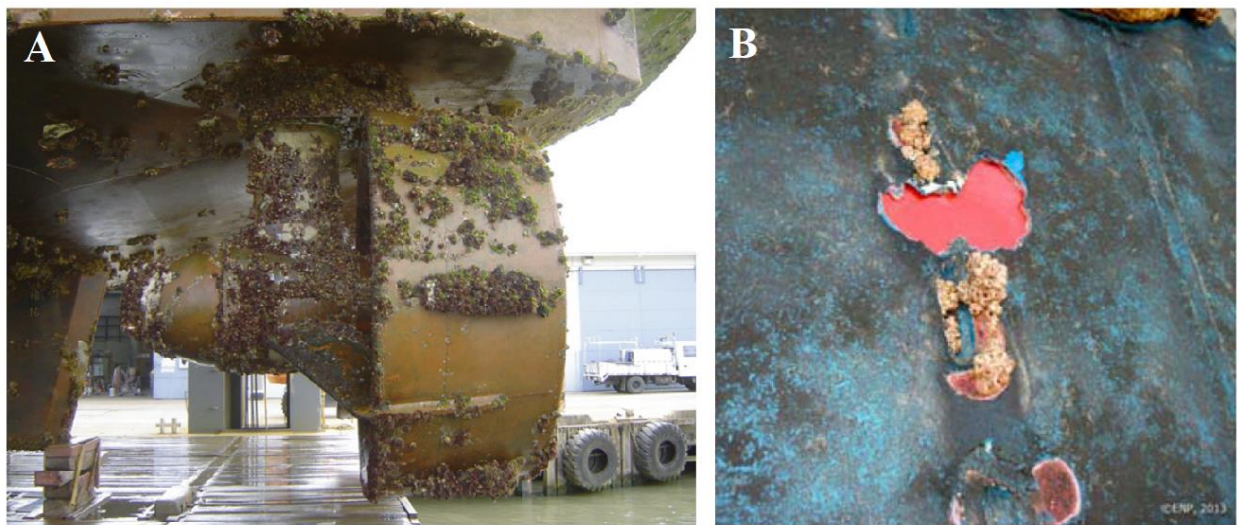


**Figure 2.** A) Vessel hull fouling [14] B) Biocorrosion [15].

To deal with the mentioned issues, various antifouling strategies have been developed, but they are either selective or with harmful side effects on the environment. Until today, no universally effective antifouling method exists, whether it uses a biological [16] or physicochemical [17] approach, just as there is no fully effective method without reporting the toxic effects and consequences for the environment [14,15]. On the other hand, apart from developing antifouling strategies, a closer look at the adhesion process as the initial stage of the biofilm, as well as monitoring the biofilm development and its dispersion, could change our view of these complex communities, reveal their characteristics and behaviour, and clarify how they initially form, develop and operate.

## 1.2. Scientific background

The biofilm can be researched after it is developed in the sea environment and taken for examination as a whole complex community that was formed. To study the structure and growth of biofilms microscopic techniques (confocal and scanning electron microscopy) and numerous biochemical analyses are used. Furthermore, for the composition and functional potential of biofilm communities, the next-generation sequencing (NGS) and phylogenetic investigation of communities by reconstruction of unobserved states (PICRUSt) are applied. The NGS could be considered a revolution in the field of genomics [18-20], which is widely used to study both the composition and diversity of biofilms developed on the substrates exposed to the sea. This can involve changing the locations of the samples, replacing the type of substrates, or exposing the substrate to different time intervals [21-24]. Some of the globally most abundant bacteria in seawater and at the phylum level are shown to be *Proteobacteria*, *Cyanobacteria*, *Bacteroidetes*, and others [24,25]. This NGS method is based on finding the relative abundances of species present in the samples, giving an insight into the composition, and also offers the calculation of phylogenetic, alpha, and beta diversity [26-29]. In summary, converting the number of 16S rRNA gene reads into the exact number and composition of bacterial species in a sample involves clustering similar sequences into OTUs (operational taxonomic units), assigning taxonomic labels to these clusters, quantifying the abundance of each taxon, and presenting the results in a taxonomic profile or abundance table. It is often combined with the PICRUSt algorithm [30,31], a bioinformatics software package for predicting the functional content or potential of microbial communities based on their taxonomic composition, which is usually derived from marker genes such as the 16S rRNA gene. It is based on the assumption that the functional potential of the community is related to the genetic content of the present microorganisms. PICRUSt uses the KEGG database (Kyoto Encyclopedia of Genes and Genomes) [32] to link the predicted composition of microbial communities to functional capabilities and to estimate the frequency of functional pathways based on taxonomic information obtained from 16S rRNA gene sequences.

Opposed to the natural sea-developed biofilm, the biofilm can be developed and studied in controlled laboratory conditions. The bacteria are provided with the necessary nutrients and the conditions under which they can divide and form complex communities. The advantage of laboratory research is that it enables the direct investigation of specific features and characteristics of the biofilm, the observation of the development of colonies or the adhesion process itself.

The adhesion process is usually studied on a single bacterium interacting with the substrate, or on a population of bacteria observed as individuals. From the individual bacterial trajectories, a mean squared displacement (MSD) was calculated, characterising their motion type as adhering, diffusing, and swimming (Figure 3A), according to the exponent on the  $\tau$  time interval that was adjusted to match the calculated MSD [33]. The number of bacteria was also counted for each type of motion, both in wild-type and flagellum-mutant bacteria [33]. While directly interacting with the substrate, bacterial near-surface motility mechanisms using flagella and pili were examined [34] (Figure 3B) and characterized as crawling, walking, twitching, and pivoting [33-36]. The rheotaxis and orientation dynamics were also described as a function of the applied shear rate [37] (Figure 3C).

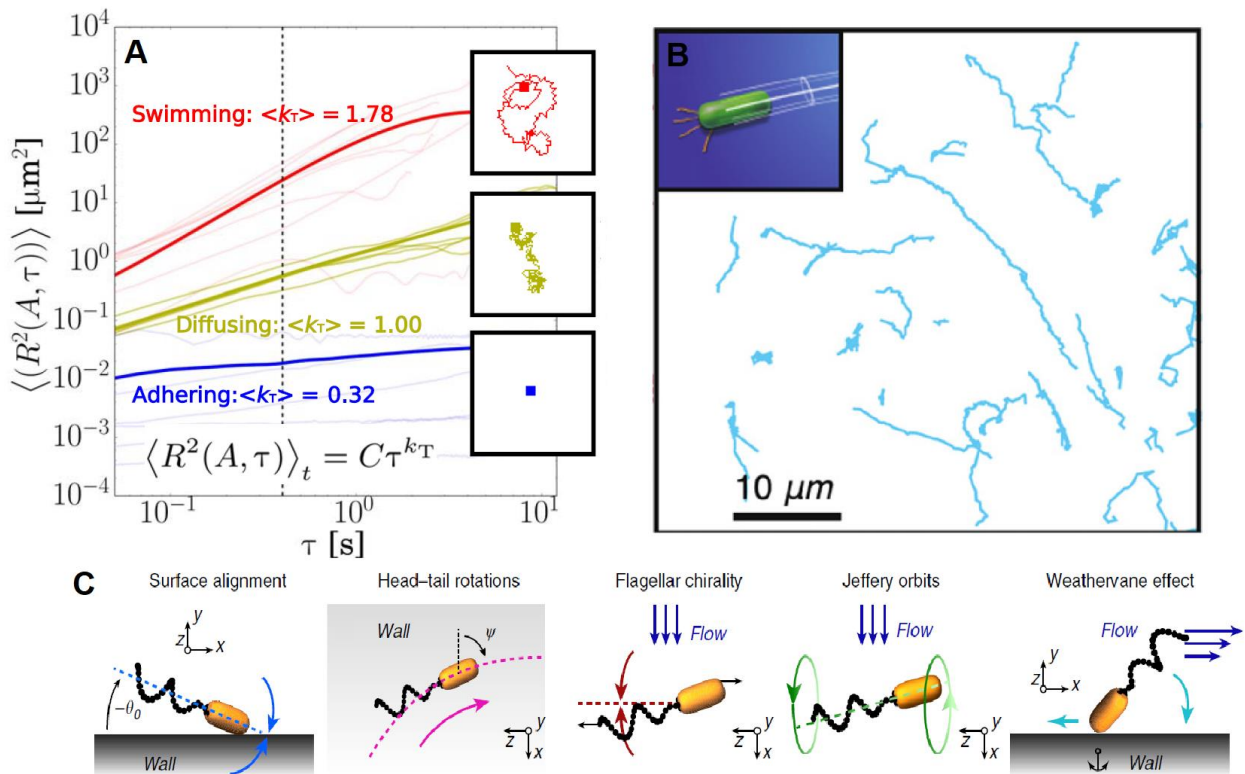


**Figure 3.** A) Calculated MSD as a function of  $\tau$  time interval. The  $k_T$  coefficient was set to match the MSD and characterise the stated types of motion [33] B) Near-surface motility: crawling trajectories [34] C) flow and wall effects on rheotaxis and orientation dynamics [37].

Moreover, bacteria can be observed as a whole community of a certain species, focusing on the development of aggregates, colonies, and biofilm. Bacterial surface attachment and surface physicochemical state were monitored on colloidal bead suspension [38]. Also, the biofilm



development and maturation process after adhesion were observed in a longer time interval for wild-type and aggregation-inducing polysaccharide mutant bacteria [3] (Figure 4A), as well as the early phase formation on stainless steel [39]. Furthermore, a reported 3D structure biofilm evolution revealed its characteristics, growth dynamics, and colony merging [13,40], but also the effect of biofilm reduction with the use of antimicrobial peptides [41]. With the description of biofilm formation mechanisms [42], its development was also simulated, predicting the growth behaviour from different initial aggregate arrangements, and compared to real growth [43,44]. After the maturation of biofilm, erosion or dispersion occurs as a result of unfavourable conditions and environmental changes, during which the bacteria leave as single cells [45] (Figure 4B).

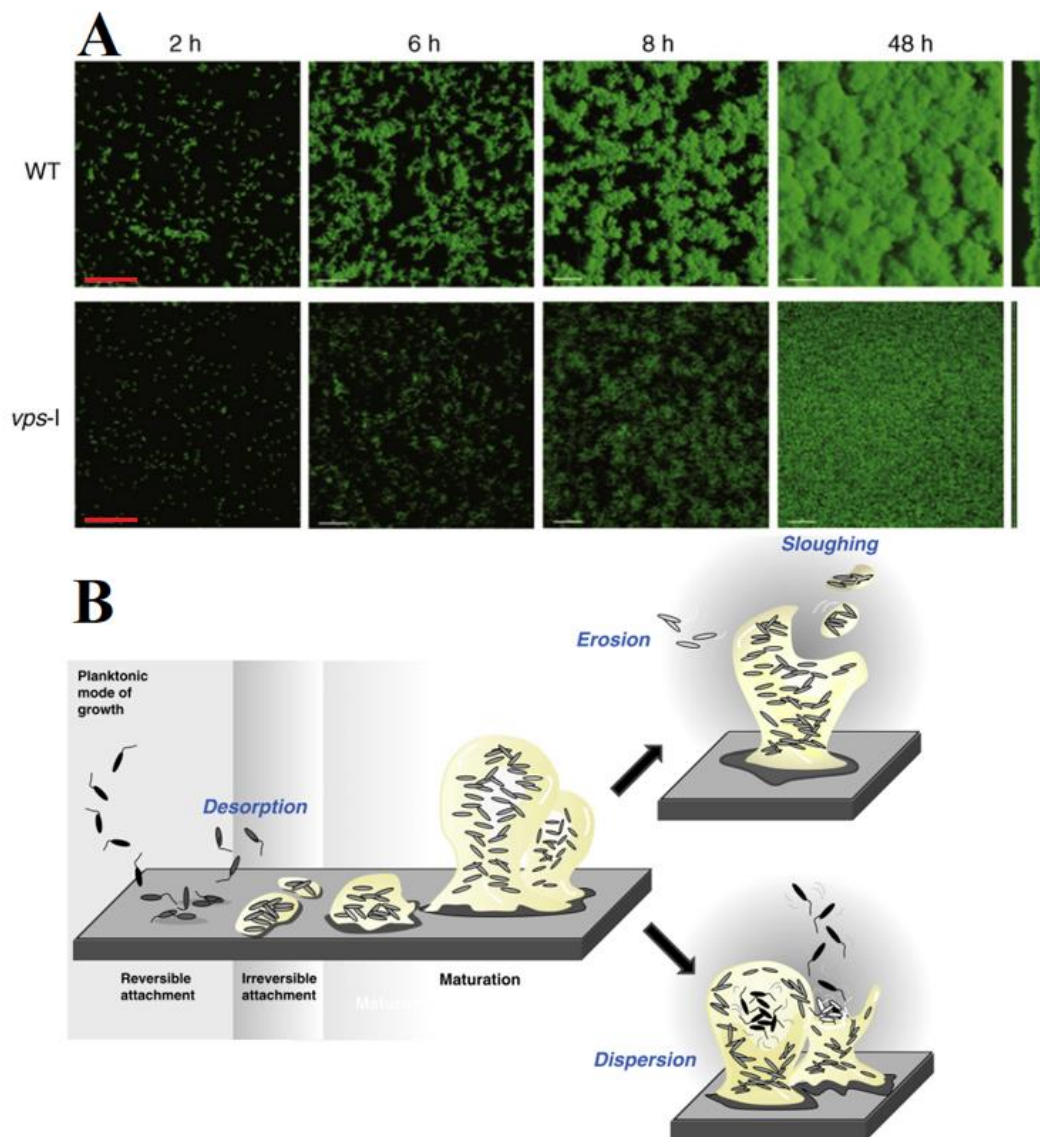


**Figure 4.** A) 3D biofilm structures of wild-type and vps-I mutant *Vibrio cholerae*, tagged with green fluorescent protein [3]. The red scale bar indicates 50  $\mu\text{m}$ . B) Modes of escape from a developed biofilm [45].

Dispersion is driven by quorum sensing [3,46], a crucial bacterial cell-to-cell communication and collective behaviour mechanism that is guided by secreted signal molecules and receptors and shown to affect both the process of biofilm formation and its regulation [47-49]. It acts as a response to mainly oxygen and nutrient depletion, as well as flow disruption [45]. The final phase of the biofilm has been studied with dispersal initiated by the interruption of nutrient flow [50] or explained by quorum sensing regulatory networks [46]. Also, it was shown that the development of a biofilm can be prevented by quorum quenching [51]. When performing the adhesion dynamics experiments, one of the key features is the rate of medium flow (flux). Based on its rate, the influence on the local repression of quorum sensing was reported [52], as well as the interaction with the biofilm development due to shear stress varying across the width of a channel and changing for different channel heights [53]. Very rarely the bacterial model was not *Escherichia coli* or *Pseudomonas aeruginosa*, which became the standard species for bacterial biofilm research. The primary and irreversible adhesion, biofilm maturation, and both interaction and genetic regulatory mechanisms, including quorum sensing, were extensively described for *Escherichia coli* [54], as well as its strongly suppressed chemotactic drift at higher cell densities [55].

Unlike the experiments where only one species was used, emphasizing its specific characteristics, observing the multiple species community mimics the more realistic environment, giving an insight into species interactions, cohabitation, and competition for resources [56] (Figure 5).

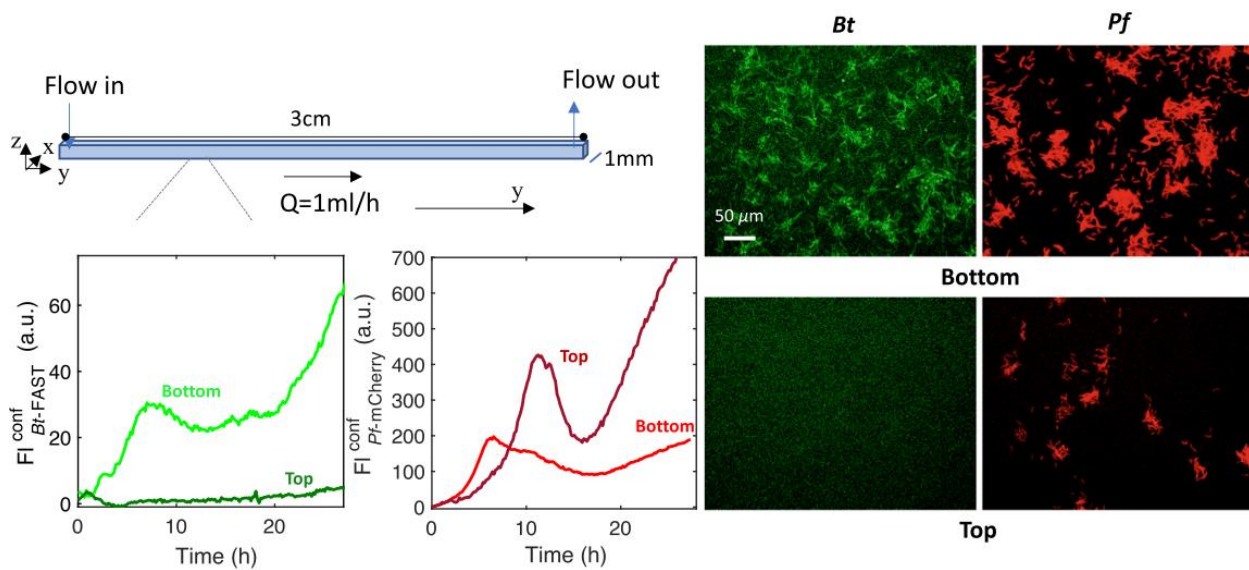


**Figure 5.** A schematic view of millifluidic channel together with surface-dwelling characteristics of two different species, both at the bottom and the top, measured as confocal fluorescence intensities [56].



Apart from the experimental background, the bacterial motion and the conditions that the bacteria are found under during experiments can be described theoretically.

Talking about diffusion, the Stokes-Einstein equation describes the diffusion of spherical particles with radius  $r$ , with relation  $D = \frac{k_B T}{6\pi\eta r}$ , where  $\eta$  is the dynamic viscosity of water at 20°C (0.001 kgm<sup>-1</sup>s<sup>-1</sup>). If this is applied on 1 to 2-micron-sized bacteria with an approximation of a spherical particle, that would result in a diffusion constant  $D = 0.215 \mu\text{m}^2\text{s}^{-1}$ . The mean squared displacement of a particle (MSD), which is  $\langle |x(\tau) - x(0)|^2 \rangle = \frac{1}{N} \sum_{i=1}^N |x_i(\tau) - x_i(0)|^2$  averaged by  $N$  particles can be calculated from diffusion constant as  $MSD = 2nD\tau$ , where  $\tau$  is the observing time interval and  $n$  is the number of dimensions. For  $\tau = 1\text{s}$  and 2D motion,  $MSD$  equals  $0.86\mu\text{m}^2$ , describing the covered area of spontaneous diffusion of a random particle. On the other hand, the bacteria with a willing and directed motion perform ballistic steps from which an average speed and crossed length can be calculated. The average speed reaches from 40 to 80  $\mu\text{m}\text{s}^{-1}$  due to their flagellum [57]. This speed exceeds by far a spontaneous diffusion motion (Figure 6A).

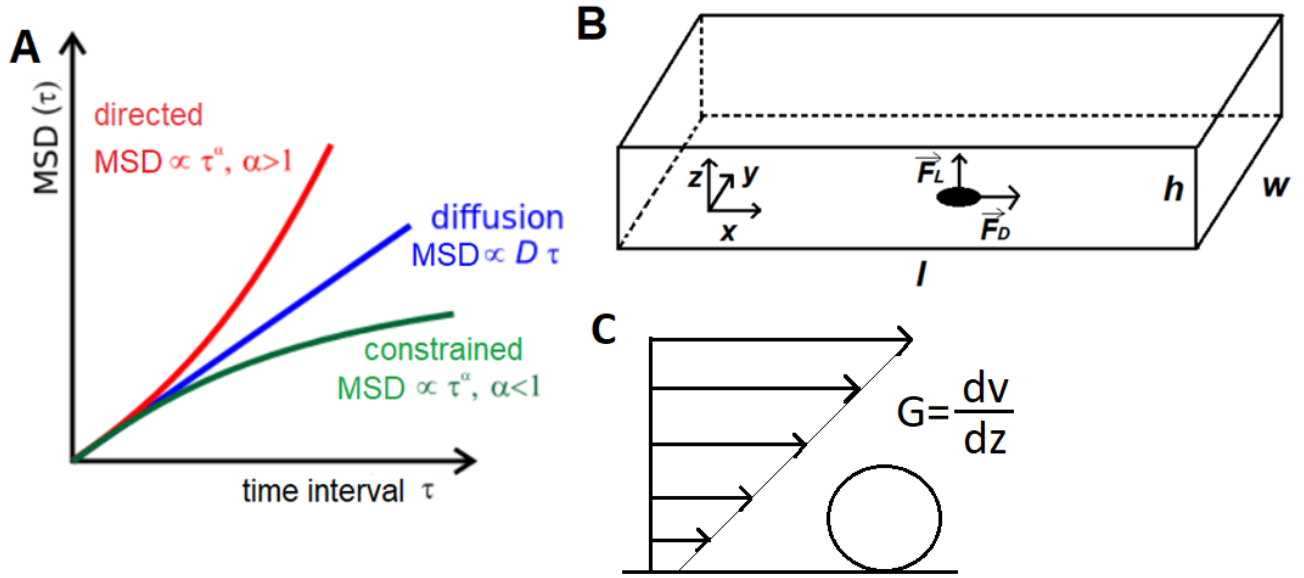


**Figure 6.** A) MSD dependence of time interval  $\tau$  for diffusion (proportional to  $\tau$ ) and directed or constrained motion. B) Rectangular microfluidic channel defined by the width  $w$ , height  $h$ , and length  $l$ , with specified axes. A bacterium adhered at the surface is shown with drag and lift forces that act upon it. C) A schematic representation of the shear rate of ambient flow  $G$ .

On the other hand, the adhered bacteria perform slight movements at the beginning of adhesion, finally becoming anchored and immobile after some time. The bacteria dwelling at the surface of a substrate inside a rectangular microfluidic channel defined by the width  $w$ , height  $h$ , and length  $l$  as in Figure 6B, experience shear stress as a result of shear forces, and resist the drag  $F_D$  and lift force  $F_L$ .

In the case of  $h \ll w$ , if the middle height is set to zero and it ranges from  $-h/2$  to  $+h/2$ , velocity as a function of height could be written as  $v(z) = v_{max}(1 - \frac{4z^2}{h^2})$  [58], where the maximum velocity is achieved at the middle height ( $z = 0$ ). The volume flow  $Q$  is then defined as  $Q = \bar{v} \cdot h \cdot w$ , where  $\bar{v}$  is the average velocity across the length direction. The average velocity equals two thirds of its maximum value  $\bar{v} = \frac{2}{3}v_{max}$  [58], transforming the velocity as a function of height into

$$v(z) = \frac{3}{2}\bar{v}\left(1 - \frac{4z^2}{h^2}\right) = \frac{3Q}{2hw}\left(1 - \frac{4z^2}{h^2}\right).$$

Deriving this velocity by the height results in the shear rate of the ambient flow  $G$  (Figure 6C), which describes the flow field, the change of velocity with height.

Therefore,  $\frac{dv}{dz} = G = -\frac{12Q}{h^3w} \cdot z$ , where for the  $z = -\frac{h}{2}$  at the surface it becomes  $G = \frac{6Q}{h^2w}$ . The shear

Reynolds number is defined as  $Re_s = \frac{|G|Ld}{\nu}$  [59], where  $L$  is the height at which it is calculated and  $d$

is the diameter of a spherical-like particle (bacterium), while  $\nu$  is the kinematic viscosity of water ( $10^{-6}m^2s^{-1}$  at  $20^\circ C$ ). Since the drag and lift forces for the fluid density  $\rho$  are defined as

$$F_D = C_{Ds} \frac{\pi}{8} \rho G^2 L^2 d^2 \text{ and } F_L = C_{Ls} \frac{\pi}{8} \rho G^2 L^2 d^2 \text{ [59], where drag shear coefficient and lift shear}$$

$$\text{coefficient are calculated as } C_{Ds} = \frac{40.81}{Re_s} (1 + 0.1Re_s^{0.753}) \text{ and } C_{Ls} = \frac{3.66}{(Re_s^2 + 0.12)^{0.22}} \text{ [59], the drag and}$$

lift forces could be estimated. For the approximate volume flow of  $20\mu l/min$ ,  $120\mu m$  channel height

and  $2mm$  channel width (conditions used in this dissertation), the shear rate of the ambient flow would

be  $G = 69.6 s^{-1}$ . Furthermore, if the shear Reynolds number is calculated at the height of the half

bacterium diameter ( $L = \frac{d}{2}$ ), for the bacterium diameter of  $1\mu m$  and at  $20^\circ C$  of the water medium, it

would be  $Re_s = 34.8 \cdot 10^{-6}$ . Thus, for the  $C_{Ds} = 1.17 \cdot 10^6$  and  $C_{Ls} = 5.95$ , the bacterium at the

bottom would feel the drag force of  $F_D = 5.6 \cdot 10^{-13}N$  and negligible lift force of only

$F_L = 7 \cdot 10^{-19}N$ . In case of decreasing the channel height  $n$  times, the drag force would increase

roughly  $n^2$  times and vice versa, hence it is inversely proportional to the square of channel height,

$F_D \propto h^{-2}$ . Also, if the bacteria grew in time and from one individual a colony evolved, the observed

particle would increase its diameter and the height at which the drag force was calculated. The drag

force is directly proportional to the square of the particle diameter,  $F_D \propto d^2$ . In the end, it is directly proportional to the flux change,  $F_D \propto Q$ .

These forces are caused by the fluid motion i.e. its velocity that varies along the  $yz$  plane for a fixed  $x$  position. Calculation of the velocity field  $v(y, z)$  (Figure 7A) [53] along the width of the channel  $w(y)$  as in Figure 6B reveals that the bacteria at the same height  $z$  will feel different shear stress across the width, as a result of velocity variation  $v(y)$ . Furthermore, for a steady flow of incompressible fluid, the shear stress was modelled across the 1 mm-wide channel for different channel heights (Figure 7B) [53].

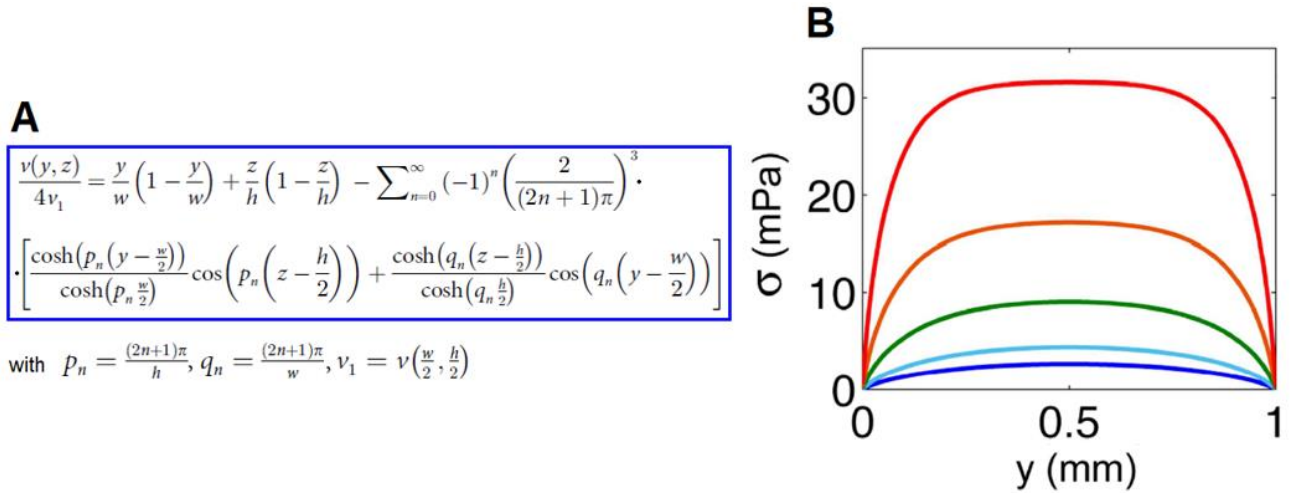


**Figure 7. A)** Velocity field calculation for a steady viscous flow of an incompressible fluid in a rectangular channel [53]. **B)** Bottom shear stress variation across the channel width as a result of velocity field  $v(y, z)$ , given for 5 rectangular 1mm-wide channels, ranging in height from 250  $\mu\text{m}$  (red) to 1000  $\mu\text{m}$  (dark blue), under a flow rate of 1 ml/h [53].

Using this formula from Figure 7A, the velocity field can be calculated for any type of rectangular channel. For instance, a 1.8 mm-wide and 120  $\mu\text{m}$ -high channel (conditions used in this dissertation) at a fixed height of 60  $\mu\text{m}$  (half of the height) would have a velocity profile as in Figure 8A (blue dots), with velocity reaching the maximum value at around 200  $\mu\text{m}$  of width and being constant until 1600  $\mu\text{m}$  of width is reached. The profile is symmetrical regarding the middle width (900  $\mu\text{m}$ ). On the other hand, at the lower height of  $z = 10\mu\text{m}$ , the highest reached velocity is only at around 31% of the maximum velocity in the channel (Figure 8A, orange dots), confirming that the velocities decrease while approaching the boundary, both in the  $y$  and  $z$  direction. Observing the bacteria that are adhered on the surface, their height would be around 1  $\mu\text{m}$ , hence the velocity field at this height

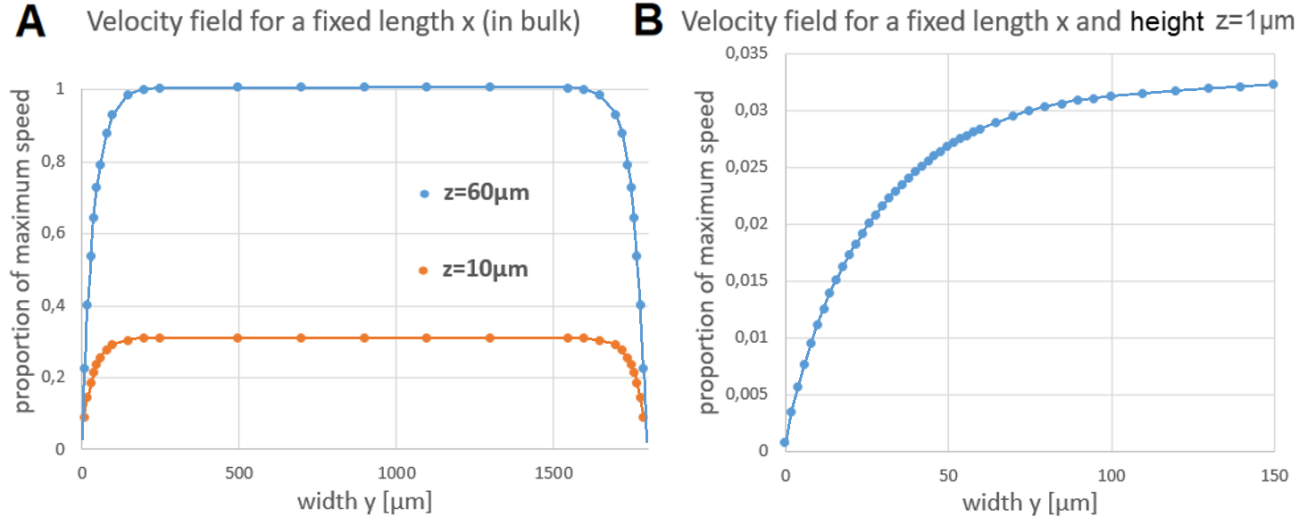


**Figure 8.** **A)** Velocity field at a fixed  $x$  position and at the heights of  $z = 60\mu\text{m}$  and  $z = 10\mu\text{m}$ , in a  $1.8\text{ mm}$ -wide and  $120\mu\text{m}$ -high channel. **B)** Velocity field at the height of  $z = 1\mu\text{m}$ , at which the bacteria is situated while adhered at the surface.

is particularly interesting and shown in Figure 8B. The presented width ranges only to  $150\mu\text{m}$ , since from that point on, the velocity becomes constant. Again, the profile is symmetrical and identical variation is found on the other side. The maximum velocity value that is reached at this height is only around 3% of the maximum velocity of the whole channel, making it noticeably lower. Also, the bacteria that adhere in the region of  $50\mu\text{m}$  from the boundary feel even smaller shear stress (Figure 8B).

Talking about bacterial interaction, quorum sensing is a crucial cell-to-cell communication, enabling collective behaviour driven by secreted signal molecules. Since it affects biofilm formation and regulation [47-49], but also dispersion [3,46], it is necessary to estimate the MSD of these signal molecules. Autoinducer-2 (AI-2), as a standard quorum sensing molecule consists of 23 atoms and based on its 3D model, its diameter can be estimated as 7 linear atoms,  $7 \cdot 10^{-10}\text{m}$ . Stokes-Einstein equation for  $T = 293\text{K}$  then gives  $D = \frac{k_B T}{6\pi\eta r} \approx 6 \cdot 10^{-10}\text{m}^2\text{s}^{-1}$ . For  $\tau = 1\text{s}$  and 1-dimensional diffusion ( $z$ ), mean squared displacement  $MSD = 2D\tau = 1200\mu\text{m}^2$  and mean displacement is around  $35\mu\text{m}$ . Also, for the volume flow of  $20\mu\text{l}/\text{min}$ ,  $120\mu\text{m}$  channel height and  $2\text{mm}$  channel width (conditions used in this dissertation), the average velocity is  $\bar{v} = \frac{Q}{h \cdot w} = 1.4\text{mms}^{-1}$  and  $v_{max} = \frac{3}{2}\bar{v} = 2100\mu\text{ms}^{-1}$ . The bacteria at the bottom experience only around 3% of the maximum velocity,  $v \approx 60\mu\text{ms}^{-1}$ , making the diffusion of AI-2 molecule somewhat “quicker” than the ambient flow at the

bottom of such a channel since the average displacement in the  $z$  direction should be  $\approx 35\mu\text{m}$  after 1 second. For  $\tau = 0.1\text{s}$ , the bottom velocity would be  $\approx 6\mu\text{ms}^{-1}$  and the MSD of  $120\mu\text{m}^2$  with a mean displacement of  $11\mu\text{m}$ . On the other hand, the time needed for the same molecule to diffuse to half of the height ( $60\mu\text{m}$ ) is 3 seconds, after which it could be said that AI-2 molecules cover all the heights in the channel. In the same time interval, the medium passes around  $180\mu\text{m}$  at the bottom and  $6000\mu\text{m}$  at the middle ( $\frac{w}{2}, \frac{h}{2}$ ), in the 10 cm long channel. Therefore, it is questionable if the AI-2 molecule could reach the neighbouring bacteria before diffusing to the bulk, but it could reach them afterwards since all heights should be covered while it is diffusing. Hence, the effect of quorum sensing could be diminished, but not neglected.

### 1.3. Goals and Hypothesis

Despite all these findings, there is no widely used non-pathogenic autochthonous marine bacterium model species for adhesion dynamics and colony and biofilm evolution research. Moreover, the quantification of adhesion as a substrate coverage, and colony evolution is rarely presented. A particularly interesting dispersion phenomenon of colonies and biofilm, which has some reported causes [10,60-62], remained unclear and unquantified regarding its time dependence and dependence on the position in the channel, as well as the substrate coverage at which it is triggered.

The aim of this dissertation is the identification of a representative primary biofilm-forming model species from Kaštela Bay: its (I) isolation and (II) cultivation in laboratory conditions, (III) quantitative determination of its potential regarding the adhesion mechanics and genetic potential, (IV) quantification of its adhesion/desorption dynamics, (V) identification of main events of this dynamics on the single cell level and (VI) identification of the collective effects in different stages of adhesion/dispersion dynamics. To achieve this, the following goals were set and accomplished.

To begin with, the first goal was to extract, isolate, cultivate, and identify autochthonous marine bacterial species from the sea that participate in the early stages of biofilm formation. To distinguish which of the isolated species was the best choice for model species in studying the adhesion dynamics, preliminary adhesion tendency measurements were performed. Also, the NGS analysis was carried out to acquire the relative abundances of all marine bacterial species that were found in early-formed

biofilm, as well as their representations in various phases of complex biofilm samples, thus confirming the importance of their presence. To further confirm the choice of a suitable model bacterial species, genes critical for bacterial adhesion, quorum sensing and cell motility in the species of interest were predicted using the PICRUSt method.

In general, successful bacterial adhesion is an elementary step for often harmful and undesirable biofilm development in seawater and other environments. Each pathogenic action also occurs after adhesion and colonisation. To better describe the rate and characteristics of adhesion for a chosen bacterial model, another goal was to design and produce a bio-reactor that could enable the quantification of adhesion dynamics on the solid substrate and monitor the distribution of their aggregates of different sizes. This was achieved by measuring the surface of the covered substrate at the chosen time points. Achieving this led to the question of real-time bacterial adhesion dynamics. With the aim of calculating it, the adhesion dynamics was measured first in large volume (in bulk conditions) of around 5 ml, with no height restriction, where the bacteria could swim freely and not interact with the ceiling, possibly being forced to adhere. For this, a barrel-like container with different flow rates of medium mixing was predicted. Compared with the adhesion in a microfluidic device with a constant flow of the medium, which was a confined space where the height was restricted, the optimal experimental setup for the following research was to be decided, as well as finding the parameters that could drive their behaviour.

Changing the focus from the adhesion of individual bacteria from the medium and their collective behaviour, the next goal was to comprehend how colonies evolve in time. The idea was to conduct the experiment for measurement of colony sizes (surfaces), from the starting individual cell until the evolved colony dispersion, and also compare it with standard growth models. Here, an inevitable bacterial division could be controlled better and the essential supplies ensured easier. Additionally, whether the colonies were affected by the change in the initial concentration of bacteria set on the substrate was to be checked and the critical parameters confirmed. Also, the question to be answered was whether and how the dispersion time depends on the position in the microchannel. To understand that, specifically designed Polydimethylsiloxane (PDMS) microchannels were created for simultaneous monitoring of two different positions in the channel, but also to quantify collective dispersion phenomenon, and offer an explanation for its triggering mechanisms.

The hypothesis of this dissertation: A marine bacterium can be isolated from early-phase formed biofilm from Kaštela Bay and serve as a convenient and versatile model for quantitative investigation of adhesion dynamics and pioneer biofilm formation, as well as potential prevention strategies. The regulation of the early stages of biofilm includes collective phenomena guided by interactions between cells.

## 2. Materials and methods

### 2.1. Choosing the bacterial model species

#### 2.1.1. Isolation and identification of biofilm-forming species

To isolate the biofilm-forming bacterial species from the early phase of biofilm formation, three microscopic slides were cleaned three times with 70% ethanol and kimwipes and inserted into the gaps made in Styrofoam using a sterile scalpel. The Styrofoam carrier was also cleaned the same way and placed on the sea surface, with the slides (substrates) immersed in the sea. Precisely, into a pool with a free circulation of seawater, at the Institute of Oceanography and Fisheries in Split, Croatia (43°30'28.8"N, 16°23'18.1"E). The slides were exposed to the marine environment for three days to ensure that there was sufficient biodiversity in the biofilm, but also that the biofilm did not develop too much from the early phase, which was the aim. After three days, the biofilm formed on three slides was scraped and diluted with 300 ml of sterile distilled water. An aliquot of 100 µl and its dilutions of 1:2, 1:10, 1:20, and 1:100 were spread on Marine agar plates. Marine agar was prepared from 37.4 g/L of Marine broth (BD Difco, USA), to which 15 g/L of technical agar (Biolife, Italy) was added. To allow colony formation for all the present species, agar plates were left for three days at room temperature. The colonies formed were then randomly selected based on different morphology and sizes and subcultured i.e. spread onto new agar plates to ensure monocultures, all resulting in 16 different isolated species. To identify them taxonomically, their genomic DNA was extracted using the NucleoSpin Microbial DNA Kit (Macherey-Nagel, Germany), according to the manufacturer's instructions. The partial 16S rRNA gene of the representative strains was amplified with primers 27f (5' -AGAGTTTGATYMTGGCTCAG-3') and 1492r (5' -TACGGYTACCTTGTTACGACT-3') under standard PCR conditions [63], and subjected to Sanger sequencing of both strands in Macrogen Europe service (Amsterdam, Netherlands). The obtained sequences were then compared with those available in the GenBank database using the BLAST software (<http://www.ncbi.nlm.nih.gov/>). All isolates were stored in glycerol-containing stocks at -80 °C.



### 2.1.2. Preliminary adhesion tendency tests

The isolated species were identified taxonomically and showed to participate in the early phase of biofilm formation. To verify whether these species actually have adhesion preferences in laboratory conditions and consequently could be used in future adhesion dynamics experiments, they were tested for adhesion tendencies one by one. After a single colony was transferred into 5 ml of Marine broth for each species separately, around 20 hours-old overnight culture was directly inserted into a simple transparent microchannel as in Figure 9A. A microscopic coverslip was used as a substrate, and a hollowed two-sided sticking tape as the frame, ensuring the height. Above the frame, a transparent thin plastic with an “in” and “out” hole was placed. The medium was left in stationary conditions without any flux or medium exchange. The microchannel was placed onto a stage of the PicoTwist apparatus (Figure 9B), which was used as an inverted microscope. The bottom (substrate) of the microchannel was monitored and filmed with a uEye camera (IDS, Germany). The adhesion process was quantified as a percentage of substrate surface coverage in time and calculated in the FIJI image processing package [64]. The results of this preliminary experiment were used, together with the results of the following methodology sections 2.2. and 2.3. to decide which isolated biofilm-forming monoculture has the potential to serve as model species for future experiments and will be used.

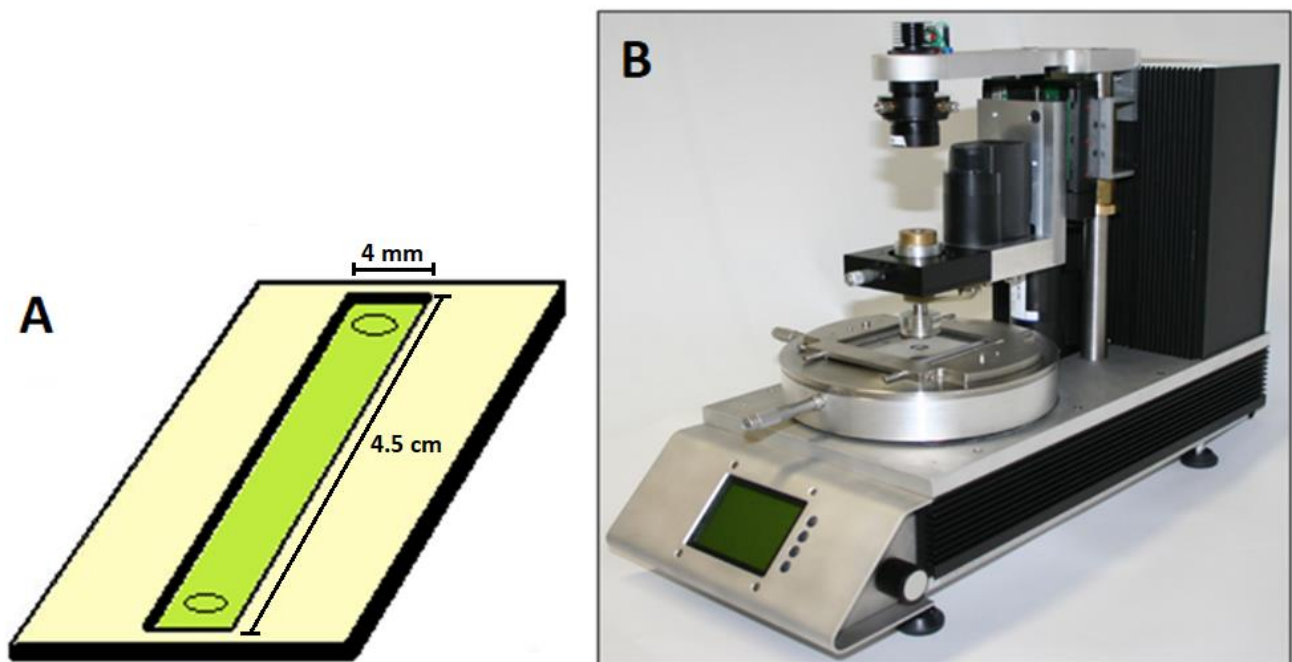


**Figure 9.** A) 30  $\mu\text{m}$  high microchannel with an insertion and ejection hole. B) PicoTwist apparatus, used simply as an inverted microscope, onto which the microchannel was placed.

## **2.2. NGS (Next generation sequencing) analysis**

### **2.2.1. DNA isolation and preparation of samples**

To collect the samples for NGS, a similar procedure was used as in section 2.1.1. but this time a larger number of microscopic slides was used to ensure that sufficient biofilm and its amount of DNA was collected. Based on the estimate of how much DNA can be collected on a single slide, it was decided to use exactly one hundred and ten glass slides to achieve the required amount of DNA for each sample. Both the slides and Styrofoam carrier were cleaned three times with 70% ethanol and kimwipes and the slides were inserted into the Styrofoam gaps made with a sterile scalpel. Again, the carrier was placed at the same location (Institute of Oceanography and Fisheries in Split, Croatia (43°30'28.8"N, 16°23'18.1"E)), so that the slides (substrates) were immersed beneath the sea level (Figure 10). The experiment was conducted in the late November of 2019, at a sea temperature of (18±1) °C. At the moment of immersion, 1200 ml of seawater was collected below the surface and immediately filtered through 0.22 µm pore-size MCE membrane filters (Whatman, UK) to obtain the first sample S0. This sample was taken mainly to show which species were present in the environment at the beginning of the experiment and in what abundance, but also to distinguish the species present in the biofilm from the others which presumably do not adhere at all and are only present in this sample. After 24, 48, and 72 hours from the immersion, exactly 50, 30, and the remaining 30 slides were recovered from the sea. For each day a separate sample of one, two, and three days old biofilm (B1-B3) was obtained, by thoroughly scraping the formed biofilm from the slides with a sterile razor blade. The scraping was combined with a gentle rinsing of the slides with sterile distilled water. In the end, the fully scraped biofilm from each sample was filtered the same way as the seawater from the S0 sample. Apart from the S0 sample which contained metagenomic DNA from the seawater at the time of submergence, the other three samples (B1-B3) contained DNA from organisms involved in the early phase of biofilm formation at different time points, thus giving an insight into which species were present in which abundance during these phases, but also on development and evolution of the biofilm. To extract genomic DNA from the seawater and biofilm samples, the DNeasy PowerWater Kit (Qiagen, Germany) was used. Samples B1, B2, and B3 consisted of DNA taken from N individual slides that were pooled together. This generated a unique one-value result for each different operational taxonomic unit (OTU) found in separate biofilm samples B1, B2, and B3, acquired from a larger number of individual and independent slides representing a biofilm sample (data pooling).

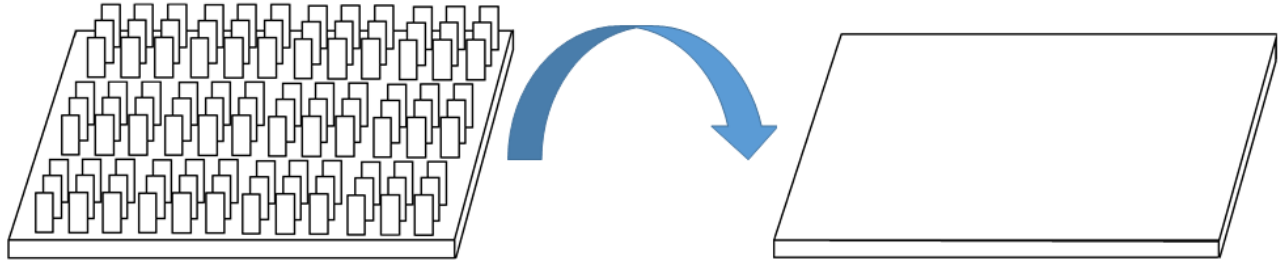


**Figure 10.** Schematic view of the Styrofoam carrier with 110 inserted microscopic slides that were immersed into the sea and used as substrates for biofilm formation.

### 2.2.2. 16S rRNA amplicon sequencing and data accession

Before the DNA samples from seawater and biofilm were sent for analysis, the DNA concentration and quality were analysed using a NanoDrop® Spectrophotometer 1000 (Thermo Scientific, USA). The samples were then sent to Novogene Europe (Cambridge, UK) for NGS sequencing of the microbial 16S rRNA gene, using custom V3-V4 primers. The raw data obtained were merged and quality-filtered to remove reads that did not meet the desired quality. This was done using the QIIME pipeline (version 1.7.0, [http://qiime.org/scripts/split\\_libraries\\_fastq.html](http://qiime.org/scripts/split_libraries_fastq.html) [65]). The sequences that met the desired quality were grouped into operational taxonomic units (OTUs) by clustering with a 97% identity threshold. The OTUs were obtained from the SILVA database [66] and they corresponded to certain and unique species, genera, and other taxonomic levels in the samples. This finally led to obtaining the taxa information and taxa-based relative abundance distribution among the samples. The relative abundance of any OTU was calculated as the number of sequences attributed to a given OTU divided by the total of sequences of all OTUs. The 16S rRNA gene sequences have been deposited in the European Nucleotide Archive (ENA) at EMBL-EBI under project accession number PRJEB48750 as follows: SAMEA10944843 (sample S0), SAMEA10944844 (sample B1), SAMEA10944845 (sample B2), SAMEA10944846 (sample B3).

### 2.2.3. NGS analysis and $\alpha$ - and $\beta$ -diversity calculation

The main objective of the NGS analysis was to observe the NGS results and the relative abundances in the samples in relation to the 16 isolated species from section 2.1. Apart from the species isolated from the biofilm and their preliminary adhesion tendency tests, the idea was to confirm the presence of these species in biofilm samples and compare their relative abundances with those of other species, as well as to analyse how they change as biofilm evolves. With that in mind, it could be estimated

how relevant the isolated species are for biofilm formation and how frequently they occur at different stages of biofilm formation, also knowing that they are cultivable. Additionally, what can be calculated from the relative abundances and examined in terms of relevant species are diversities in a sample or among the samples. The  $\alpha$ -diversity describes the diversity of a single sample and its characteristics, such as richness and evenness, were calculated from the relative abundances of each OTU in a sample ( $p_i$ ) for  $n$  OTUs. Shannon diversity index ( $H$ ) describing richness and Simpson diversity index ( $\lambda$ ) describing evenness were calculated as in [27]:

$$H = - \sum_{i=1}^n p_i \cdot \log_2(p_i) \quad \lambda = 1 - \sum_{i=1}^n p_i^2$$

$\beta$ -diversity, on the other hand, describes the diversities among any of two samples based on a phylogenetic tree generated for those samples, the lengths of branches in the tree, and the abundance of species in the branch (weighted value). For the length of the  $i$ -th branch  $b_i$  among  $n$  branches, the numbers of sequences descending from the  $i$ -th branch in samples A ( $A_i$ ) and B ( $B_i$ ), and the total number of sequences in samples A ( $A_T$ ) and B ( $B_T$ ), the weighted UniFrac value for  $\beta$ -diversity is calculated as in [67]:

$$u = \sum_i^n b_i \cdot \left| \frac{A_i}{A_T} - \frac{B_i}{B_T} \right|$$

Furthermore, the principle coordinate analysis (PCoA) was carried out [67,68]. It maps the distance between objects in distance matrices and displays dissimilarities among objects by finding the characteristics that explain/contain most of the variation between the data sets. The variations between samples are represented on two orthogonal coordinates.

## 2.3. Prediction of metagenome functional potential

Another indicator that could highlight the adhesion potential of bacteria from biofilm samples and the cultured bacteria is the prediction of genes that are crucial for biofilm formation. Using the bioinformatics software package PICRUSt (Phylogenetic Investigation of Communities by Reconstruction of Unobserved States), the functional potential of each sample can be predicted based on the relative abundances of the OTUs contained in the sample (taxonomic profiling) and the genes

annotated in their genomes (functional profiling). Not only is the functional potential of a sample predicted, but it is also assigned to specific OTUs that could potentially exhibit the functions of interest as a result of their gene expression, if they possess these genes. A simple workflow of this algorithm is presented in Figure 11.

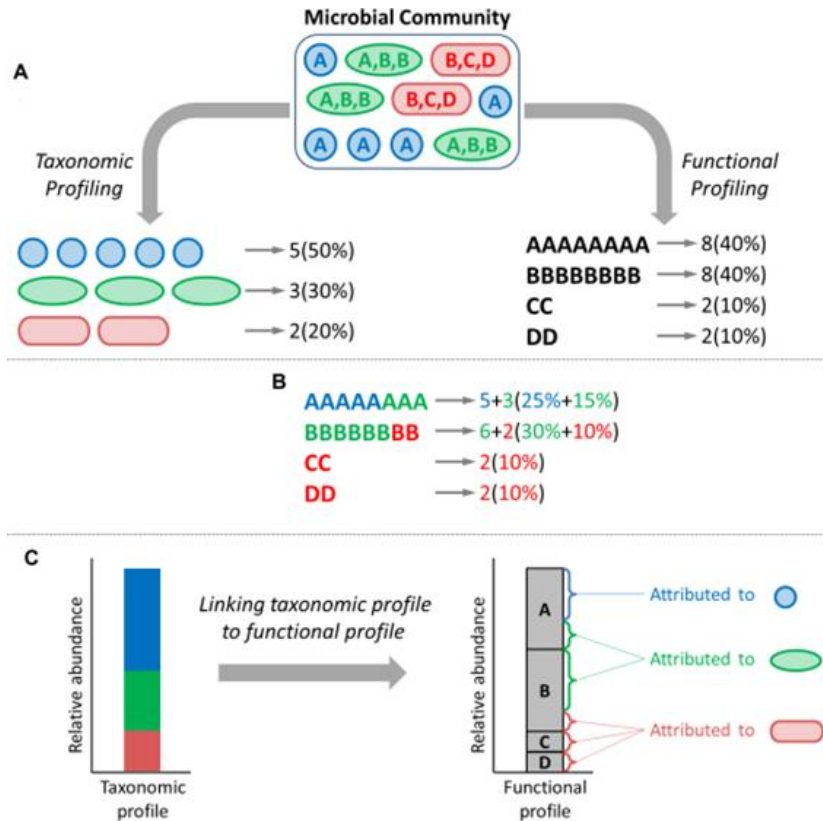


**Figure 11.** A simple workflow of the PICRUSt algorithm [69]. A Taxonomically identified microbial community (taxonomic profile) with its genetic potential (functional profile). B Functional profile represented as shares of each function attributed to each taxon. C The final representation.

During the analysis, PICRUSt normalizes the relative abundance of operational taxonomic units (OTUs) based on their respective 16S rRNA gene copy number. This contributes to a more accurate representation of the true abundance of each taxon in the community, taking into account the inherent variations in gene copy number. The desired OTUs, in this case, the isolated species and those more abundant ones from the samples, or even genera to which they belong, can be observed and compared to see if they contain the genes relevant for biofilm formation. Therefore, the genes involved in cell motility, quorum sensing and translation of surface adhesion proteins are of interest. To predict the involvement of a particular taxon in overall functional potential and metabolic pathways, PICRUSt

uses information from the Kyoto Encyclopedia of Genes and Genomes (KEGG) Orthology (KO) genomic database [32]. The predicted functions can be observed at several hierarchical levels, ranging from L1 to L4, where L4 representation corresponds directly to genes, L3 to molecular functions that require a smaller genetic network, and in the end L1, being the most general and complex functional level. The OTUs can also be observed at different taxonomic levels, ranging from species and genus to class or phylum level.

To perform this analysis, the following was done. The resulting OTU sequence abundance table from NGS was stored in BIOM file format. It was then used to predict functional potential by referring to the KEGG database [32], using the PICRUSt v2.3.0 software package [31]. This generated the functional attribution table for each taxon, thus relating the OTUs with their potential KO functions from the KEGG database. From the functional attribution table, the relative taxon abundance table was created, taking the relative abundances of OTUs into account. In order to convert the representation of data from the OTU/KO view to the taxa/function view, the following actions were taken. OTU-to-taxa lookup table was used to form a table that relates taxons of chosen taxonomic levels to different OTUs. From this table, a specific taxonomic level and selected taxons from the same level were used for further processing. Similarly, to observe specific molecular functions, the KO database was converted into a hierarchical table, from which specific molecular functions (L3) or exact genes of interest (L4) from the same hierarchical level were selected and used in further data processing. With the chosen taxons of the same taxonomic level and molecular functions or genes of interest, desired taxa/function tables were created.

## **2.4. Adhesion dynamics in a bioreactor**

For the following experiments, *Vibrio gigantis* was chosen as a model bacterial organism among the isolated species from a formed marine biofilm. A newly-designed experiment in a bioreactor was set to monitor bacterial adhesion and aggregate formation on a glass substrate and at the chosen time points, during a one-hour and three-hour time interval. From this point on, the Marine Broth (MB) medium used in the experiments (BD Difco) was filtered through a sterile 0.45  $\mu\text{m}$  pore-size syringe filter (Millex- HA, Germany), to ensure the transparency of the medium and improve the visibility of bacteria without affecting bacterial growth.

### **2.4.1. Premeasurements**

The colony forming units (CFU) of viable plate counts of *V. gigante* were determined at  $OD_{600}$  values of 0.2 and 0.4, using a spread plate method. The counted approximate number of bacteria at these OD values was also determined on a McFarland densitometer (Biosan, Latvia) so the initial concentration could be more easily adjusted.

The overnight culture was diluted 1:20 in fresh and filtered MB and incubated for one hour to reach the exponential phase. The exponentially grown culture was adjusted to a density of  $5 \cdot 10^5$  CFU/ml by diluting it appropriately. The growth dynamics of *V. gigante* was then analysed over 24 hours at 28°C. Triplicate absorbance values of a sample and a blank probe were measured at a wavelength of 600 nm using a Synergy HTX multi-mode reader (BioTek, USA).

### **2.4.2. Bioreactor experiment setup**

To quantify the adhesion dynamics at chosen time points, the percentage of substrate surface covered with *V. gigante* was calculated. Eight clean microscopic slides used as a substrate were cleaned three times with 70% ethanol and kimwipes and inserted into the Styrofoam gaps made with a sterile scalpel (Figure 12A). The Styrofoam was also previously cleaned with 70% ethanol. It was all set under ultraviolet light inside a digester before the start of the experiment. A sterile 250 ml volume glass beaker, containing a 2 cm long magnetic stirring bar, was used as a container and put on a magnetic stirrer that enabled the constant bar spin of approximately 3-4 rps, to prevent the settling of bacteria. A filtered MB overnight culture of *V. gigante* was prepared at room temperature. 15 ml of culture was diluted with 200 ml of fresh MB, incubated for one hour until density reached 0.5 McFarland units (McF), and then poured into a glass container. The Styrofoam was then flipped and the slides were partially immersed into the broth (Figure 12B), which determined the start of the experiment. At the first time point, a randomly selected slide was gently removed from the container. The removed slide was then slowly dipped in sterile distilled water and gently moved around for approximately 10 seconds to remove bacteria that did not sufficiently attach to the surface. The slide was then dried on a burner to fix the attached cells and stained with 1:5 diluted carbol fuchsin (Fluka, Switzerland) for two minutes, to achieve a better contrast for the latter imaging. This in the only experiment configuration where carbol fuchsin was used. After staining, the slide was slowly immersed in sterile distilled water again, to remove the stain excess and dried in the same manner as before. The remaining

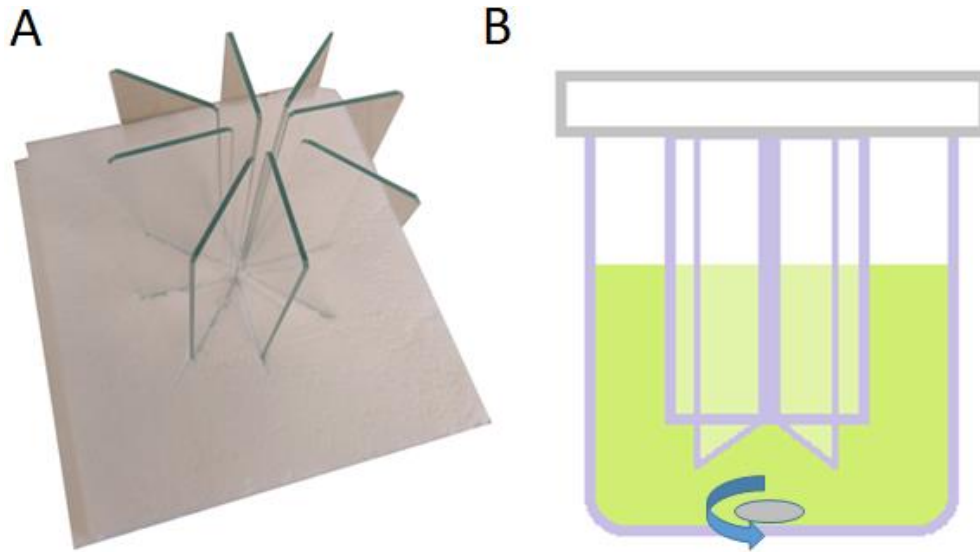


**Figure 12.** A) Styrofoam carrier with 8 microscopic slides used as substrates. B) A simple schematic view of a bioreactor, with the slides being partially immersed into the broth.

slides were taken out at different time points, in clockwise order and were processed identically. After all the slides were processed, they were ready for imaging. The experiment was repeated three times.

### 2.4.3. Image analysis

After the slides with the attached bacteria were collected and processed, each slide was examined on an upright microscope in brightfield microscopy mode (Zeiss Axio-imager M1 microscope) with a high-resolution camera (Carl Zeiss Axio-Cam MR Rev3) using Axio Vision Rel. 4.7 software (Zeiss, Austria). To ensure a justified surface analysis, the identical regions of interest were examined for each slide (Figure 13). During the first measurements, the images were taken with a 40× magnification objective, but when compared with the images from a 10× magnification objective, the results were almost identical, so the latter was used further on, allowing more surface area to be analysed. After obtaining 10 images for each region of interest (Figure 13), 30 images for each slide were selected as the representative ones and processed in ImageJ software [70]. A total of 240 images were imported and subjected to a threshold procedure, identical for each image. After the binarized images were obtained that way (Figure 14), the “analyze particles” option was performed. This resulted in a calculated percentage of the covered surface for each image, which was taken as a measure of the adhesion rate. The average percentage of the 30 representative images was taken for each slide or time



point. Furthermore, the aggregate size distribution was also analysed, as the average number of various-size aggregates in time, by limiting the surfaces taken into account.

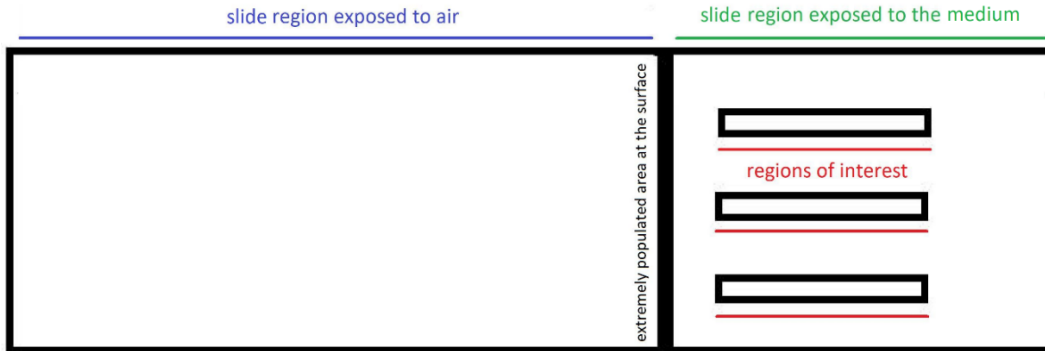


**Figure 13.** A slide was partially immersed into the bacterial sample (medium). Three examined regions of interest are shown (10 images for each region), resulting in a total of 30 images per slide. The average percentage of surface coverage from 30 representing images was taken for each slide. At the border of the medium and air, an extremely populated area was noticed. The slide dimensions were 75x25 mm.

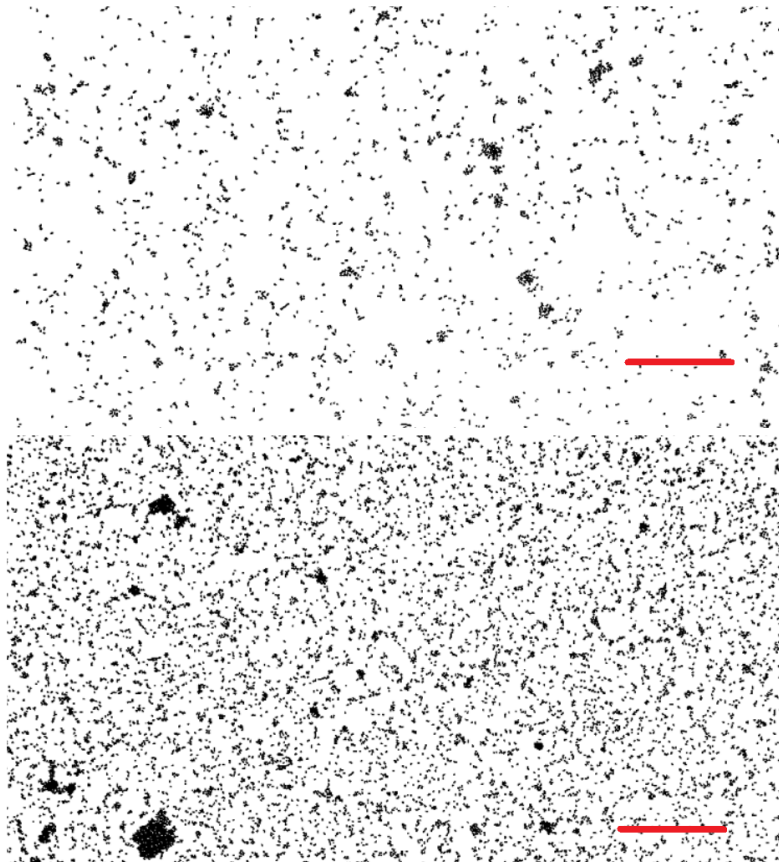


**Figure 14.** An example of two random fragments of images at the earlier (upper, coverage percentage 3.8%) and later phase (lower, coverage percentage 11.7%) of the experiment after binarization. High contrast was achieved using the carbol fuchsin, enhancing the visualization of bacteria. The red scale bar represents 100  $\mu\text{m}$ .

[Redacted]

[Redacted]

[Redacted]

[Redacted]

[Redacted]

[Redacted]

[Redacted]

[Redacted]

[Redacted]

[Redacted]

[Redacted]

[Redacted]

[Redacted]

[Redacted]

[Redacted]

[Redacted]

[Redacted]

[Redacted]

[Redacted]

[Redacted]

[Redacted]

[Redacted]

[Redacted]

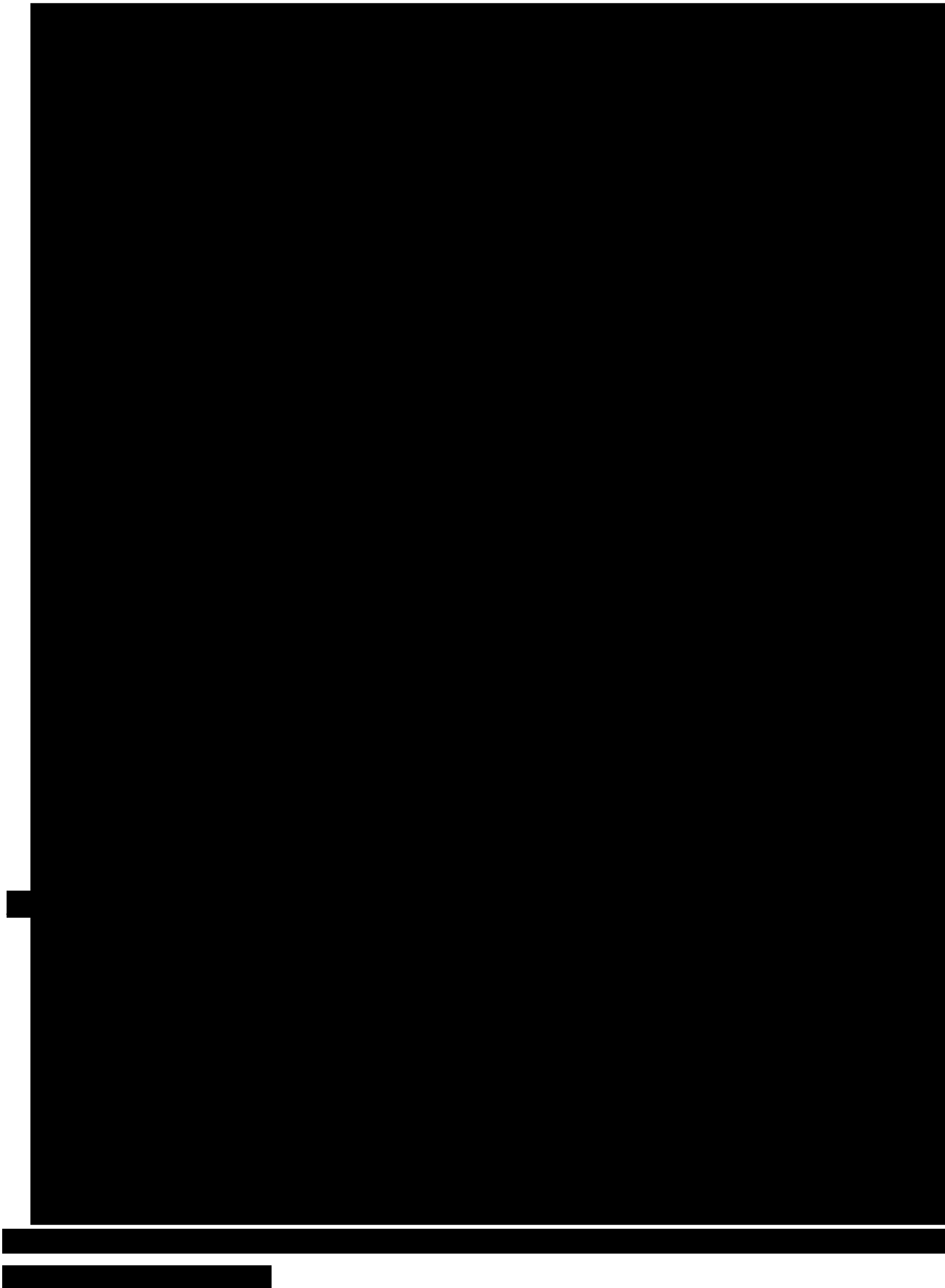
[Redacted]

[Redacted]

[Redacted]

[Redacted]

[Redacted]



[Redacted]

[Redacted]

[REDACTED]

[REDACTED]

[REDACTED]

[Redacted text block]

[Redacted text block]

[Redacted text line]

[Redacted text block]

[Redacted]

[Redacted]

[Redacted]

[Redacted]

[Redacted]

[Redacted]

[Redacted]

[Redacted]

[Redacted]

[Redacted]

[Redacted]

[Redacted]

[Redacted]

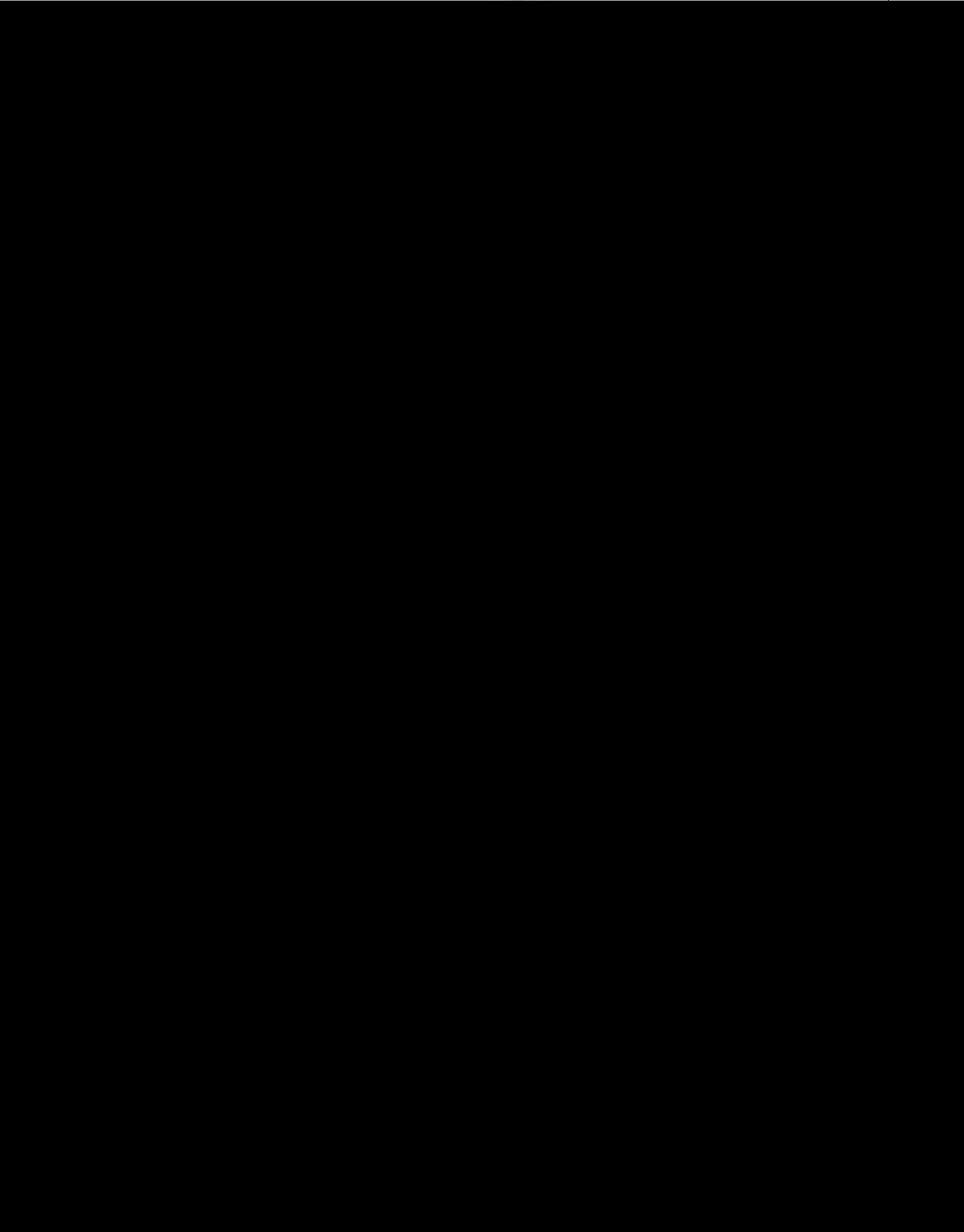
[Redacted]

[Redacted]

[Redacted text block]

[Redacted text block]

[Redacted text block]



[Redacted line of text]

[Redacted line of text]



[REDACTED]

[REDACTED]

[REDACTED]

[REDACTED]

[REDACTED]

[Redacted text block]

[Redacted text block]

[Redacted text block]

[Redacted text block]

[Redacted text block 1]

[Redacted text block 2]

[Redacted]

[Redacted]

[Redacted]

[Redacted]

[Redacted]

[Redacted]

[Redacted]

[Redacted]

[Redacted]

[Redacted]

[Redacted]

[Redacted]

[Redacted]

[REDACTED]

[REDACTED]

[REDACTED]

[Redacted]

[Redacted]

[Redacted]

[Redacted]

[Redacted]

[REDACTED]

[REDACTED]

[REDACTED]

[Redacted text block]

[Redacted text block]

[Redacted text block]

[Redacted text block]

[Redacted text block]

[Redacted text block]



[Redacted text block]

[Redacted text block]

[Redacted text block]

[Redacted text block]

[Redacted text block]

[Redacted text block]

[Redacted text block]

[Redacted text block]

[Redacted text block]

[Redacted text block]

[Redacted text block]

[Redacted text block]

[Redacted text block]

[Redacted text block]

[Redacted text block]

[Redacted text block]

[REDACTED]

[REDACTED]

[REDACTED]

[REDACTED]

[REDACTED]

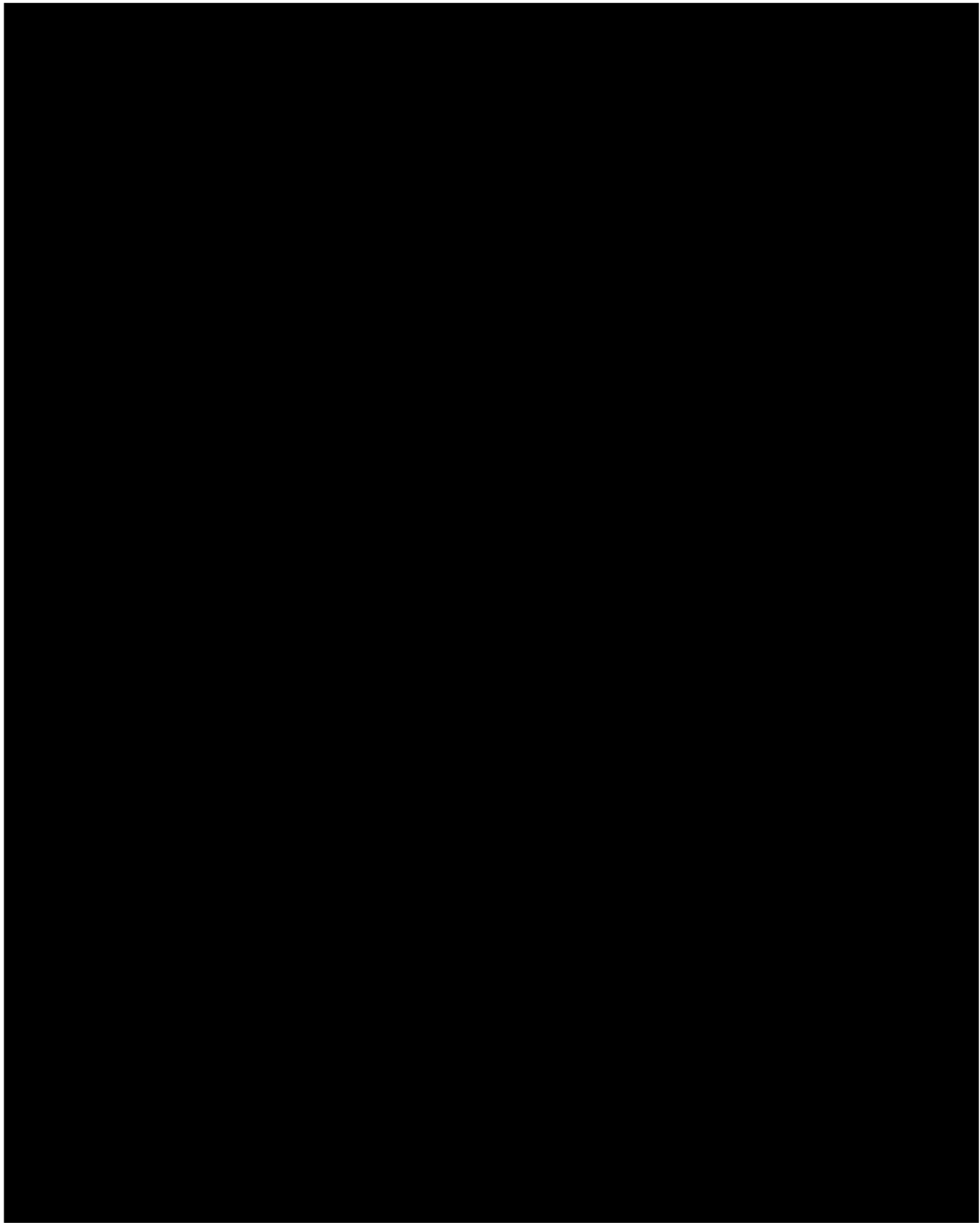
[REDACTED]

[REDACTED]

[REDACTED]

[REDACTED]

[REDACTED]



## 3. Results and Discussion

### 3.1. Choosing the bacterial model species

#### 3.1.1. Isolation and identification of biofilm-forming species

To identify the pioneer biofilm-forming species, the microscopic slides were exposed to the marine environment for three days. At the moment of extraction, one of the slides was examined under a microscope to qualitatively describe the condition and characteristics of a developed biofilm. The presence of differently-shaped bacterial cells was noted (Figure 30ABC), but also more complex communities, probably consisting of several species (Figure 30BC), and diatoms as representatives of eukaryotic cells (Figure 30AC). A variety of bacterial species involved in the early phase of biofilm development was found, as well as species participating in the latter phases, when more complex structures were formed.

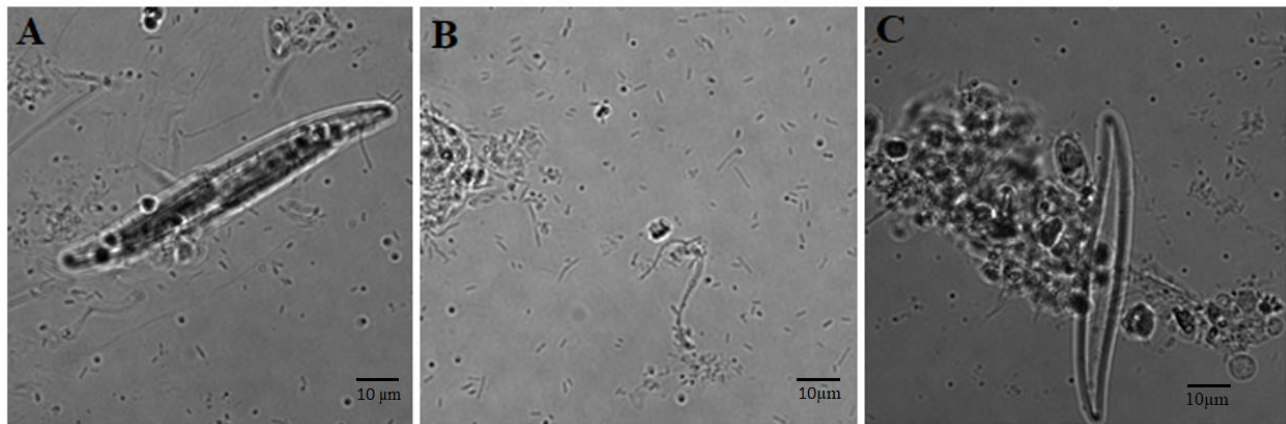


**Figure 30.** Common pioneer species that form a biofilm in the marine environment within three days.

The remaining slides were aseptically scraped, and the biofilm samples were then subjected to serial dilution, with aliquots from different dilutions plated onto solid agar media. The resulting plates had varying colony densities (see Figure 31), and a dilution that had approximately 30 well-isolated colonies was selected for further study. Subsequently, colonies with discrete growth and non-overlapping morphology were subcultured individually on fresh agar plates to obtain pure monocultures. After isolation of 16 monocultures, morphological examination by visual inspection

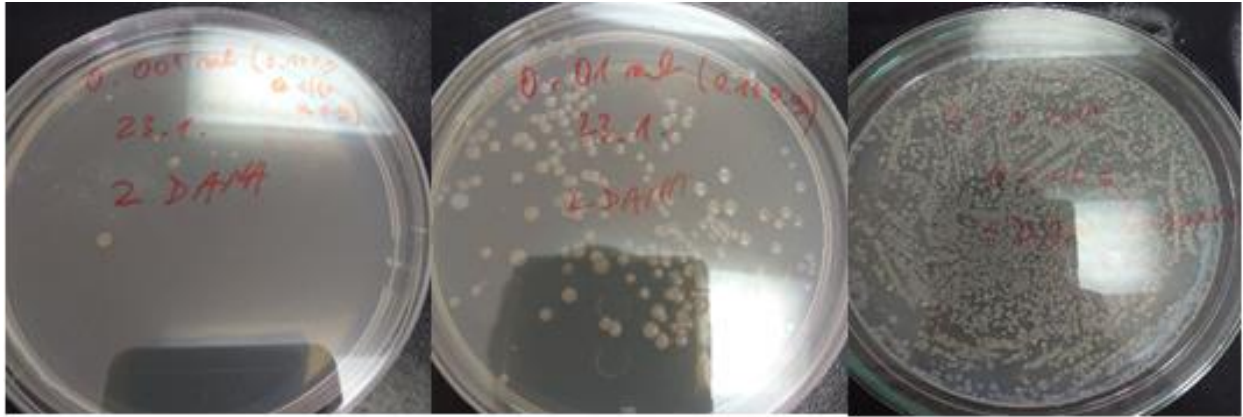


**Figure 31.** The scraped biofilm was serially diluted to facilitate subcultivation with the aim of isolating pure bacterial cultures at the optimal conditions. The plates had a diameter of 10 cm.

ensured that there were no discernible differences between the individual bacteria within each isolate, indicating phenotypic uniformity (see Figure 32).

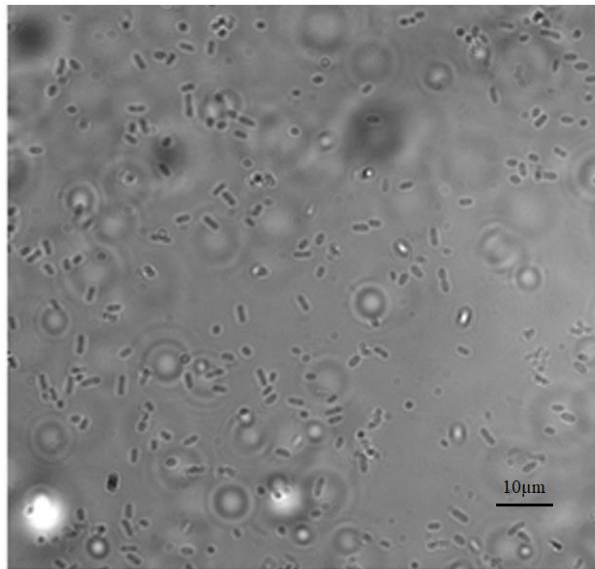


**Figure 32.** Morphological and morphotypic evaluation of the bacterial isolate 1.

These isolates were sent for the 16S rRNA paired-end sequencing (Table 1A). Most species were taxonomically identified as the species from genera *Vibrio* and *Pseudoalteromonas*. The reason why the species came from almost exclusively two different genera may be that not all bacteria can be cultivated on the marine agar plates. The isolate number 1 was confirmed as *Vibrio gigantis*, which was of particular interest due to its high adhesion tendency (see next subsection). The sequencing was repeated twice for the isolate number 1 (Table 1B).



Query					Identities		
Name	Gene	Length	Start	End	Match	Total	Pct.(%)
1F	Halomonas sp. SK18 16S ribosomal RNA gene, partial sequence	1433	1	36	35	36	97
1R	Vibrio gigantis strain S-44 16S ribosomal RNA gene, partial sequence	1456	1450	829	534	627	85
2F	Pseudoalteromonas sp. strain 70365 16S ribosomal RNA gene, partial sequence	1427	10	274	238	265	90
2R	Pseudoalteromonas sp. strain 70320 16S ribosomal RNA gene, partial sequence	1429	1429	776	641	657	98
3F	Epicoccum nigrum, ribosomal RNA gene and internal transcribed spacer 2	816	1	815	797	828	96
3R	Bacterium QM35 16S ribosomal RNA gene, partial sequence	1427	1424	568	792	861	92
4F	Vibrio sp. P1S6 16S ribosomal RNA gene, partial sequence	1453	4	822	805	821	98
4R	Vibrio gigantis strain PJ-21 16S ribosomal RNA gene, partial sequence	1456	1451	239	1199	1213	99
5F	Pseudomonas sp. O-NR7 16S ribosomal RNA gene, partial sequence	1416	2	35	33	34	97
5R	Microbacterium phyllosphaerae strain QT8 16S ribosomal RNA gene, partial sequence	1491	1450	1107	260	350	74
6F	Vibrio sp. 57S-9 16S ribosomal RNA gene, partial sequence	933	2	858	835	860	97
6R	Vibrio sp. An91 partial 16S rRNA gene, isolate An91	1462	1450	162	1243	1294	96
7F	Pseudoalteromonas marina strain D5053 16S ribosomal RNA gene, partial sequence	1012	8	787	756	784	96
7R	Pseudoalteromonas sp. NBRC 101701 gene for 16S rRNA, partial sequence	1461	1448	274	1149	1175	98
8F	-	-	-	-	-	-	-
8R	Pseudoalteromonas sp. 29 16S ribosomal RNA gene, partial sequence	1419	1411	298	1065	1130	94
9F	Vibrio sp. H1309/3.3 partial 16S rRNA gene, isolate H1309/3.3	1465	2	285	270	287	94
9R	Uncultured bacterium clone Woods-Hole_a1941 16S ribosomal RNA gene, partial sequence	1513	1491	536	927	961	96
10F	Bacillus sp. enrichment culture clone DWSRK116 16S ribosomal RNA gene, partial sequence	963	268	299	31	32	97
10R	Microbacterium ginsengisoli strain HKS03 16S ribosomal RNA gene, partial sequence	1440	1420	682	623	762	82
11F	Uncultured bacterium clone YD100-50 16S ribosomal RNA gene, partial sequence	1513	29	913	863	888	97
11R	Uncultured bacterium clone SanDiego_a2785 16S ribosomal RNA gene, partial sequence	1513	1481	265	1205	1217	99
12F	Pseudoalteromonas marina strain I 17 16S ribosomal RNA gene, partial sequence	1503	21	893	834	877	95
12R	Uncultured bacterium clone T8 16S ribosomal RNA gene, partial sequence	1497	1468	186	1239	1290	96
13F	Uncultured bacterium clone T8 16S ribosomal RNA gene, partial sequence	1497	30	1173	1091	1148	95
13R	Uncultured Pseudoalteromonas sp. clone K4S72 16S ribosomal RNA gene, partial sequence	1497	1467	319	1123	1150	98
14F	Staphylococcus pasteurii strain HN-35 16S ribosomal RNA gene, partial sequence	1460	3	623	576	625	92
14R	Staphylococcus warneri partial 16S rRNA gene, isolate OCAT13	1116	1075	117	773	982	79
15F	Bacterium strain NBTE-T4 16S ribosomal RNA gene, partial sequence	1425	4	949	919	947	97
15R	Pseudoalteromonas undina strain RA4 16S ribosomal RNA gene, partial sequence	1360	1360	70	1268	1292	98
16F	Pseudoalteromonas marina partial 16S rRNA gene, isolate M7	1416	16	736	698	723	97
16R	Pseudoalteromonas sp. SBS2-1 16S ribosomal RNA gene, partial sequence	1461	1451	166	1257	1293	97

**Table 1A.** Taxonomic identification of 16 isolates from 16S rRNA paired-end sequencing. Length denoted the size of a sequence that was sequenced, with the position of a Start and End base. Match was the number of identical bases between the reference 16S rRNA sequence and the sequenced fragment, while the Total number was the number of bases of the fragment.

Query					Identities		
Name	Gene	Length	Start	End	Match	Total	Pct.(%)
1(1)F	Vibrio sp. VibC-Oc-039 16S ribosomal RNA gene, partial sequence	1469	29	1219	1141	1198	95
1(1)R	Vibrio gigantis partial 16S rRNA gene, isolate LPD 1-1-47	1463	1439	106	1304	1334	98
1(2)F	Vibrio sp. VibC-Oc-057 16S ribosomal RNA gene, partial sequence	1478	31	1056	1004	1030	97
1(2)R	Vibrio gigantis strain S-32 16S ribosomal RNA gene, partial sequence	1455	1449	278	1139	1173	97

**Table 1B.** The taxonomic identification of isolate 1 gave compatible results for forward and reverse sequencing of the two technical replicates, also with a large amplified fragment and a high percentage of concordance.

To this point, 16 pioneer biofilm-forming and cultivable isolates were selected, among which the majority were taxonomically identified to a species or genus level.

### 3.1.2. Preliminary adhesion tendency tests

Each of the bacterial isolates was tested individually for its adhesion tendency by placing 20-hour-old bacterial overnight culture in a simply designed microchannel with a microscopic coverslip as a substrate. The idea was to check whether and at which rate a certain species adhered in the

microchannel without a flow, which was expected since they were found in the biofilm samples. In Figure 33, the surface condition at two different moments is shown for *Vibrio gigantis* (isolate 1), presenting the evolution of the adhesion process.

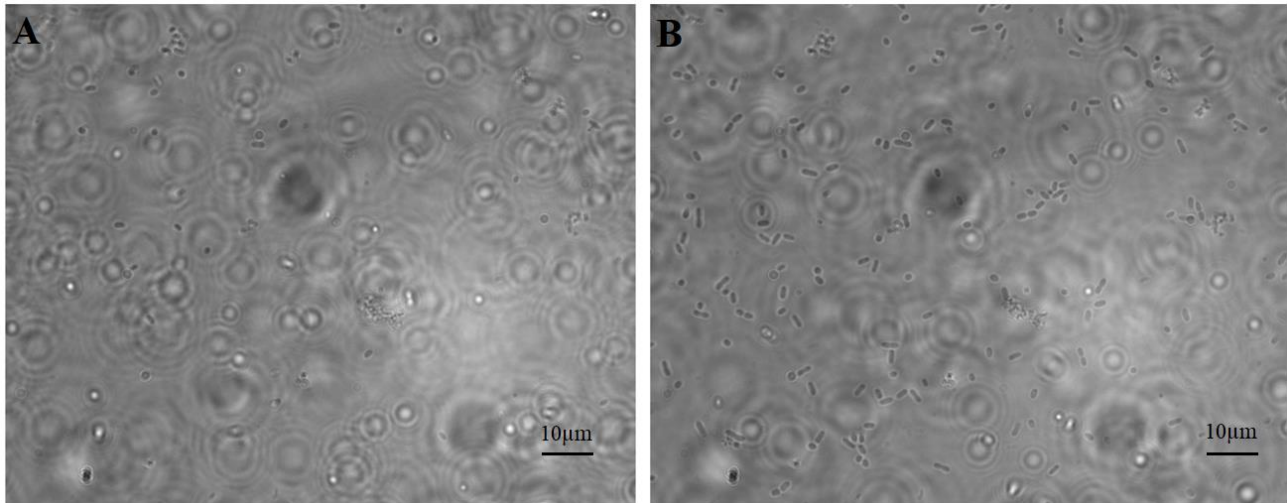


**Figure 33.** The surface of the microchannel with the adhering *V. gigantis* bacteria at the initial (A) and the latter phase (B), after around 20 minutes.

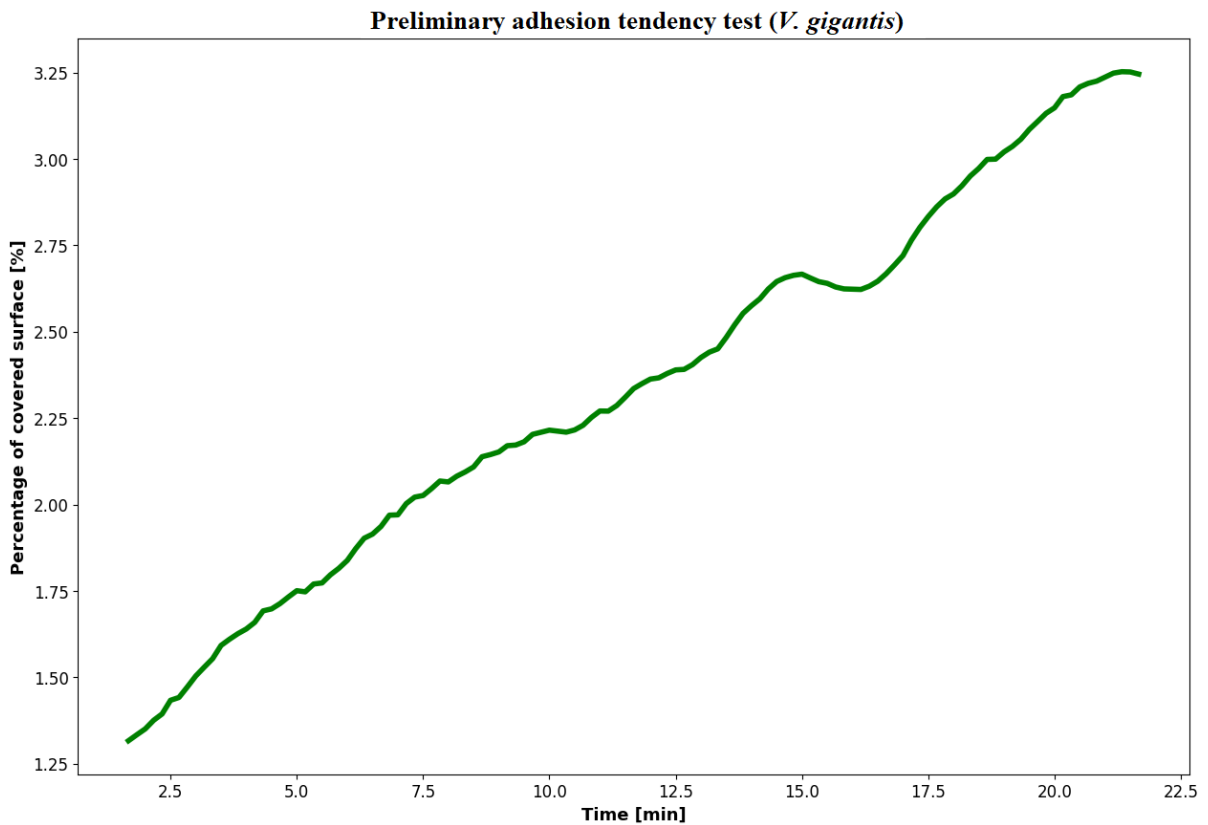


**Figure 34.** Percentage of covered surface as a measure of adhesion of *V. gigantis*.

Adhesion was measured as the percentage of substrate covered by bacteria and its evolution over a 20-minute period is shown in Figure 34.

Other isolates were also tested, but the progress of their adhesion as an essential and obligatory feature was not as rapid and effective as in *V. gigantis*, making them less desirable as biofilm-forming model species. Since *V. gigantis* was one of the few isolates that were taxonomically identified at the species level after the isolation and also preliminarily showed a strong and promising adhesion tendency, it was decided to proceed with this species as the model organism for future experiments. Also, the results of the following two sections were in favour of doing so.

The transition from a free-swimming to a surface-attached state of *V. gigantis* was recorded ([Pre-video](#) in the Appendix). Together with a high motion activity and fast swimming, its surface motility modes such as twitching, crawling, pivoting, rotating, and detachment after division were seen ([Pre-video](#)), all being standard bacterial behaviour in the early stages of surface adhesion [34-36]. The swimming individuals were recorded moving at the rate of 50 to even 120  $\mu\text{m s}^{-1}$  in accordance with what was reported [57].

## 3.2. NGS (Next generation sequencing) analysis

### 3.2.1. Sequencing depth

The DNA material from the biofilm samples was collected as described in the “Methods” section (Figure 35), as was that from the seawater sample. After the sequences were obtained, quality-filtered, and grouped into OTUs, a rarefaction measure was done to determine whether the samples were sequenced to the depth sufficient to represent their real diversity. In other words, it measured how the number of newly observed OTUs changed by increasing the number of examined sequences in a sample. After the plateau was reached for each sample, it could be said that the sample was sequenced deep enough and all the relevant OTUs were found (Figure 35). Increasing the number of the remaining examined sequences would produce only a few more unique OTUs (those with only one sequence found). The number of species observed was the highest in the seawater sample, indicating a higher diversity of species. It decreased with the development of the biofilm, especially on the third day of the biofilm, when certain species were found more frequently and were predominant.

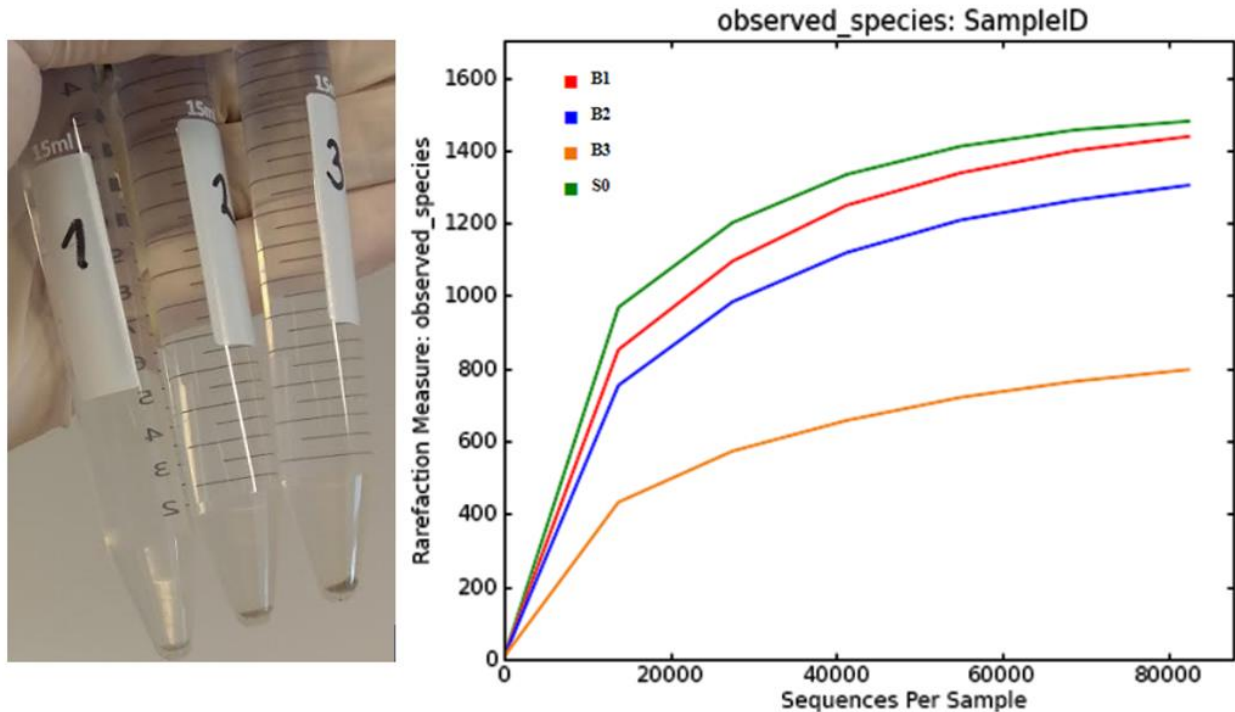


**Figure 35.** Genomic DNA extracted from biofilm samples reached rarefaction saturation, as shown by the observed species plateau, indicating sufficient sequencing depth.

Not all of the sequences organized in Operational Taxonomic Units (OTUs) could be taxonomically identified to species level. This limitation may be due to technical inaccuracies or, more importantly, to the incomplete annotation of all marine species genomes, leading to the recognition of new and unique species. As a result, certain sequences could not be associated with certain OTUs at the species level with certainty and were instead summarized at higher taxonomic levels, mainly at the genus or family level (see Figure 36). The exact enumeration of sequences at different taxonomic levels per sample is also recognizable. In particular, the predominance of sequences belonging to OTUs at the genus level indicates possible limitations in the current SILVA database, although it is regularly updated [66]. After genus-level OTUs, species-level OTUs were the most frequent in all samples, followed by a comparable frequency of family-level OTUs. In contrast, OTUs at higher taxonomic levels were less frequent or only insignificantly represented (see Figure 36).

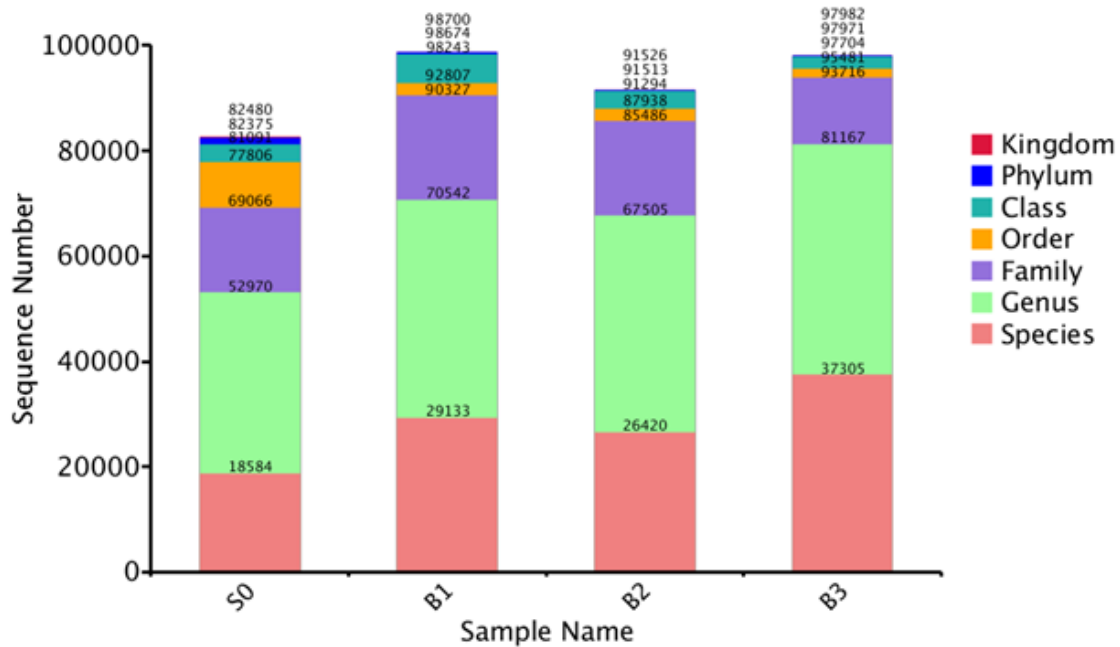


**Figure 36.** Taxonomic depth of OTUs per sample, with the exact number of sequences at each taxonomic level. The top number represents a total number of sequences in samples, which is 82480, 98700, 91526, 97982 in order of appearance.

### 3.2.2. Relative abundances analysis

After each read sequence was grouped into OTUs, relative abundances for each OTU could easily be calculated by dividing the absolute count of read sequences of any OTU in the sample by the total number of read sequences of the same sample, thus describing the composition of biofilm and seawater samples. Among more than 2000 OTUs and around 220 OTUs at the species level, a few dozen stood out as more frequent and with higher relative abundances (Table 2). The relative abundance of *V. giganteus* in biofilm samples confirmed its adhesion effectiveness to the immersed surface. From the calculated relative abundance of only 0.73% in the seawater sample, it grew to a huge 11.83% in the first-day sample of the biofilm, meaning that more than every tenth read sequence came from the *V. giganteus* species. In the following samples (2-day and 3-day biofilm samples) it gradually decreased, to 3.76% and 0.96% respectively. This was the indicator that this species probably had an important role in the early phase of biofilm development, taken over by some other species during the following days, such as *Gamma proteobacterium\_UDC305* (10.59% in B2 and 19.75% in B3), *Thalassotalea eurytherma* (6.53% in B2, 8.19% in B3), and *Bacterium\_RFB\_D08* (5.05% in B3).

Taxonomy	Relative abundance [%]			
	S0	B1	B2	B3
gamma_proteobacterium_UDC305	0.4110	2.6322	10.5880	19.7454
<b>Vibrio_gigantis</b>	<b>0.7347</b>	<b>11.8295</b>	<b>3.7645</b>	<b>0.9590</b>
Thalassotalea_eurytherma	0.2461	2.3521	6.5398	8.1911
Vibrio_sp._EJY3	5.1916	4.9248	0.9057	0.3019
bacterium_RFB_D08	0.0436	0.3298	1.1191	5.0521
Dinophysis_acuminata	4.0470	0.0861	0.0327	0.0315
Gammaproteobacteria_bacterium_Q1	0.0909	2.4151	0.9239	0.3565
Phalacroma_mitra	1.3543	0.0170	0.0061	0.0000
alpha_proteobacterium_HIMB59	1.2488	0.0327	0.0109	0.0048
Arcobacter_nitrofigilis	0.7602	0.4898	0.4753	0.2546
Thalassomonas_sp._Ma5	0.0182	0.1600	0.4583	0.7287
Photobacterium_phosphoreum	0.6971	0.0800	0.0449	0.0073
Thalassotalea_agariperforans	0.0145	0.1164	0.4013	0.6668
Alteromonadaceae_bacterium_HSML-FTL-9e	0.0703	0.5723	0.3540	0.2922
Photobacterium_ganghwense	0.4146	0.5007	0.3589	0.2049
Serratia_marcescens	0.2376	0.3577	0.4656	0.1225
Thalassotalea_agarivorans	0.0206	0.1479	0.2958	0.3528
Aliivibrio_fischeri	0.1588	0.2255	0.0594	0.0170
Escherichia_coli	0.0727	0.2037	0.2025	0.0461
Saccharophagus_sp._MM1-2b	0.0121	0.1588	0.1382	0.0558
Pseudoalteromonas_sp._8040	0.0048	0.1467	0.1091	0.0170
Dokdonia_genika	0.0048	0.0194	0.1164	0.1103
Tenacibaculum_dicentrarchi	0.0570	0.0776	0.0170	0.0048
Lewinella_agarilytica	0.0109	0.0170	0.0267	0.0497
Staphylococcus_epidermidis	0.0206	0.0485	0.0170	0.0048
Paramoritella_sediminis	0.0412	0.0424	0.0073	0.0024

**Table 2.** Relative abundances of most frequent species in seawater (S0) and biofilm (B1, B2, B3) samples.

There are two possible explanations for the decrease in the relative abundance of *V. gigantis*. The first one is that after active adhering during the early phase of biofilm formation on the first day, it simply began leaving the biofilm during the following days. The other possibility was that its absolute abundance (real number) remained unchanged, while the absolute abundances of other species or genera increased substantially, causing its relative abundance to decrease. Since *V. gigantis* had the highest relative abundance among all species in the initial phase of biofilm evolution (Figure 37), it is definitely a very desirable model species for the study of adhesion dynamics.



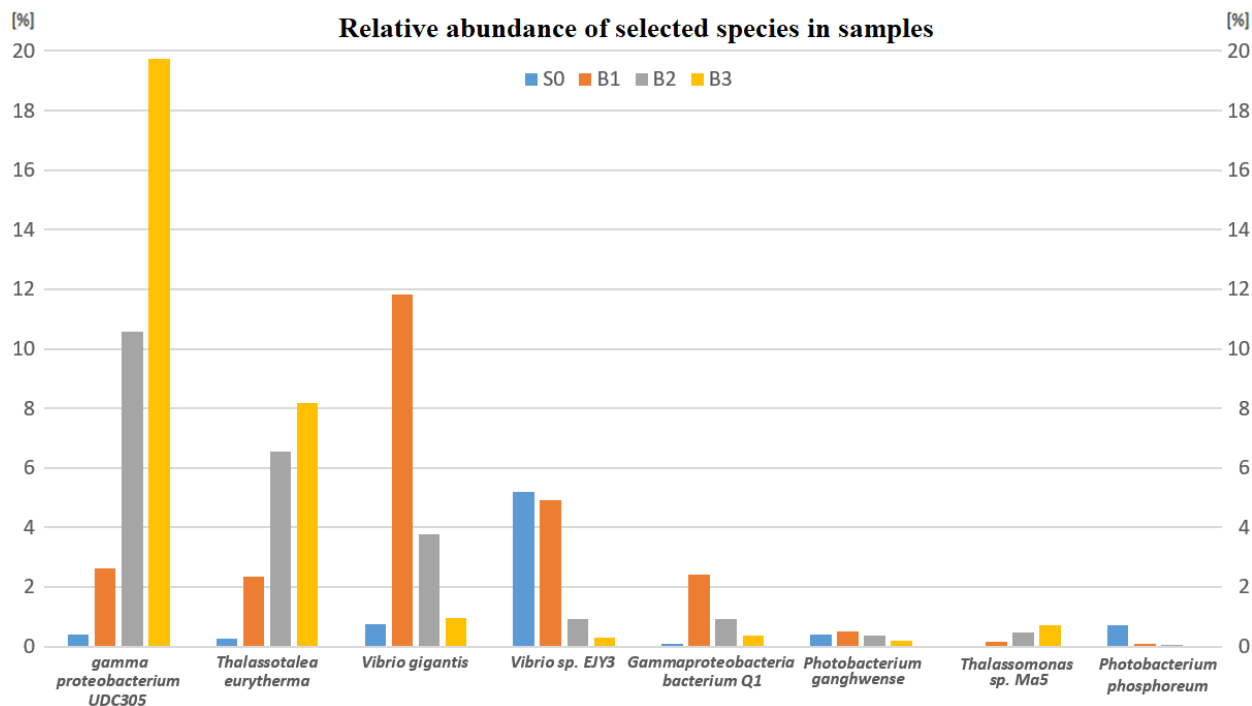


**Figure 37.** Relative abundance of pioneer bacterial species in seawater (S0) and during the first three days of biofilm formation on the surface of immersed slides (B1, B2 and B3).

Also of interest is *Dinophysis acuminata*, a eukaryotic planktonic species, which was much more abundant in the seawater sample with a relative abundance of 4%, while its relative abundance in the biofilm samples fell far below 0.1%, probably due to insufficient development of the biofilm at that time, as more complex organisms attach later. Taking a look at the genus taxonomic level, the *Vibrio* genus was one of the most dominant with a relative abundance of 7.33% in the seawater sample, 20.68% in B1, and 6.03% in the B2 sample (Table 3). To a certain extent, it followed the trend of *V. gigantis* but not entirely. Other mostly occurring genera were *Thalassotalea* (19.44% in B2 and 29.73% in B3), *Colwellia* (10.99% in B2 and 20.38% in B3), *Loktanella* (9.46% in B3), and *Agarivorans* (6.42% in B1 and 8.68% in B2 sample) (Table 3). Moreover, at the phylum taxonomic level, mostly *Proteobacteria*, *Cyanobacteria*, and *Bacteroidetes* were found (Supplementary Figure 1 in the Appendix), which were globally shown to be the most frequent phyla [21, 22, 24, 25].

Taxonomy	Relative abundance [%]			
	S0	B1	B2	B3
Thalassotalea	0.7675	8.4918	19.4399	29.7345
<b>Vibrio</b>	<b>7.3363</b>	<b>20.6826</b>	<b>6.0306</b>	<b>1.5701</b>
Colwellia	0.4450	2.7886	10.9930	20.3831
Loktanella	0.3383	0.6462	2.9413	9.4690
Agarivorans	0.2340	6.4197	8.6833	3.7452
Pseudoalteromonas	0.3892	6.9096	4.6229	0.9796
Psychrosphaera	0.1200	2.8819	2.1799	1.1760
Asciaceihabitans	2.8067	0.4765	0.8135	0.4910
Psychrobium	0.0558	0.7335	2.0466	1.3785
Photobacterium	1.6671	0.7347	0.4559	0.2291
Arcobacter	1.5422	1.1809	0.9736	0.5092
Glaciecola	1.4149	0.0812	0.0897	0.0849
Marinobacterium	0.3237	1.1773	0.5335	0.2049
Reinekea	0.1212	1.0997	0.5553	0.3310
Octadecabacter	0.1018	0.1188	0.4001	1.0621
Pseudohongiella	0.8887	0.0800	0.0449	0.0206
Propionigenium	0.6280	0.8075	0.2170	0.1855
Candidatus_Actinomarina	0.6996	0.0121	0.0133	0.0000

**Table 3.** Relative abundances of most frequent genera in seawater (S0) and biofilm (B1, B2, B3) samples.

Apart from *V. giganteis*, the only other identified species of the *Vibrio* genera was *Vibrio sp. EJY3*. Its relative abundance had a value of around 5%, both for the seawater sample S0 and the B1 biofilm sample, which was quite different behaviour when compared to *V. giganteis*. In the other samples, it dropped quite similarly as to the relative abundance of *V. giganteis*. In Figure 38 the relative abundances for the most dominant genera are shown together with those of *V. giganteis* and *V. sp. EJY3*, which are compared next to each other and shown as a subset of genus *Vibrio*. Here the trend of the presence of *Vibrio* species is clearly in favour of *V. giganteis*, also when it is compared to the whole genus *Vibrio*. When summing up the relative abundances of the two species mentioned (see Figure 38), the cumulative proportion still does not match the relative abundance attributed to the genus *Vibrio*. This discrepancy results from the presence of additional *Operational Taxonomic Units* (OTUs) associated with the genus *Vibrio* that could not be confidently identified to species level despite sequence similarity at the 16S level, as they show considerable sequence dissimilarity with annotated *Vibrio* species in the database. Specifically, 19 different *Vibrio* species were identified in these samples.

With the exception of *Vibrio sp. EJY3* (OTU7) and *Vibrio giganteis* (OTU 11), the remaining *Vibrio* species were assigned specific OTUs without further identification at the species level (see Table 4).



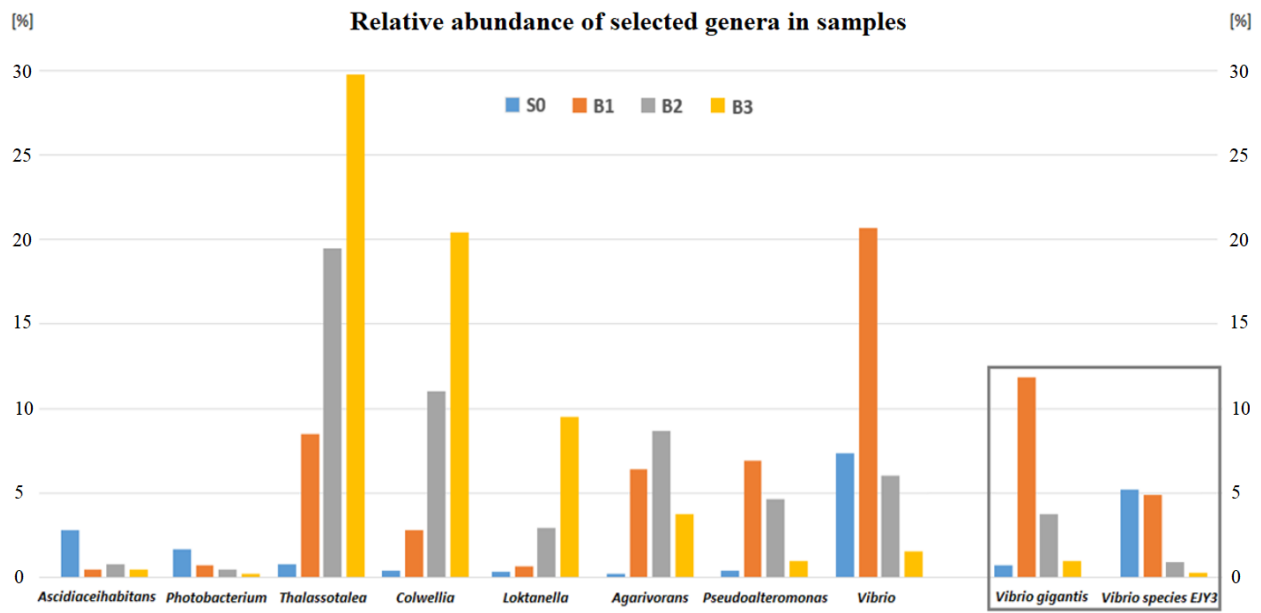


**Figure 38.** Genera with the highest relative abundances among the samples. The exceptions are the two framed species, shown as a subset of the genus *Vibrio*.

The observed sequence variations between these *Vibrio* OTUs were substantial enough to justify their classification as distinct OTUs (Table 4), implying their taxonomic differentiation.

	Tax_detail
OTU_7	k_Bacteria;p_Proteobacteria;c_Gammaproteobacteria;o_Vibrionales;f_Vibrionaceae;g_Vibrio; s_Vibrio_sp._EJY3
<b>OTU_11</b>	<b>k_Bacteria;p_Proteobacteria;c_Gammaproteobacteria;o_Vibrionales;f_Vibrionaceae;g_Vibrio; s_Vibrio_gigantis</b>
OTU_32	k_Bacteria;p_Proteobacteria;c_Gammaproteobacteria;o_Vibrionales;f_Vibrionaceae;g_Vibrio
OTU_121	k_Bacteria;p_Proteobacteria;c_Gammaproteobacteria;o_Vibrionales;f_Vibrionaceae;g_Vibrio
OTU_143	k_Bacteria;p_Proteobacteria;c_Gammaproteobacteria;o_Vibrionales;f_Vibrionaceae;g_Vibrio
OTU_210	k_Bacteria;p_Proteobacteria;c_Gammaproteobacteria;o_Vibrionales;f_Vibrionaceae;g_Vibrio
OTU_247	k_Bacteria;p_Proteobacteria;c_Gammaproteobacteria;o_Vibrionales;f_Vibrionaceae;g_Vibrio
OTU_367	k_Bacteria;p_Proteobacteria;c_Gammaproteobacteria;o_Vibrionales;f_Vibrionaceae;g_Vibrio
OTU_586	k_Bacteria;p_Proteobacteria;c_Gammaproteobacteria;o_Vibrionales;f_Vibrionaceae;g_Vibrio
OTU_618	k_Bacteria;p_Proteobacteria;c_Gammaproteobacteria;o_Vibrionales;f_Vibrionaceae;g_Vibrio
OTU_752	k_Bacteria;p_Proteobacteria;c_Gammaproteobacteria;o_Vibrionales;f_Vibrionaceae;g_Vibrio
OTU_765	k_Bacteria;p_Proteobacteria;c_Gammaproteobacteria;o_Vibrionales;f_Vibrionaceae;g_Vibrio
OTU_1042	k_Bacteria;p_Proteobacteria;c_Gammaproteobacteria;o_Vibrionales;f_Vibrionaceae;g_Vibrio
OTU_1268	k_Bacteria;p_Proteobacteria;c_Gammaproteobacteria;o_Vibrionales;f_Vibrionaceae;g_Vibrio
OTU_1443	k_Bacteria;p_Proteobacteria;c_Gammaproteobacteria;o_Vibrionales;f_Vibrionaceae;g_Vibrio
OTU_1602	k_Bacteria;p_Proteobacteria;c_Gammaproteobacteria;o_Vibrionales;f_Vibrionaceae;g_Vibrio
OTU_1860	k_Bacteria;p_Proteobacteria;c_Gammaproteobacteria;o_Vibrionales;f_Vibrionaceae;g_Vibrio
OTU_2018	k_Bacteria;p_Proteobacteria;c_Gammaproteobacteria;o_Vibrionales;f_Vibrionaceae;g_Vibrio
OTU_2130	k_Bacteria;p_Proteobacteria;c_Gammaproteobacteria;o_Vibrionales;f_Vibrionaceae;g_Vibrio

**Table 4.** All Operational Taxonomic Units (OTUs) within the genus *Vibrio*, delineated on the basis of their highly conserved DNA sequences.

It is particularly interesting to note that when the relative abundance of *V. gigantis* from each individual sample is divided by the sum of the relative abundances of all *Vibrio* OTUs from the same sample, it becomes clear how this particular species stands out from the genus *Vibrio* in terms of occurrence in the biofilm samples (the last row of Table 5). The proportion of *V. gigantis* in the entire genus *Vibrio* was only 10% when the marine environment or the S0 sample was observed. However, when the biofilm samples were considered, its proportion in the genus *Vibrio* was about 60%. This confirmed that *V. gigantis* adheres much more frequently to the substrate, not only among the other genera, but also among the species of its own genus, which should have similar characteristics due to their close taxonomic relationship. This bacterium was originally isolated in France, from the Pacific oyster (*Crassostrea gigas*) [72], but has also been found in China, Malaysia, and Sweden. The complete genome sequences of these strains are deposited in the NCBI database. *V. gigantis* has not been recorded for infections in humans, but vibriosis has been reported in cage-farmed marine fish [73,74]. It is also a plastic coloniser with potential participation in its degradation [75].

	Relative abundance			
	S0 [%]	B1[%]	B2 [%]	B3 [%]
OTU_7	5.19	4.92	0.91	0.30
<b>OTU_11</b>	<b>0.73</b>	<b>11.83</b>	<b>3.76</b>	<b>0.96</b>
OTU_32	0.66	1.66	0.53	0.12
OTU_121	0.06	0.52	0.22	0.03
OTU_143	0.12	0.30	0.08	0.02
OTU_210	0.02	0.19	0.07	0.03
OTU_247	0.23	0.12	0.01	0.00
OTU_367	0.03	0.09	0.03	0.01
OTU_586	0.07	0.19	0.05	0.02
OTU_618	0.09	0.17	0.09	0.03
OTU_752	0.04	0.15	0.06	0.01
OTU_765	0.01	0.01	0.00	0.00
OTU_1042	0.00	0.01	0.00	0.00
OTU_1268	0.01	0.02	0.00	0.00
OTU_1443	0.02	0.01	0.01	0.00
OTU_1602	0.00	0.00	0.01	0.00
OTU_1860	0.04	0.43	0.18	0.02
OTU_2018	0.00	0.00	0.00	0.00
OTU_2130	0.02	0.04	0.02	0.01
<b>OTU_11/g__Vibrio</b>	<b>0.1001</b>	<b>0.5720</b>	<b>0.6242</b>	<b>0.6108</b>

**Table 5.** All the OTUs from genus *Vibrio* with their relative abundance in seawater (S0) and biofilm (B1, B2, B3) samples. In the last row of the table, the relative abundance of OTU11 (*V. gigantis*) was divided by the sum of the relative abundances of all *Vibrio* OTUs of the same sample.

### 3.2.3. Samples diversities

To obtain additional information on how the biofilm samples developed and how they differed from the seawater sample, diversity indices were calculated. First, a simple measure of phylogenetic diversity was calculated from constructed cladograms [26] and is presented in Figure 39. A quick glance at Figure 36 clearly separates the three-day biofilm sample B3 from the other samples which did not vary substantially in phylogenetic diversity. This is a further indication that the biofilm became more specific on third day in terms of the composition and variety of the species found in it.

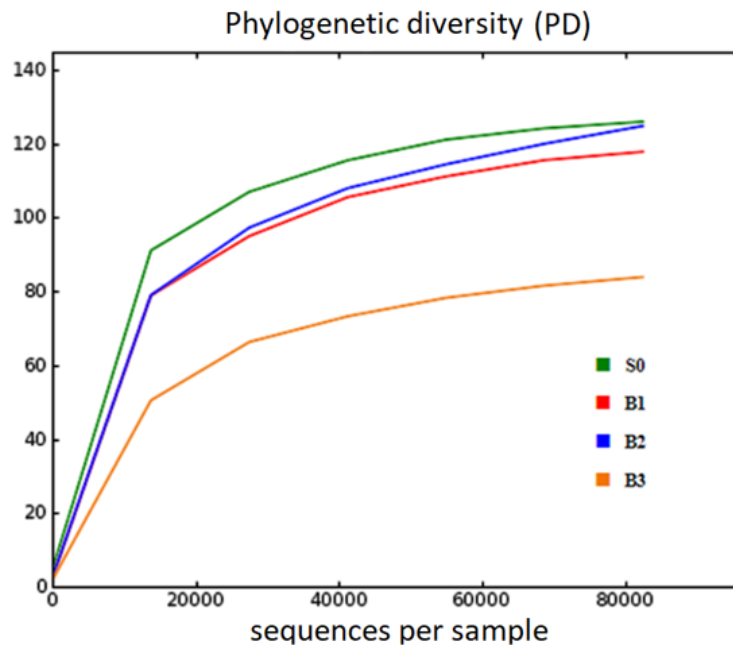


**Figure 39.** Phylogenetic diversity calculated from a constructed cladogram for one seawater (S0) and three biofilm samples (B1, B2, B3). As the number of considered sequences increased, so did the current diversity value.

This represents the most fundamental metric of  $\alpha$ -diversity and provides a characterization of each sample without comparing it to others. Other, more specific,  $\alpha$ -diversity measures are those describing the richness of a sample (Shannon [H]) and the evenness/dominance of the sample (Simpson diversity index [ $\lambda$ ]). The Shannon index estimates the richness of heterogeneous samples and takes into account both the relative abundance and the total number of species in a sample [27]. Its values are shown in Figure 40. Simpson index, on the other hand, is calculated as the sum of squares of relative abundances in a sample, or by subtracting that value from 1 [27], as in Figure 40, thus calculating the dominance or the evenness respectively. In other words, it describes if there are dominant and more frequent

species in a sample or if the occurrence among the species is more evenly distributed. It always varies from 0 to 1.

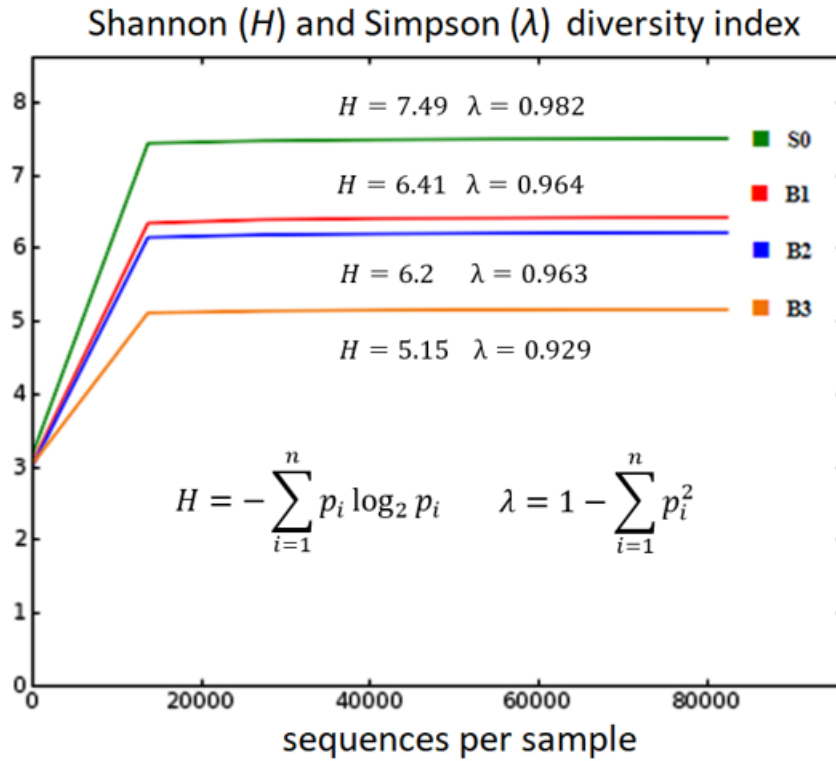


**Figure 40.** Shannon ( $H$ ) and Simpson ( $\lambda$ ) diversity indices, describing the richness and evenness of a sample with given formulas, where  $p_i$  is the relative abundance of the  $i$ -th OTU and  $n$  is the number of OTUs in a sample. Simpson index is not presented graphically, but only shown numerically.

As expected, the richness the highest in the seawater sample (7.49), gradually decreased in samples B1 (6.41) and B2 (6.2) and finally reached a value of 5.15 in sample B3, again confirming that the biofilm became more specific as it developed. In contrast to the Simpson index which did not vary much between the samples, ranging from 0.982 for S0 to 0.929 for the B3 sample. However, a clear trend was observed, showing that species were most evenly distributed in the S0 sample, while evenness decreased and dominance increased in the B3 sample, suggesting that certain species were more abundant due to others. All  $\alpha$ -diversity measures were compatible.

The  $\beta$ -diversity measurements compared the community composition directly between the samples, again separating the B3 sample from the others. Weighted UniFrac values were calculated, taking into account the compositions of the samples both quantitatively and qualitatively [67]. The diversity was the highest between the seawater sample S0 and the biofilm samples B1-B3 (Figure 41.) These

differences were to be expected, as it cannot be assumed that everything present in the environment would also be found in the biofilm samples. Among the biofilm samples, the most similarities were found between B1 and B2 samples, with a diversity measure of 0.141, while B1 and B3 were the least similar with a diversity measure of 0.281 (Figure 41).

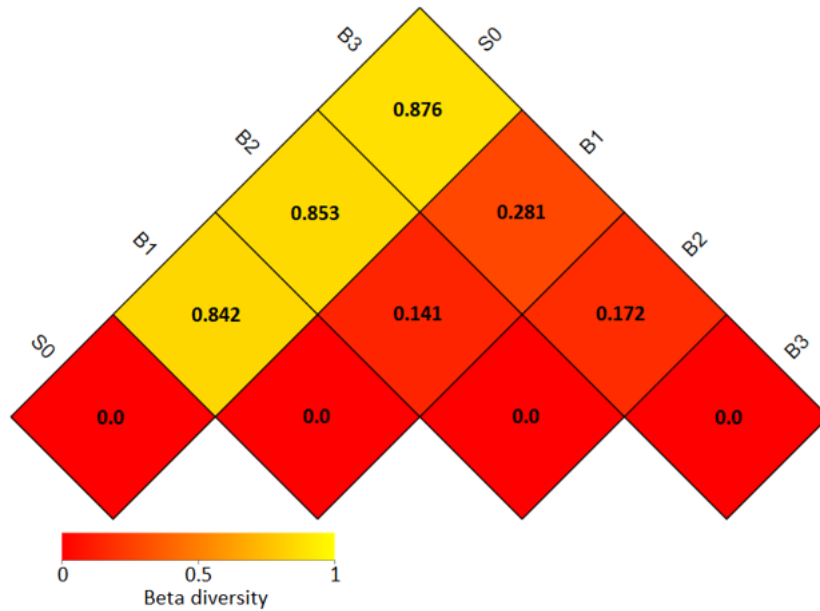


**Figure 41.** Weighted UniFrac distance metric between seawater (S0) and biofilm (B1, B2, B3) samples.

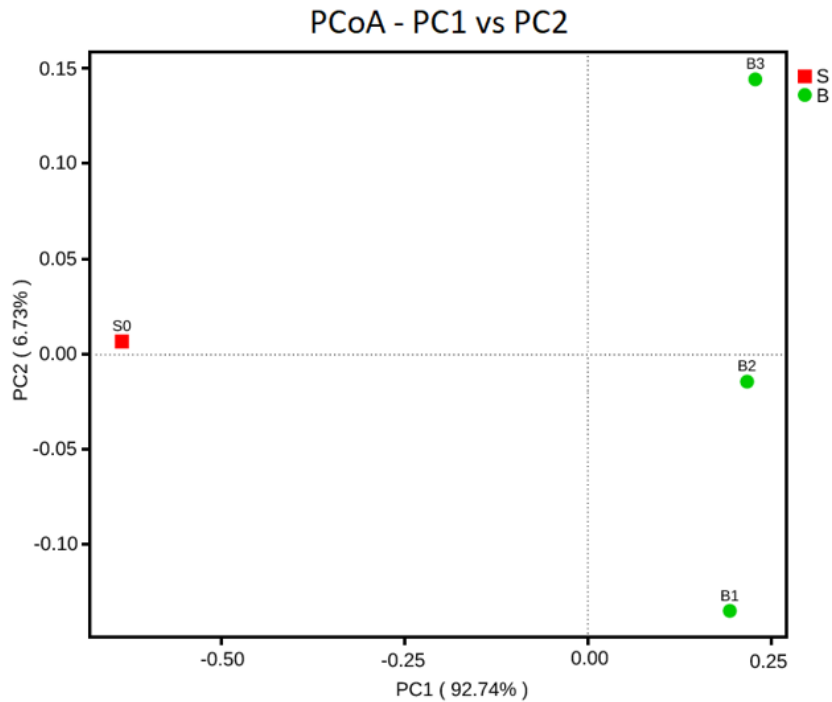


**Figure 42.** Principal coordinate analysis (PCoA), explaining the variations between seawater and biofilm samples by representation on two orthogonal axes, firstly on PC1 (92.74%) and then on PC2 (6.73%).

The  $\beta$ -diversity was also presented by principal coordinate analysis (PCoA), which is based on finding the characteristics (eigenvectors) that describe most of the variation between the samples and presenting them on two orthogonal axes [68]. With 92.74% of the described variation on the first axis, the seawater sample S0 was completely separated from the biofilm samples (Figure 42). The second axis, summarizing almost all of the remaining variability (6.73%), arranged the biofilm samples in order where B1 and B2 samples were put closer together and described as more related than they are with a B3 sample (Figure 42), which was also in agreement with Figure 41.

### **3.3. Prediction of metagenome functional potential**

While a metagenomic analysis provides insights into the overall functional potential of a sample with certain predictions, our main focus was on genes and molecular functions that are closely linked to and crucial for biofilm formation. At the hierarchical level of molecular functions (L3), the focus was on those related to cell motility, quorum sensing and secretion. Genes of particular interest considered at the L4 hierarchical level were directly related to the network of these specific molecular functions. In addition, the predicted functional potential of Operational Taxonomic Units (OTUs) was assessed at different taxonomic levels, with particular emphasis on the genus and species level. The creation of heatmaps was facilitated by using the relative abundances of OTUs in conjunction with gene annotations in their respective genomes. These annotations were determined by a PICRUSt analysis estimating the contribution of each taxon to the overall functional potential and metabolic pathways of the biofilm community [31].

#### **3.3.1. Functional capacity at the genus level**

At the genus level, the genera with the highest relative abundances were selected for their genetic, i.e. functional potential prediction (Table 6). The exact molecular functions are Bacterial motility: bacterial chemotaxis, bacterial motility proteins, and flagellar assembly; quorum sensing; biofilm

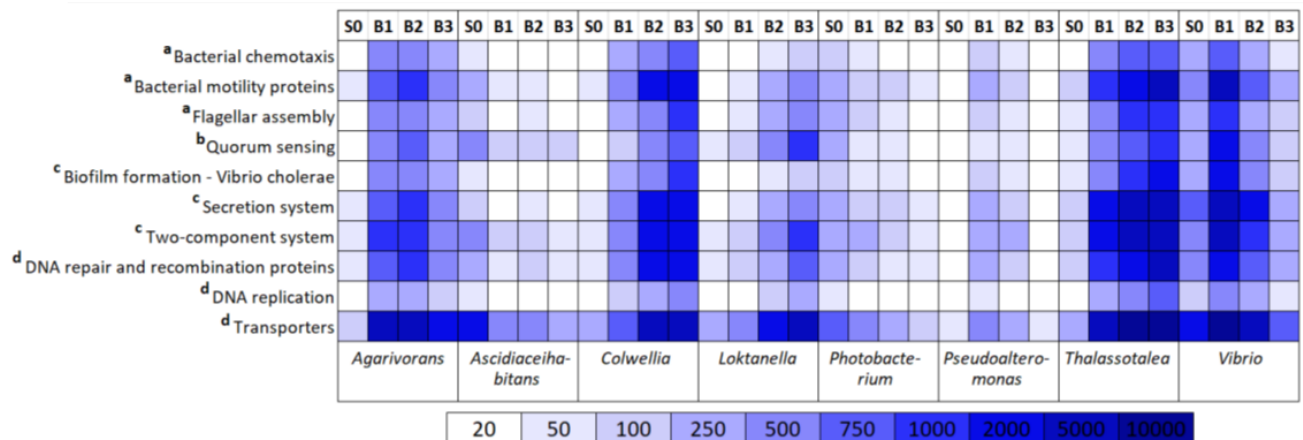


**Table 6.** Molecular function (L3) prediction of selected genera in seawater (S0) and biofilm (B1, B2, B3) samples. Colour boundaries are arbitrarily set. Denoted by a are molecular functions closely related to cell motility, b stands for quorum sensing, c for biofilm formation and secretion-related functions, and d for the essential housekeeping gene functions. C Biofilm formation – *Vibrio cholerae* was selected as the representative of the genus *Vibrio*, assuming that its biofilm-related genes were similar enough to those of the other genera.

formation and secretion-related functions: Biofilm formation – *Vibrio cholerae*, secretion system, two-component system.

The assigned categories are taken from the KEGG database [32]. The molecular function "Biofilm formation – *Vibrio cholerae*" was selected due to the taxonomic proximity between *V. gigantis* and *V. cholerae*, which both belong to the genus *Vibrio*. Hence, it is plausible that this function also applies to some extent to *V. gigantis*, although it is a different species. Furthermore, the selection of essential functions, such as DNA repair, DNA replication and transporters, reflects the inherent activities of housekeeping genes and thus justifies their consistent prediction. In the case of the genus *Vibrio*, the broad genetic potential for these functions closely matches their relative abundances, as shown by the colours of the heatmap (see Table 6). Remarkably, the genus *Vibrio* shows an increased expression of these functions, especially in the B1 sample. This analysis also improves our understanding of the functional dynamics within the biofilm community.

### 3.3.2. Functional capacity at the species level

An interesting area of research is the evaluation of predicted molecular functions at the species level to elucidate possible variations within the genus *Vibrio*, with particular emphasis on the genetic potential for biofilm formation of the bacterium *V. giganteus* (Table 7).

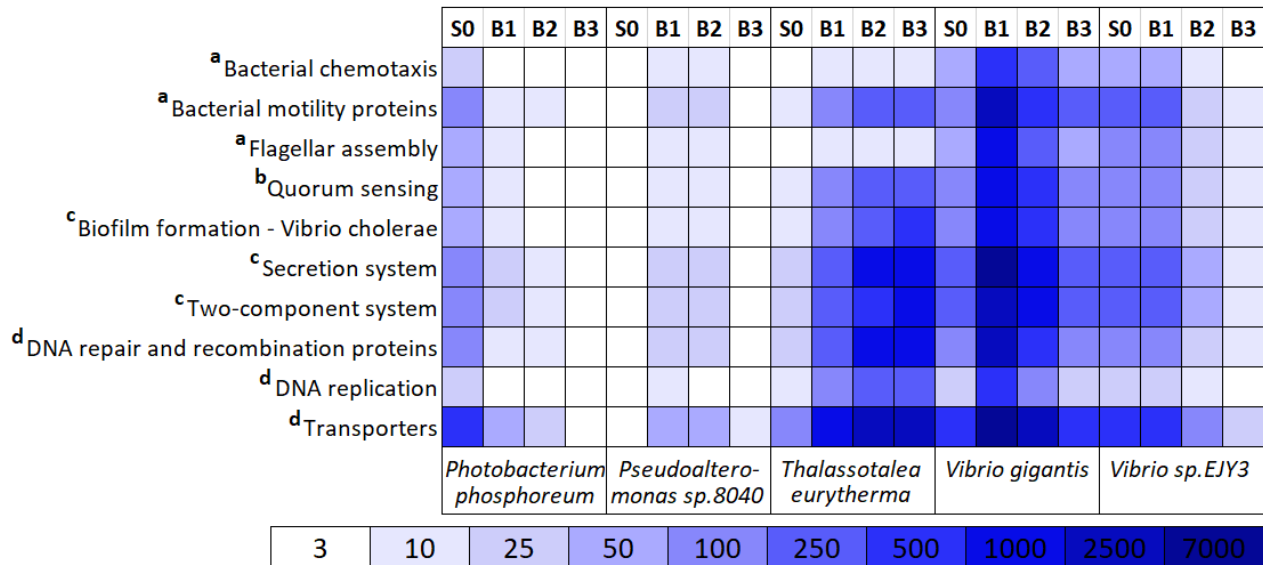


**Table 7.** Molecular function (L3) prediction of selected species in seawater (S0) and biofilm (B1, B2, B3) samples. Colour boundaries are arbitrarily set. White-coloured values are ranging from 0 to 3. Marks a, b, c, and d stand for the same roles as in the previous heatmap table.

In the S0 sample, it was moderately involved in all functions, while in the B1 sample, that substantially increased and decreased on each subsequent day, strongly depending on its relative abundance. While playing a dominant role in certain molecular pathways in the S0 and B1 samples, it was mainly replaced by *Thalassotalea eurytherma* in the B2 and B3 samples. The comparison of *V. giganteus* with *Vibrio sp. EJY3* also confirms the superior potential of *V. giganteus* among the species of its genus.

A closer look at the molecular functions reveals a network of cooperating genes. A direct genetic potential of selected genes involved in biofilm formation is shown in Table 8 for the same species as in the previous table. The genome of *V. giganteus* contains genes for the expression of aerotaxis receptors, flagellar proteins, pilus and pilin assembly proteins and the autoinducer luxP, which enable the processes of chemotaxis, bacterial motility and quorum sensing.



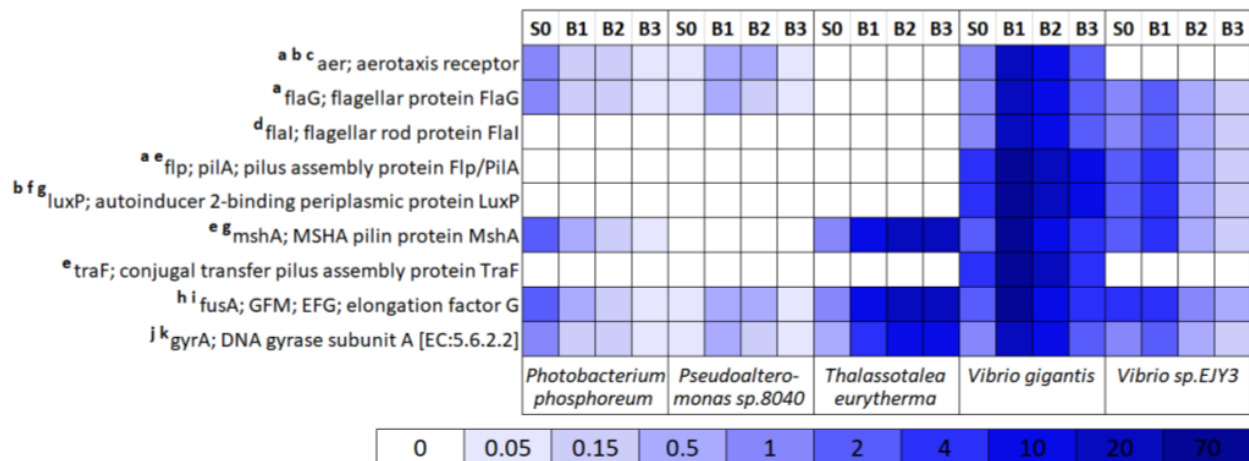


**Table 8.** Gene activity (L4) prediction of selected species in seawater (S0) and biofilm (B1, B2, B3) samples. Colour boundaries are arbitrarily set. These genes are usually involved in more than one molecular function: a – bacterial motility, b – two-component system, c – bacterial chemotaxis, d – cell motility, e – secretion system, f – quorum sensing, g – biofilm formation - *Vibrio cholerae*, h – translation factors, i – mitochondrial biogenesis, j – DNA replication proteins, k – DNA repair and recombination proteins.

Quorum sensing is an essential cell-to-cell signalling mechanism that regulates biofilm formation and gene expression using small signalling molecules. One of the most important ones is autoinducer-2 [76], which is synthesised by Lux family genes [46].

PICRUSt analysis revealed the presence of genes involved in the Lux quorum system, including the *luxN* [77], *luxQUO* [78,79], *luxP* [46,80-82] and *luxS* [46,83] genes, in the genome of *V. gigantis* (Table 9). These genes are key components of the Lux quorum signalling pathway, suggesting that this bacterium is able to communicate from cell to cell via AI-2 molecules.

However, the Lux quorum system normally also plays a key role in the regulation of bioluminescence in various species of the genus *Vibrio*. It is important to note that the presence of two critical components essential for bioluminescence in *Vibrio* species was not revealed: a transcriptional activator *luxR* and the luciferase operon (*luxCDABEG*) [84]. *LuxR* serves as a transcriptional regulator, while the luciferase operon is responsible for the production of luciferase enzymes that are crucial for the bioluminescence response [85]. The absence of these components suggests that *V. gigantis* may lack the genetic requirements for bioluminescence that distinguish it from some other species of the genus *Vibrio*.

To provide a comparative perspective, we examined the genetic content of *V. gigantis* in relation to two other bacterial species: *Photobacterium phosphoreum* and *Aliivibrio fischeri* [85], both of which

are known for their genetic predisposition to bioluminescence in seawater (Table 9). PICRUSt analysis showed that these bioluminescent species show a relatively higher share of the *luxABCDE* genes in their genomes, which indicates their bioluminescence ability. This observation is consistent with their known ability to produce light through the luciferase enzymatic pathway, which is key to their bioluminescent properties [86].

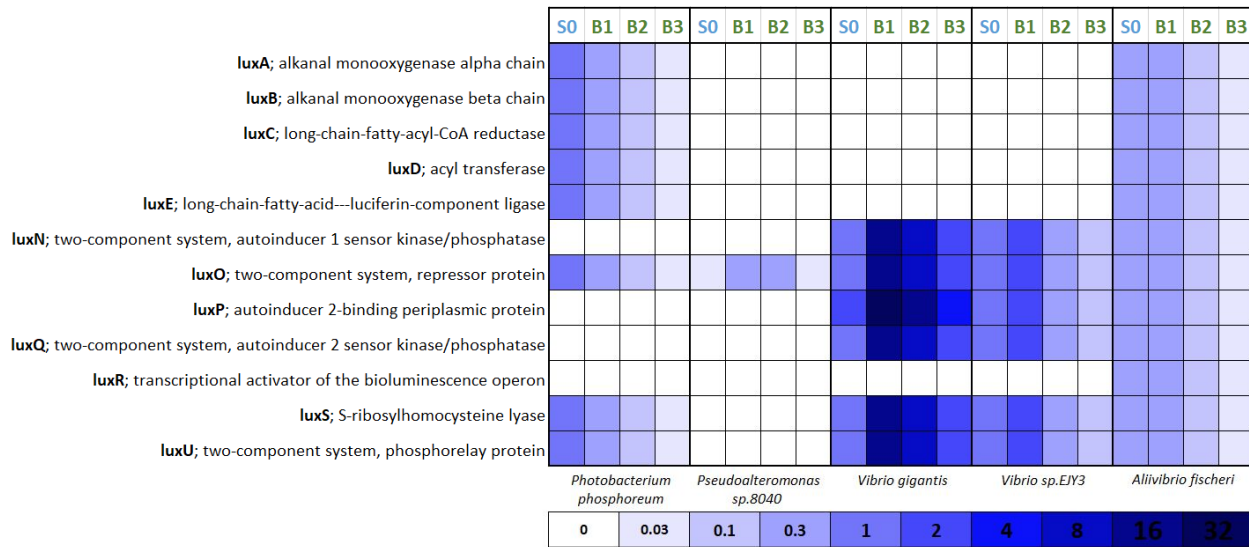


**Table 9.** Prediction of the genetic potential of cellular communication via chemical signalling molecules AI 2 in pioneer bacterial species in seawater (S0) and in the first three days of biofilm formation on the surface of immersed slides (B1, B2 and B3). Colour boundaries are arbitrarily set.

In summary, the observed dynamic involvement of *Vibrio gigantis* in functional processes within the biofilm community is closely related to its relative abundance in different samples. This comprehensive analysis improves our understanding of the genetic basis that contributes to the biofilm-forming abilities of *V. gigantis* in the studied environment.

Not only did *V. gigantis* show a promising adhesion propensity in preliminary experiments and was extremely abundant in biofilm samples, especially on the first day of biofilm, but it was also found to possess the crucial genes for quorum sensing and biofilm formation and regulation. All this made this species a perfect model for the following experiments on adhesion dynamics and colony development.

### 3.4. Adhesion dynamics in a bioreactor

In order to monitor and quantify bacterial adhesion dynamics and aggregate formation under controlled conditions at the chosen time points, a newly designed and easily-implementable experiment in a bioreactor was developed. With the idea of imitating a natural environment, there were no motion restrictions and it was performed in a large volume. *V. gigantis* was finally chosen as a model bacterial organism whose adhesion was quantified on a glass substrate as the substrate coverage percentage.

Before measuring the adhesion dynamics of *V. gigantis* in a bioreactor, its growth kinetics was determined (Figure 43) to find out how the concentration of bacteria in the medium changes as the experiment evolves. During the first 3 and a half hours, which fully covered the length of the upcoming experiments, the curve was strictly exponential, after which unusual stagnations for this phase were found (roughly around 4-5 and 6-7 hours). This could be due to low oxygen and nutrient concentration, whose lack caused the metabolic shifts and changes in behaviour. Nevertheless, the growth was more expressed after 8 hours. From 12 hours onwards, a plateau with occasional slow growth was seen, until 22 hours, as the nutrient and oxygen concentrations probably decreased to the extent of causing death and settling, lowering the measurement values.

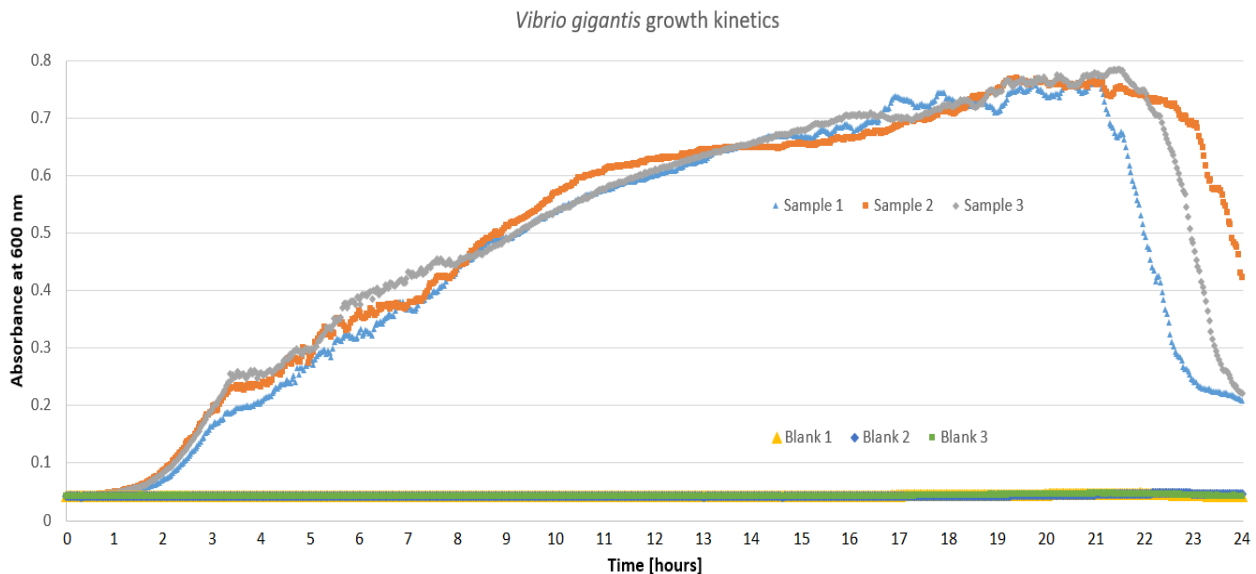


**Figure 43.** The growth kinetics of *V. gigantis* over 24 hours, at the lowest achievable temperature of 28°C. The measurements of the absorbance values of a sample and a blank probe were carried out in triplicate. The culture was adjusted to  $5 \cdot 10^5$  CFU/ml.

### 3.4.1. Adhesion quantification

The bioreactor used for the adhesion quantification of *V. gigantea* is a newly designed, simple, and low-cost setup, offering its practical and offshore application. For this experiment, the critical parameter to adjust was the duration of the entire experiment. According to the growth kinetics (Figure 43), it was decided to proceed with two experiment durations. The shorter experiment aimed to keep the bacteria at a constant concentration, i.e. in the lag phase, and therefore lasted one hour. The longer experiment lasted three hours, allowing the bacteria to enter the early exponential phase. In the shorter experiment, the slides were removed after 1, 3, 5, 10, 20, 30, 45, and 60 minutes. Removing the slides so frequently could affect and disturb the pre-adhesion dynamics, while reducing the number of slides would take away the time points, which would question the meaning of the experiment. The time points of slide removal in the longer experiment were more distant, at 10, 20, 30, 45, 60, 90, 120, and 180 minutes. In this way, a possible interference and pre-adhesion dynamics perturbation was minimized and the adhesion over a longer period was allowed. On the other hand, the bacteria in the longer experiment reached the exponential growth phase and the concentration was not relatively constant as in the shorter experiment.

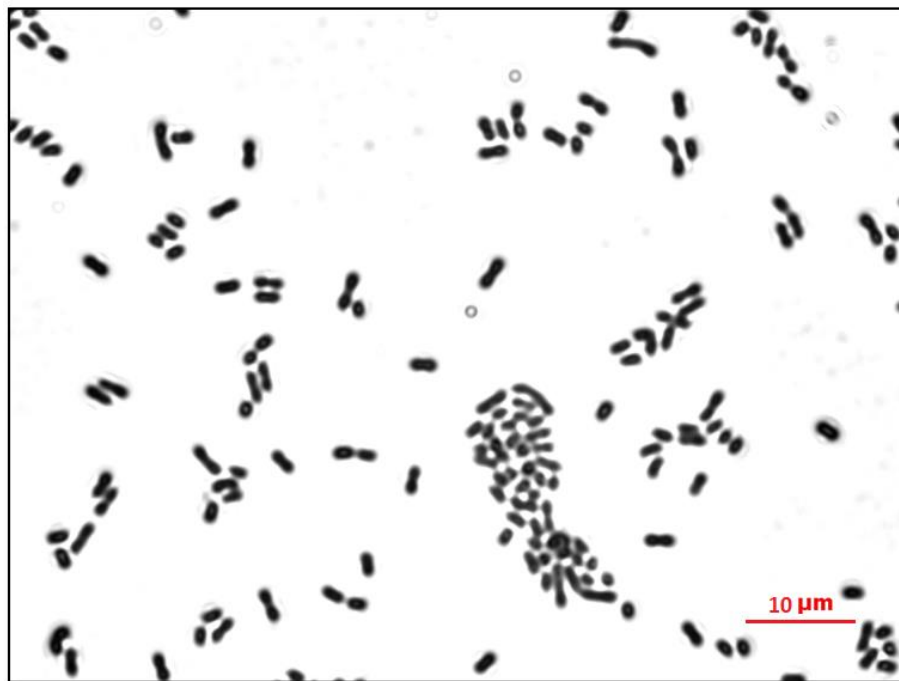


**Figure 44.** A random original image of *V. gigantea* (not processed), taken with a 100x magnification objective.

After the experiments were conducted, the images were taken with a 10x magnification objective. A random image at 100x magnification is shown (Figure 44) to present *V. gigantis* in a better resolution, showing that it is a comma-shaped species characteristic for *Vibrio* genus, with its length of around 2.5  $\mu\text{m}$  and width of around 1  $\mu\text{m}$ . This also showed how the real image looked before it was subjected to calculation later on. Also, most of the bacteria were caught at a certain stage of division, making them look more elongated than they are, or even two individuals can be distinguished.

To get an insight into the surface condition at different time points of the experiment, a set of images that best describe it was selected and presented in Figure 45. Due to the low magnification, it was difficult to observe them at the level of individual bacteria, but it did not affect the calculation of the percentage of covered substrate, a direct measure of adhesion. Qualitatively, it can be seen that the number of adhering bacteria increased with time and the aggregates began to appear in the range of 30 to 45 minutes (Figure 45). While the number of bacteria and aggregates stagnated or slightly decreased at 60 minutes, a considerable decrease was observed in most images at 90 minutes, which was far from expected. At the last two time points, a substantial increase in the covered substrate was noticed (Figure 45). This was described quantitatively as well in the following figures.

The results of the three-hour experiments are shown in Figure 46. Three measurements from independent experiments are shown together with the averaged value, confirming spontaneous adhesion. A constant increase in adhesion was observed from the beginning until a peak value was reached at 60 minutes. This was followed by a surprising decrease at 90 minutes and a further increase until the end of the experiment. The final percentage values of surface coverage ranged from 12.61% to 18.08%. A similar trend of adhesion dynamics was observed between the independent measurements with a correlation coefficient of  $R_{12} = 0.87$ ,  $R_{13} = 0.94$ , and  $R_{23} = 0.92$ .

The value dispersion at the same time points could be explained either as an interference with slides while removing them, or as the result of unequal initial concentrations. The surprising event of decline at 90 minutes is particularly interesting. At first thought, this could be interpreted as a detachment of bacterial cells after division, but probably the effect of the newly arrived bacteria would overcome the losses due to such a detachment. Hence, this could be a result of the biofilm dispersal process, which has been confirmed experimentally and theoretically in different species and is related to quorum sensing [44-46,87]. What is also intriguing is the aggregates that gradually appear, then mostly disappear, and return again to a certain extent.



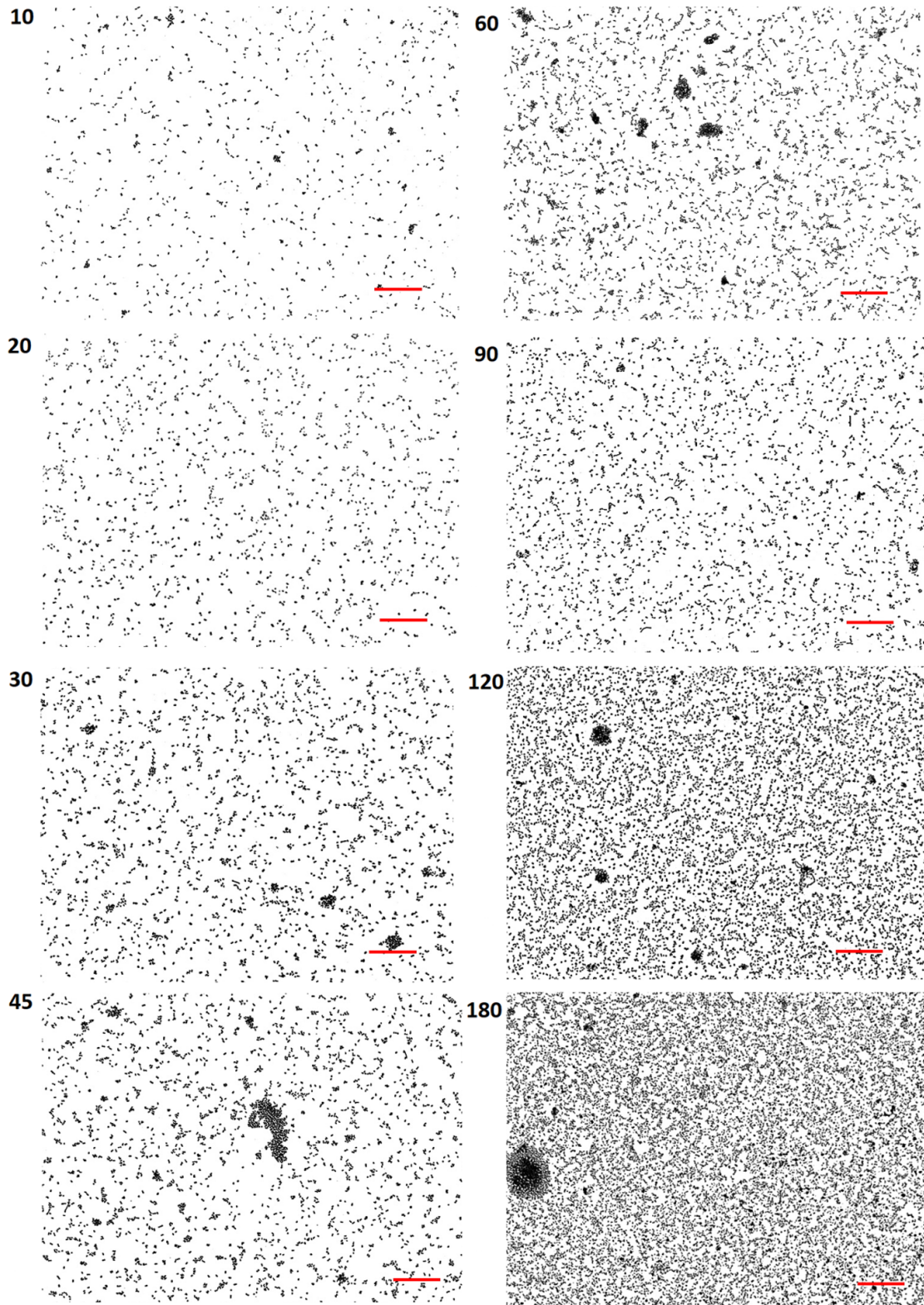


**Figure 45.** *V. gigantis* adhesion on a microscopic slide at indicated extraction times in minutes (original images). The images were taken by a 10x magnification objective (a quarter of a real image shown). The red scale bar indicates 50  $\mu\text{m}$ . The initial concentration was 0.5 McF at room temperature of 24°C.

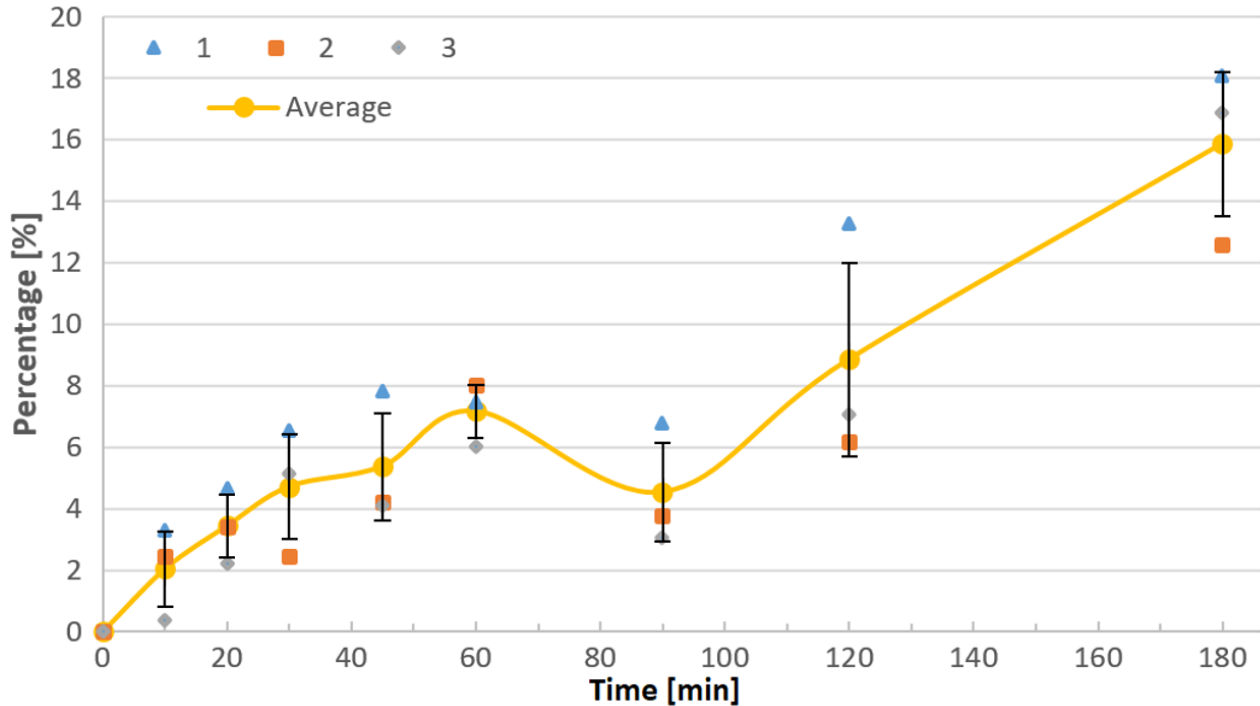


**Figure 46.** Adhesion dynamics of *V. gigantis* in the 3-hour experiment, calculated as covered surface percentage. After 1 hour of incubation, the initial concentration was 0.5 McF at room temperature of 24°C.

The independent measurements of the one-hour experiment showed a coverage increase until around 60 minutes, after which it decreased (Figure 47). These measurements varied considerably more, with a less uniform adhesion trend. It is likely that the frequent slide removals caused an unwanted interference with the system at an early stage of the experiment, where pre-adhesion dynamics is presumably a dominant effect. This interpretation is also supported by the fact that the short experiment resulted in generally lower coverages than the long experiment when the same time points are compared (Figure 46 and 47).

In order to check how the coverage would evolve with the changed initial concentration, additional two experiments were carried out: the first one with no incubation at all, and the other one with the incubation time extended by one hour. The rest of the methodology was left unchanged. The average curve from the 3-hour experiment was compared with the curves from the doubled incubation (+1h) and omitted incubation (-1h) in Figure 48.

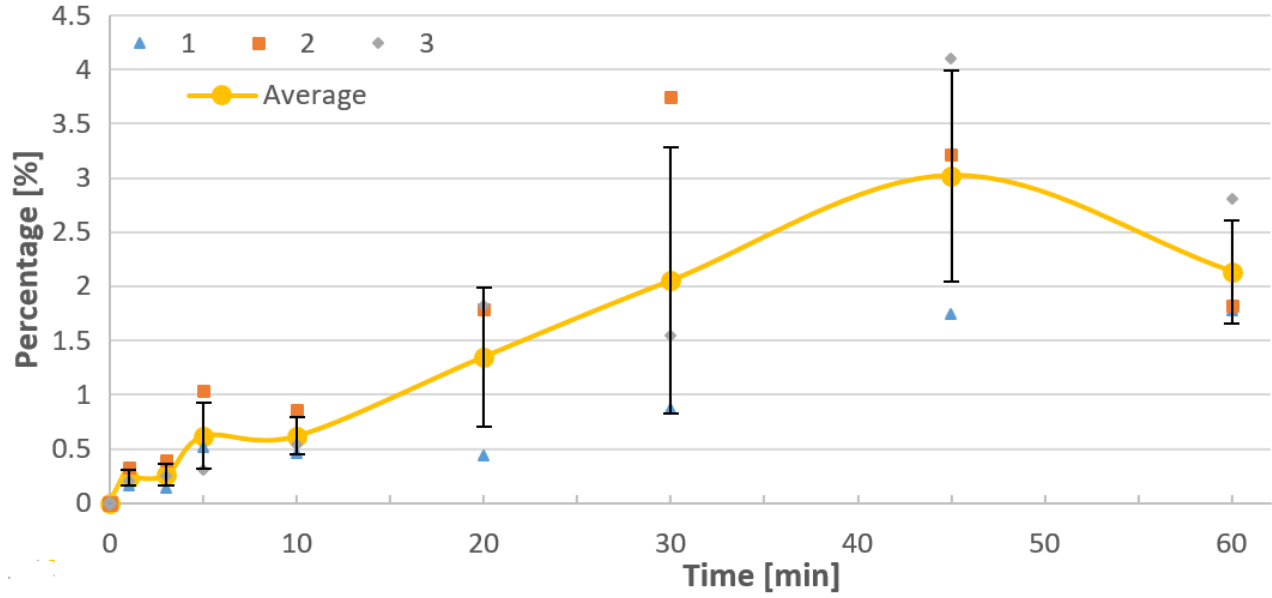


**Figure 47.** Adhesion dynamics of *V. gigantis* in the 1-hour experiment, calculated as covered surface percentage. After 1 hour of incubation, the initial concentration was 0.5 McF at room temperature of 24°C.

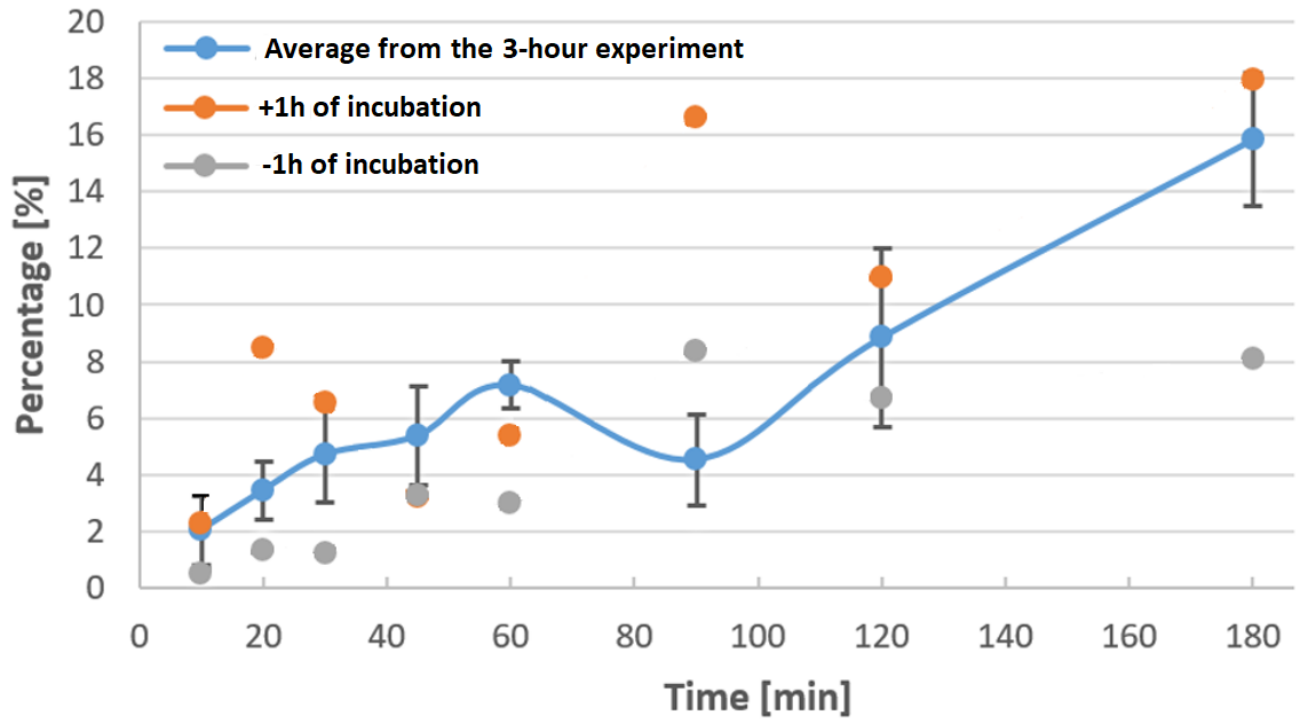


**Figure 48.** Adhesion dynamics of *V. gigantis* in the 3-hour experiment (average values from Figure 46) and the experiments with the doubled incubation (+1h) and omitted incubation (-1h).



The coverage for the added incubation increased rapidly due to a much higher initial concentration until it reached its maximum at 20 minutes. After a huge fall at 45 minutes, it grew exceptionally at 90 minutes which was in complete contrast with the average curve from regular incubation time. Followed by another strong decrease at 120 minutes, it continued to grow until the end. The coverage for the no-incubation regime behaved similarly but with much smaller amplitudes due to the lower initial concentration and the lack of exposure to a fresh marine broth before the experiment. Both regimes with added and omitted incubation time behaved like they were in the counter phase with the 3-hour average curve, resulting in opposite adhesion and detachment trends. For the additional incubation and increased initial concentration, an early decrease in the coverage at 20 minutes and the one at 90 minutes could be attributed to quorum sensing [46,62], or even to a natural response to the overcrowded substrate [61], which is perceived as an unfavourable condition. In this case, the nutrient deficit could not be the cause, because the coverage percentage grew afterward. Finally, changing the initial concentration affected the adhesion dynamics trend.

Regardless of the duration of the experiment or incubation, the slides were extremely populated at the broth and air interface in each experiment. This area was dense to the extent that the stains on the slide could be seen by the naked eye. Certainly, these areas were not taken into account because the covered surface would be 100% (see section 2.4.3.). This is also a confirmation that *V. gigantis* is a facultative anaerobe, favouring aerobic respiration when oxygen is present and switching to fermentation otherwise, like most members of the genus *Vibrio* [88].

### **3.4.2. Aggregate analysis**

From Figure 45 it is clear that aggregate forms were present at certain adhesion stages. At this point, the exact formation process was not determined since real-time evolution was not captured. These clusters could be the aggregates formed by a spontaneous accumulation of bacteria from the bulk one by one, but also could be previously formed in the bulk and adhere directly as an aggregate. Moreover, the bacteria that adhere as individuals can form a colony by a simple division and that could be what was seen in Figure 45. The last option was least probable since some aggregates were simply too large at 45 minutes for the division time of around 20 minutes, that is why the term aggregates is used in this section. Observing the aggregates of various sizes and the changes in their average number in time provides additional results for discussion (Figure 49). For each time point of the 3-hour experiment, the average number of variously-sized aggregates was calculated from a 30-image set.

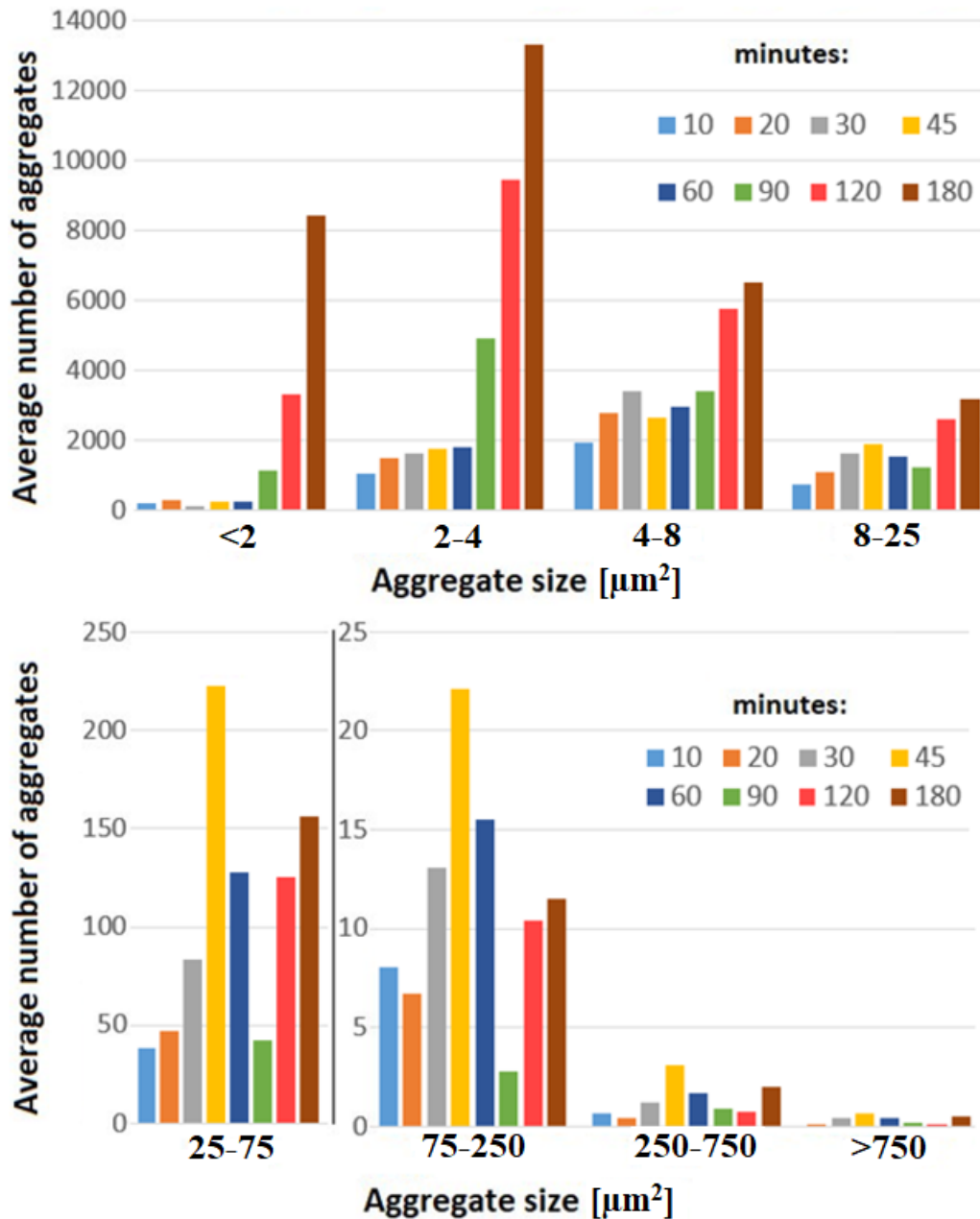


**Figure 49.** The average number of aggregates of various sizes at time points of the three-hour experiment (from Figure 46). For the sizes of <math><2</math>, 2-4, 4-8, and 8-15

The individual bacteria, pairs and various-sized aggregates were taken into account. The number of individual bacteria (<math><2\mu\text{m}^2</math>), pairs of bacteria (2-4 $\mu\text{m}^2$ ), and smaller aggregates (4-8  $\mu\text{m}^2$ ) increased

over time, with the most noticeable increase at 90 minutes (Figure 49, green column). On the contrary, medium (8-25 and 25-75  $\mu m^2$ ) and larger aggregates (75-250 and 250-750  $\mu m^2$ ) reached their peak in abundance at 45 minutes after which it was reduced by 50-70% until the 90-minute time point. At the next time points, their number increased again. The aggregates of  $>750 \mu m^2$  were too few but they also followed this trend. In other words, during the whole experiment, the number of individual bacteria, smaller and larger aggregates was increasing until the 45-minute time point, after which the number of larger aggregates dropped drastically and that way probably freed up the space for the uninterrupted increase in the number of individual bacteria and smaller aggregates which populated the substrate continuously. The bacteria acted differently on the single and aggregate level. These fluctuations in the number of different-sized aggregates (Figure 49, Figure 45) could be the result of quorum sensing, controlling a dispersal process [45,46,61] due to the surrounding bacterial concentration, overcrowding, or a localized nutrient and oxygen deficiency. Furthermore, although the surprising growth kinetics stagnations from Figure 43 occurred outside the time interval of this experiment, clearly there is some behaviour regulation and possible metabolic shifts due to oxygen and nutrient concentration deficiency caused by their consumption and cell division with bacterial concentration increase. This could act as an initiator for these aggregate number fluctuations, but also for the decrease in the substrate coverage percentage at given time points. Also, the exact fraction of bacteria, coming from the adhered bacteria and from the divided bacteria could not be known. The division was, as an inevitable and inseparable event from the adhesion, considered under the adhesion process and added to its measure.

To sum up, in order to achieve a better insight into the adhesion dynamics, the detachment process, and aggregate dynamics, and also to provide more specific explanations and conclusions, real-time monitoring of *V. gigantis* is fundamental. In the following sections, the results of experiments on additional experimental setups, designed or adjusted from the existing ones, are shown and discussed.

[Redacted]

[Redacted]

[Redacted]

[Redacted]

[Redacted]

[Redacted]

[Redacted]

[Redacted]

[Redacted]

[Redacted]

[Redacted]

[Redacted]

[Redacted]

[Redacted]

[REDACTED]

[REDACTED]

[REDACTED]

[Redacted text block]

[Redacted text block]

[Video 1](#) [Video](#)

[2](#) [Video 3](#)

[Redacted text block]

[REDACTED]

[REDACTED]

[REDACTED]

[Redacted text block]

[Redacted text block]

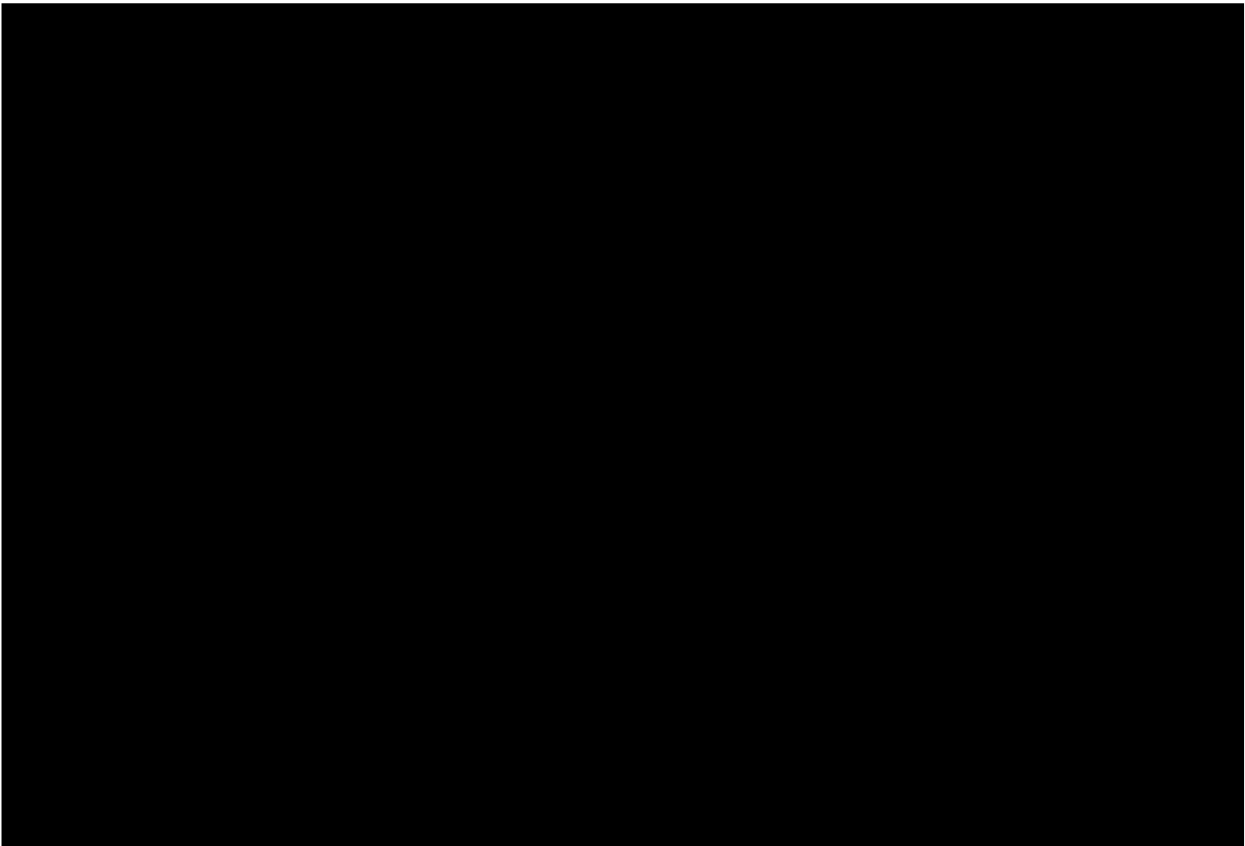
[Redacted text block]



[Redacted text block]

[Video 4](#)

[Redacted text block]



[Redacted text block]

[REDACTED]

[REDACTED]

[REDACTED]

[REDACTED]

[Redacted text block]

[Redacted text block]

[Redacted text block]

[Redacted text block]

[Redacted text block]

[Video 6](#)

[Redacted text block]

[Redacted text block]

[Redacted text block]

[Redacted text block]

[Redacted text block]

[Redacted text block]

[Video 7](#) [Video 8](#)

[Redacted text block]

[Video 8](#)

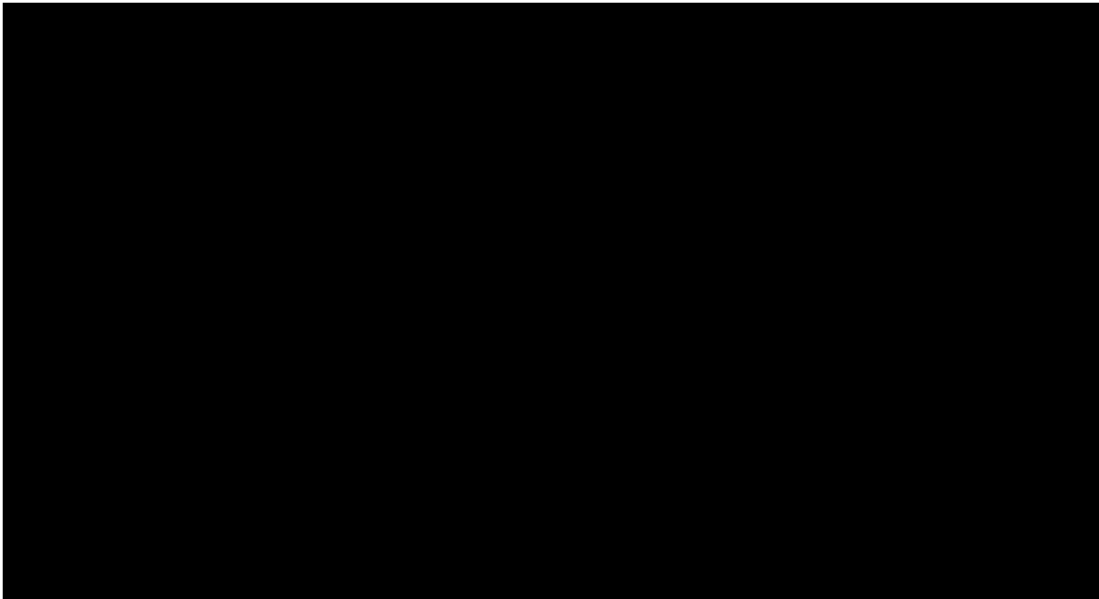


[Redacted text block]

[Redacted text block]

[Redacted]

[Redacted]



[Redacted]

[Redacted]

[Redacted]

[Redacted]

[Redacted]

[Redacted]

[Redacted]

[Redacted]

[Redacted]

[Redacted]

[Redacted] [Video 9](#) [Video 10](#) [Video 11](#)

[Redacted]

[Redacted]

[Redacted]

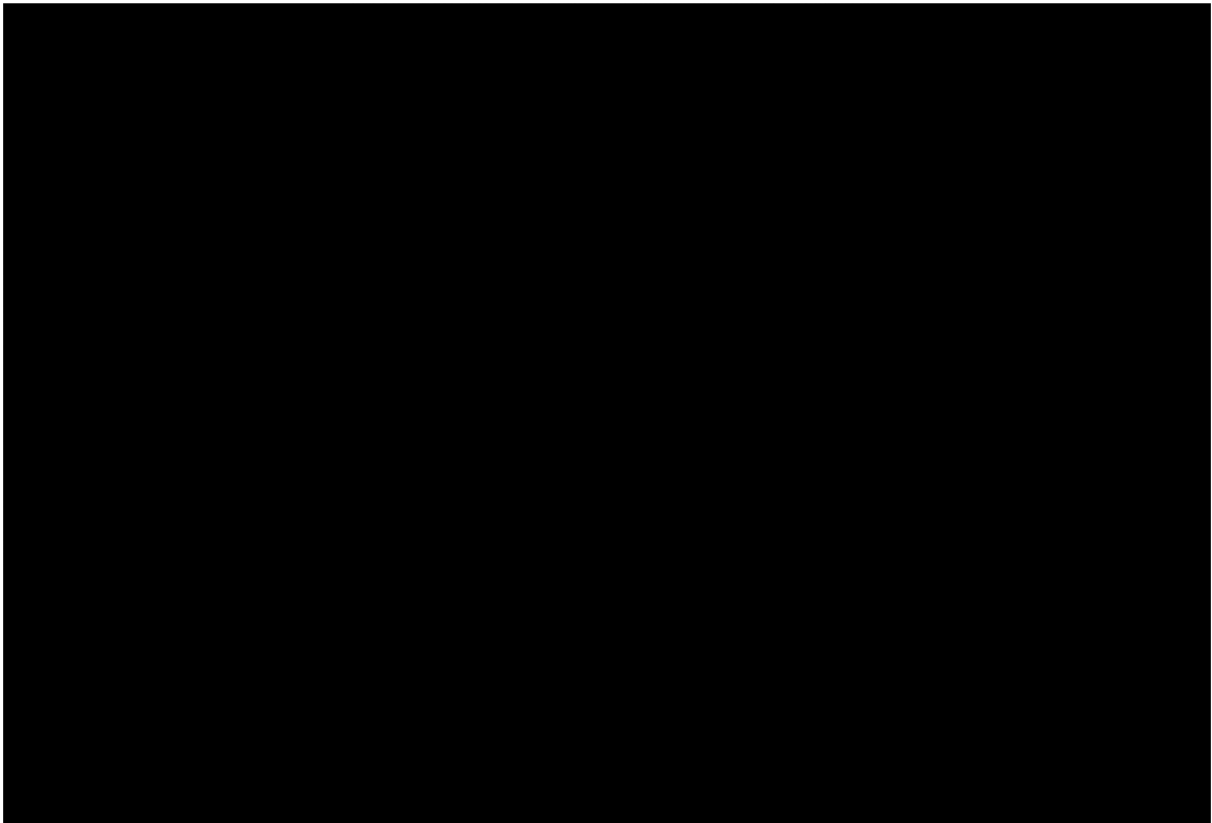
[Redacted]

[Redacted]

[Redacted]

[Redacted]

[Redacted text block]



[Redacted text block]

[Redacted text block]

[Redacted text block]

[Redacted text block]

[Redacted text block]

[Redacted text block]



[Redacted text block]

[Large redacted text block]

[Redacted text block]

[Redacted]

[Redacted]

[Redacted]

[Redacted]

[Redacted]

[Video 12](#)

[Redacted]

[Redacted]

[Redacted]

[Redacted]

[Video 13\(1\)](#) [Video 13\(2\)](#)

[Redacted]

[Redacted]

[Redacted]

[Redacted]

[Redacted]

[Redacted]

[Redacted]

[Redacted]

[Redacted]

[Redacted]

[Redacted]

[Redacted]

[Redacted text block]

[Redacted text block]

[Redacted text block]

[Redacted text block]

[Redacted text block]

[Redacted text block]

[Redacted text block]

[Redacted text block]

[Large redacted text block]

[Redacted text block]

[Redacted text block]

[REDACTED]

[REDACTED]

[REDACTED]

[Redacted text block]

[Video 14](#)



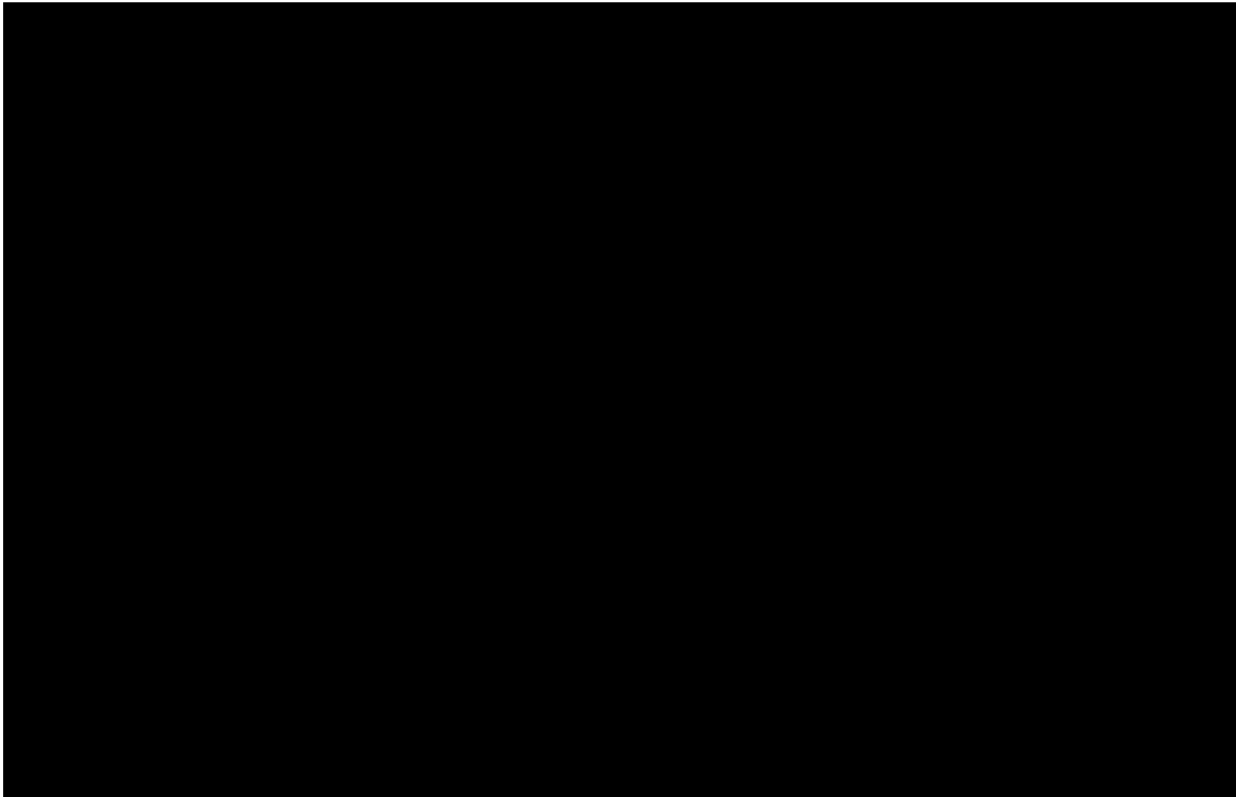
[Redacted text block]



[Redacted text block]

[Video 14](#)

[Redacted text block]



[Redacted text block]

[Video 14](#)

[Redacted text block]

[Video 15](#)

[Redacted text block]

[Large redacted text block]

[Redacted text block]

[Redacted text block]

[Large redacted text block]

[Redacted text block]

[Redacted text block]

[Redacted text block]

[Redacted text block]

[Video 13 \(2\)](#)

[Video 15](#)

[Redacted text block]

[Redacted text block]

[REDACTED]

[REDACTED]

[REDACTED]

[REDACTED]

[REDACTED]

[REDACTED]

[REDACTED]

[REDACTED]

[REDACTED]

[REDACTED]

[REDACTED]

[REDACTED]

[REDACTED]

[REDACTED]

[REDACTED]

[Redacted]

[Redacted]

[Redacted]

[Redacted]

[Redacted]

[Redacted]

[Redacted]

[Redacted]

[Redacted]

[Redacted]

[Redacted]

[Redacted]

[Redacted]

[Redacted]

[Redacted]

[Redacted]

[Redacted]

[Redacted]

[Redacted]

[Redacted]

[Redacted]

[Redacted]

[Redacted]

[Redacted]

[Redacted]

[REDACTED]

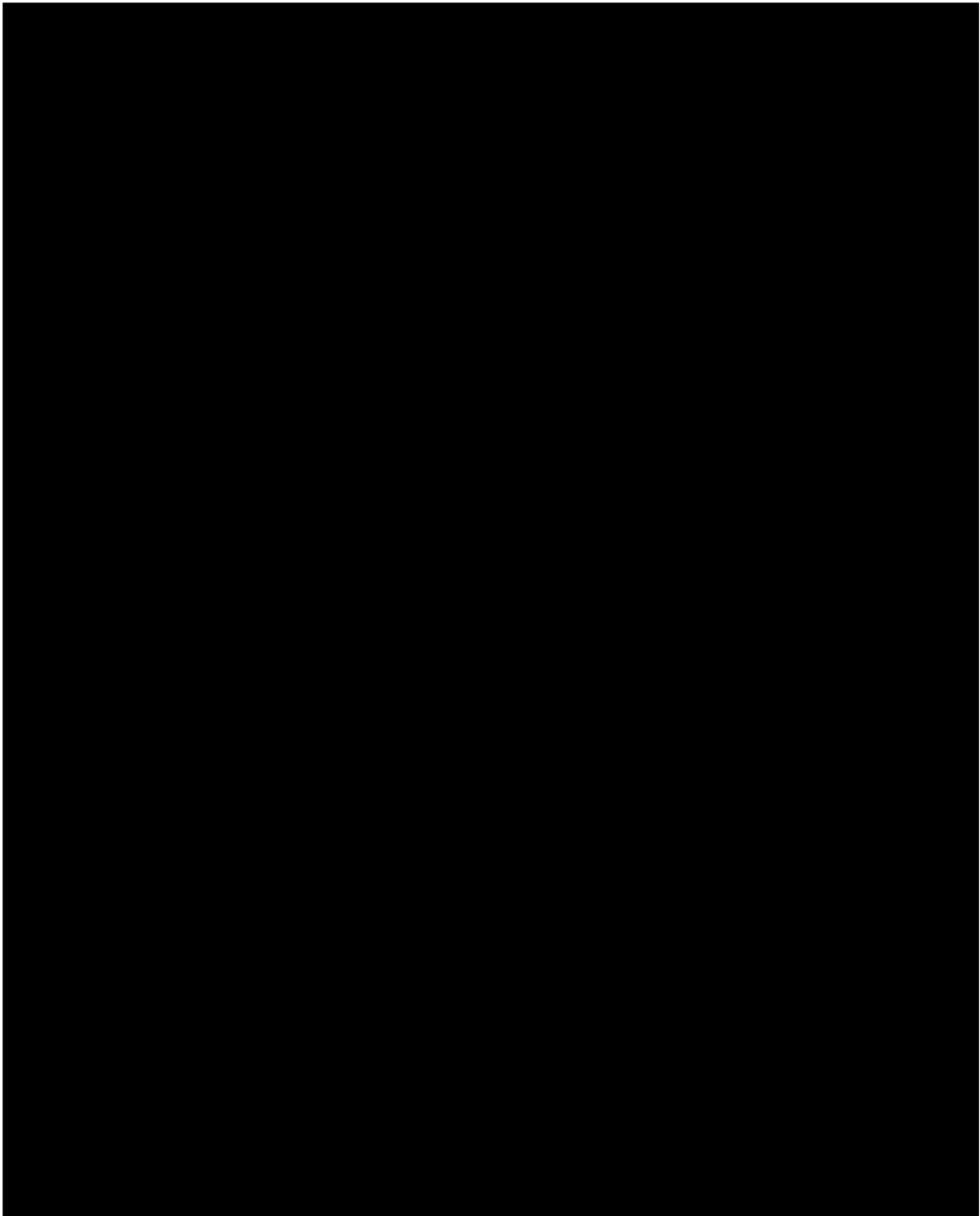
[REDACTED]

[REDACTED]

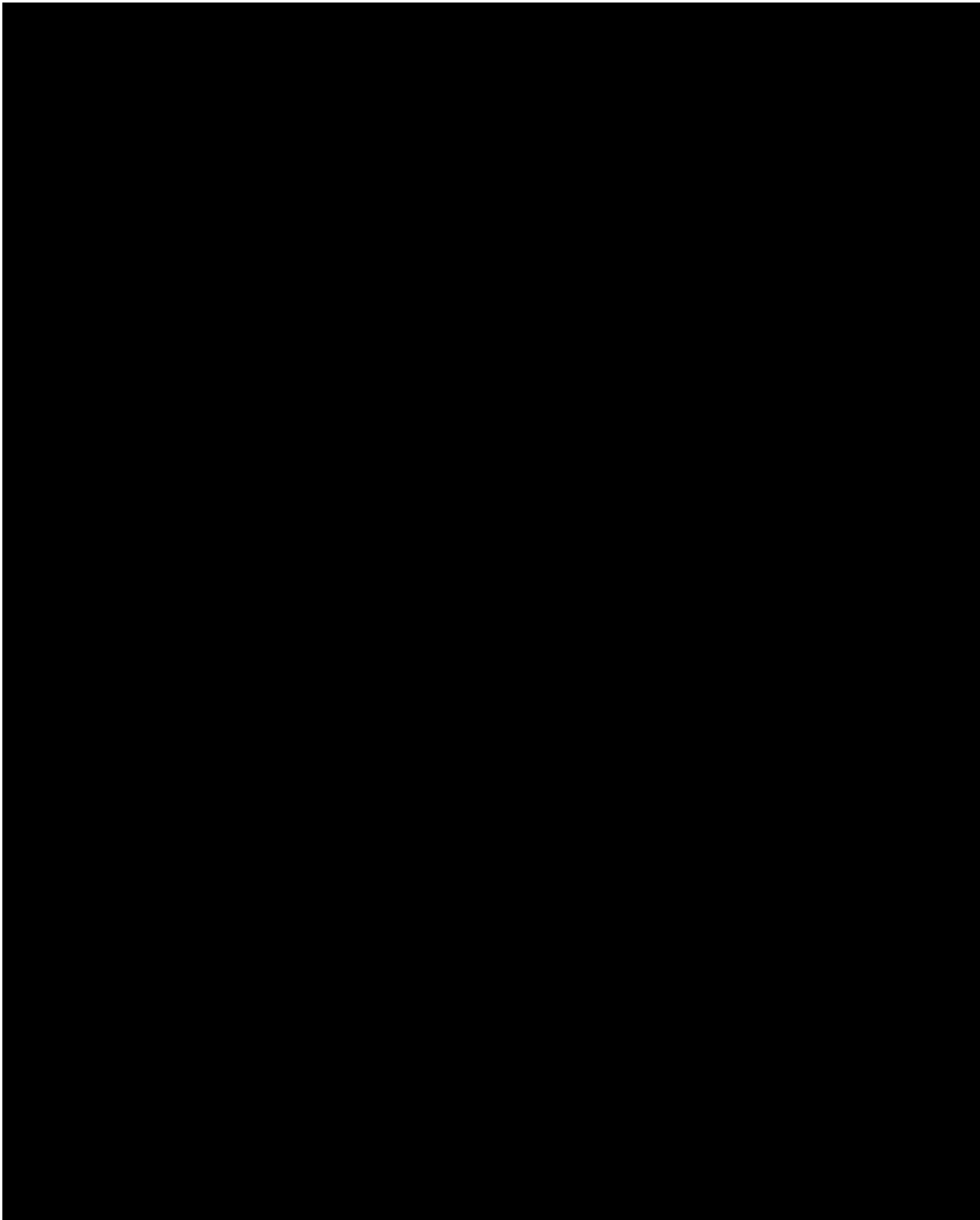
[REDACTED]

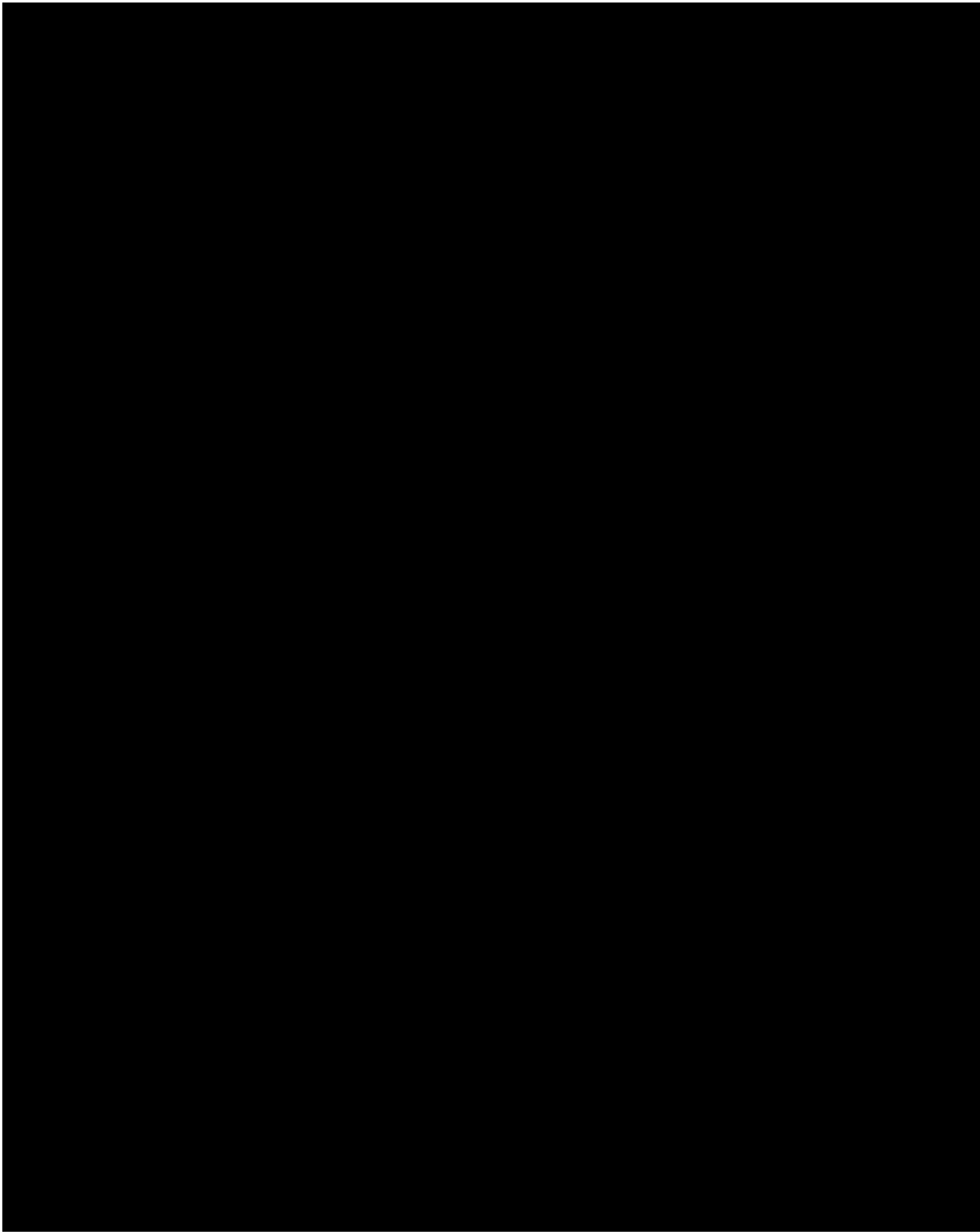
[REDACTED]

[REDACTED]









[Redacted line of text]

[Redacted line of text]

[Redacted line of text]

[Redacted line of text]

[Redacted text block]

[Redacted text block]

[Redacted text line]

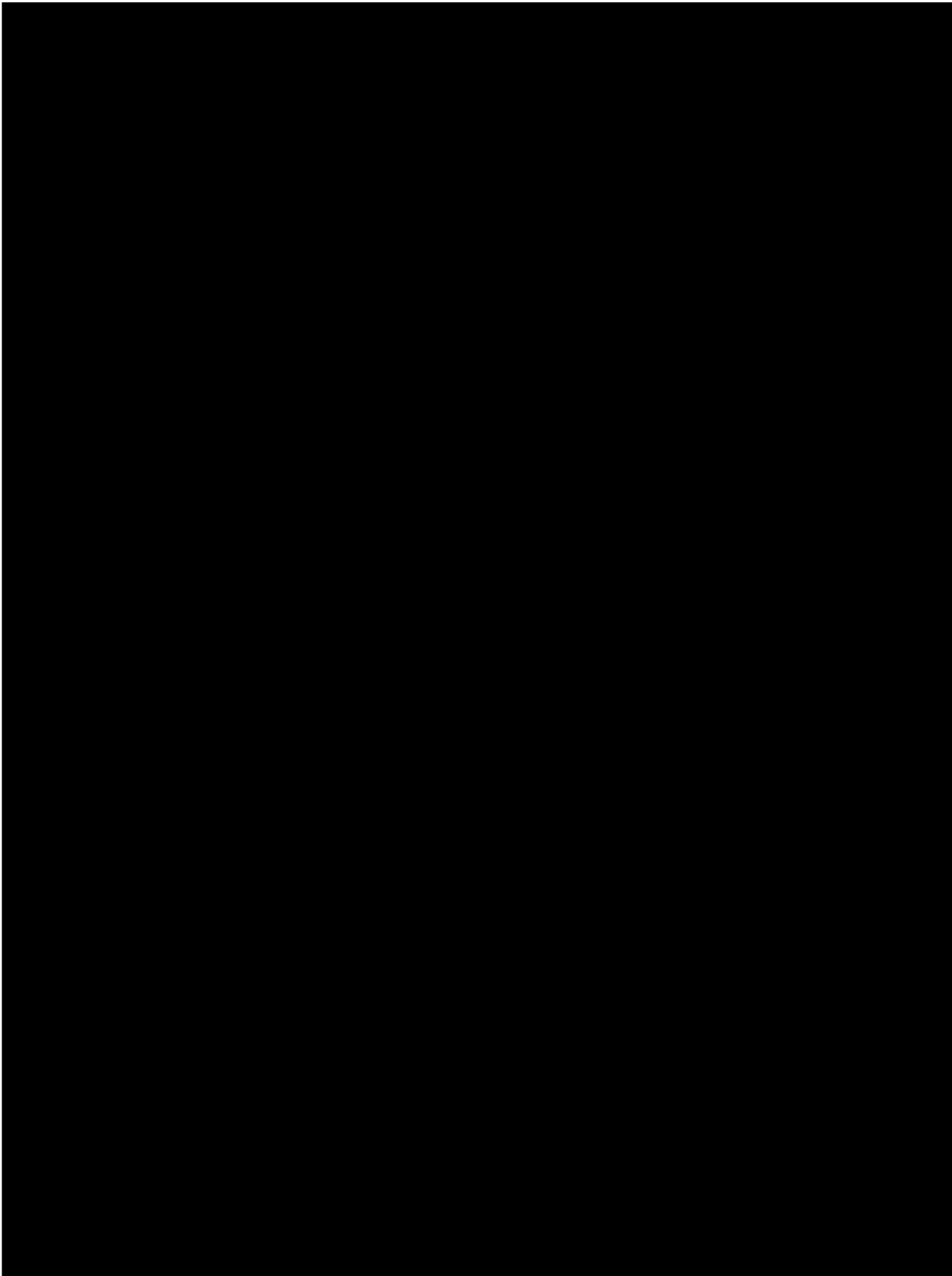
[Redacted text block]

[Redacted text block]

[Redacted text block]

[Redacted text block]

[Redacted text block]



[REDACTED]

[REDACTED]

[REDACTED]

[REDACTED]

[REDACTED]

[REDACTED]

[REDACTED]

[REDACTED]

[REDACTED]

[REDACTED]

[REDACTED]

[REDACTED]

[REDACTED]

[REDACTED]

[REDACTED]

[Redacted text block]

[Video 16](#)   [Video 17](#)   [Video 18](#)   [Video 19](#)   [Video 20](#)   [Video](#)

[21](#) [Redacted text block]

[Redacted text block]

[Redacted]

[Redacted]

[Redacted]

[Redacted]

[Redacted]

[Redacted]

[Redacted]

[Redacted]

[Redacted]

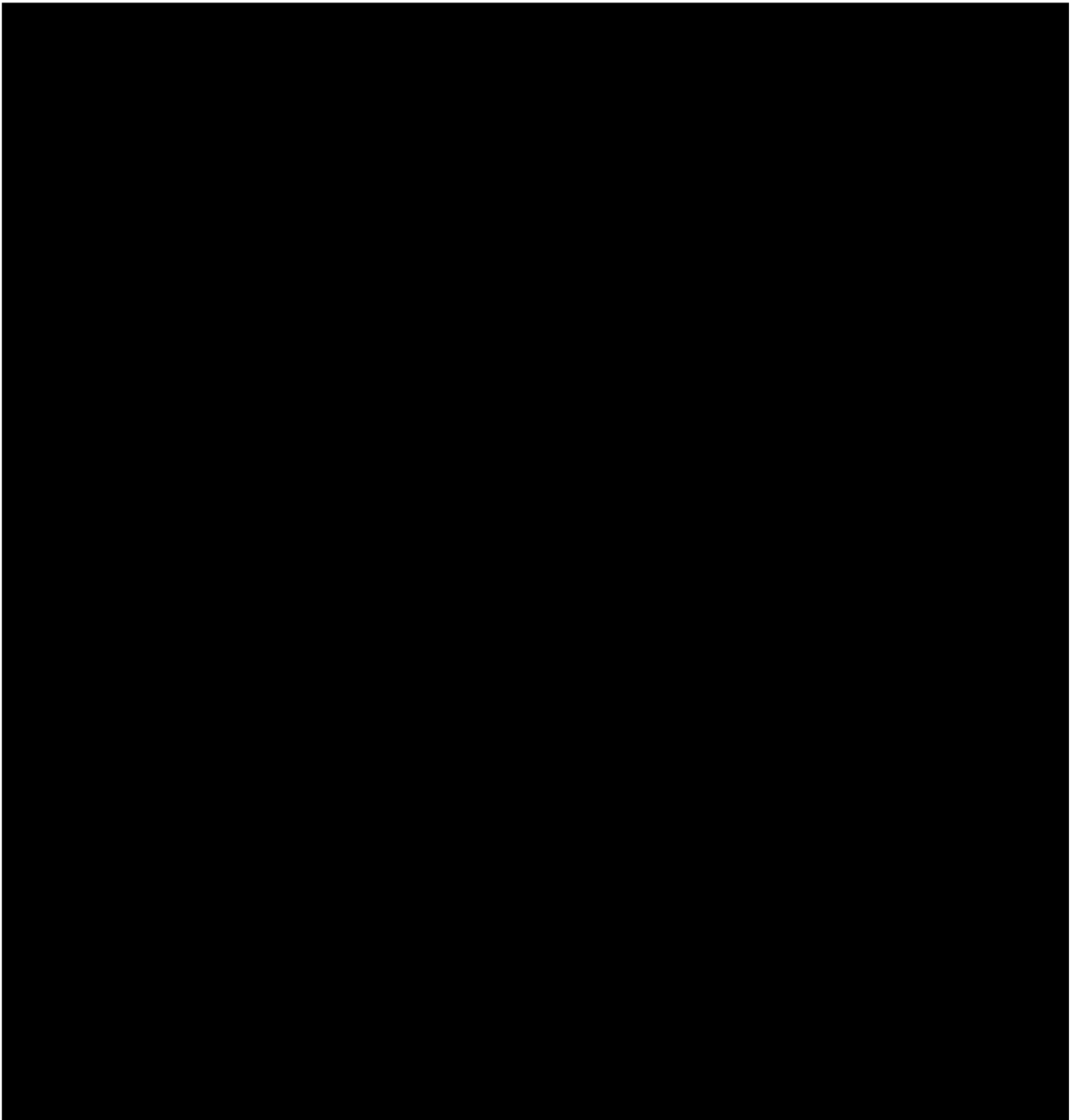
[Redacted]

[Redacted]

[Redacted]

[Redacted]





[Redacted line of text]

[Redacted line of text]

[Redacted line of text]

[Redacted line of text]

[Redacted line of text]

[Redacted line of text]

[Redacted line of text]

[REDACTED]

[REDACTED]

[REDACTED]



[Video 22](#)



[Redacted text block]

[Redacted text block]

[Redacted text block]

[Redacted text block]

[Redacted text block]

[Video 23](#)

[REDACTED]

[REDACTED]

[Redacted text block]

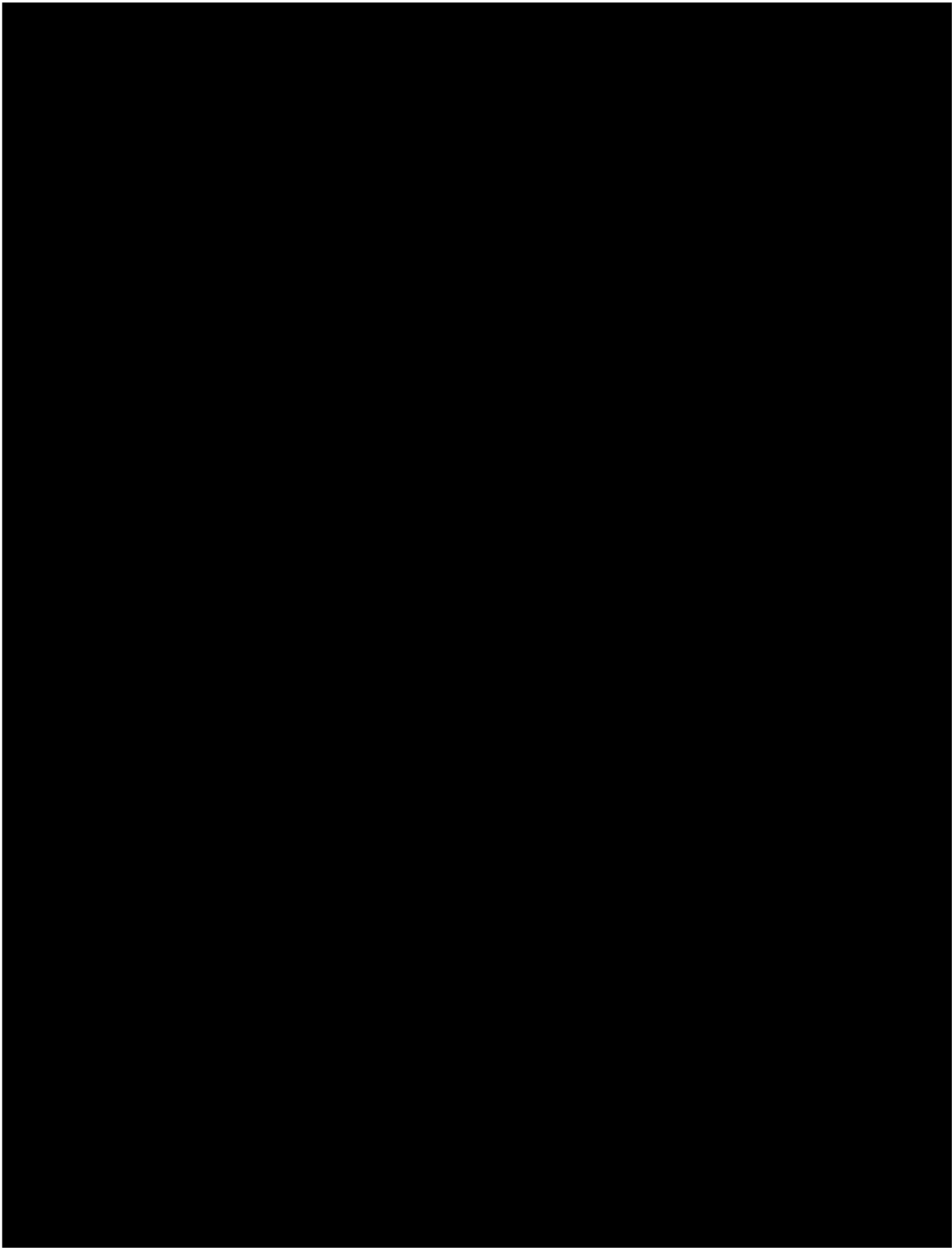
[Redacted text block]

[Redacted text block]

[Video 24](#)

[Video 25](#)

[Redacted text block]



[Redacted line of text]

[Redacted line of text]

[Redacted line of text]

[Redacted line of text]

[Redacted]

[Redacted]

[Redacted]

[Redacted]

[Redacted] [Video 26](#) [Video 27](#) [Redacted]

[Redacted]

[Redacted]

[Redacted]

[Redacted]

[Redacted]

[Redacted]

[Redacted]

[Redacted]

[Redacted]

[Redacted]

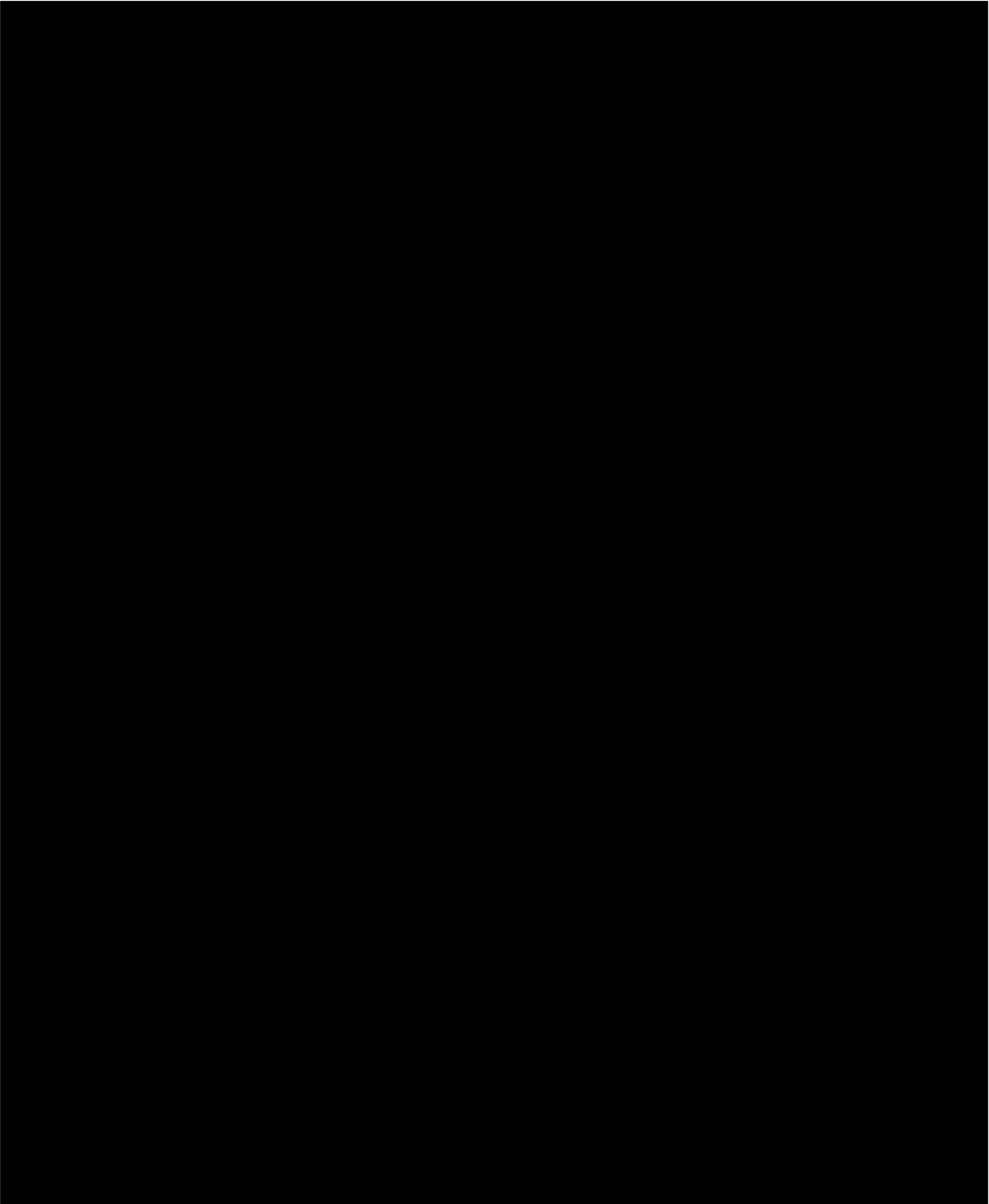
[Redacted]

[Redacted]

[Redacted]

[Redacted]





[Redacted line of text]

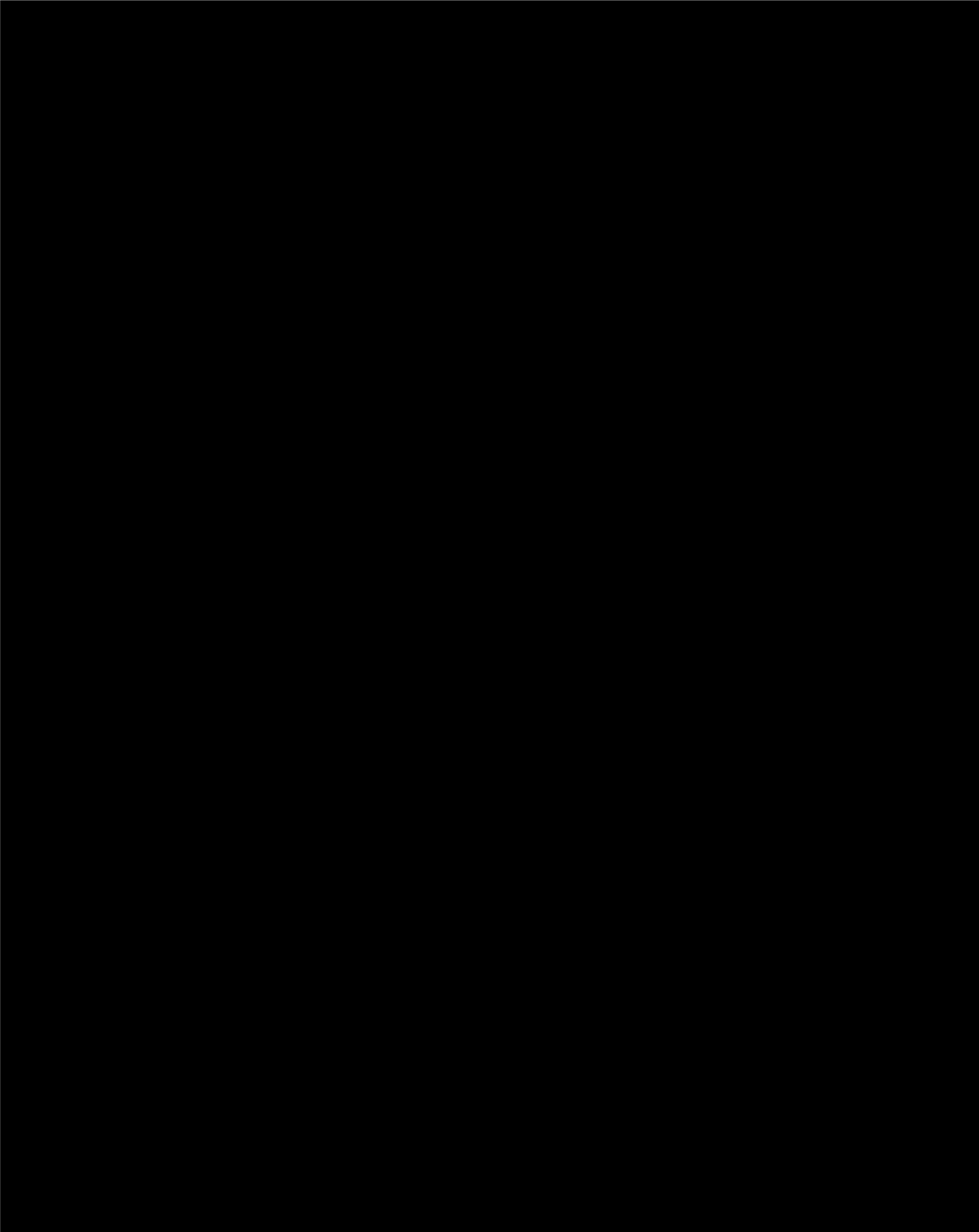
[Redacted line of text]

[Redacted line of text]

[Redacted line of text]

[Redacted text block]

[Redacted text block]



[Redacted line of text]

[Redacted line of text]

[Redacted line of text]

[Redacted line of text]

[Redacted]

[Redacted] [Video 26](#)

[Redacted]

[Redacted]

[Redacted]

[Redacted]

[Redacted]

[Redacted]

[Redacted]

[Redacted]

[Redacted]

[Redacted]

[Redacted]

[Redacted]

[Pre-Video](#)

[Redacted]

[REDACTED]

[REDACTED]

[REDACTED]

[REDACTED]

[REDACTED]

[REDACTED]

[REDACTED]

[REDACTED]

[REDACTED]

[REDACTED]

[REDACTED]

[REDACTED]

[REDACTED]

[REDACTED]

[REDACTED]

[REDACTED]

[REDACTED]

[REDACTED]

[REDACTED]

[REDACTED]

[REDACTED]

[Redacted text block]

[Redacted text block]

[Redacted text block]

[Redacted text block]

[Redacted text block]

[Redacted text block]

[Redacted text block]

[Redacted text block]

[Redacted text block]

[Redacted text block]



[Redacted]

[Redacted]

[Redacted]

[Redacted]

[Redacted]

[Redacted]

[Redacted]

[Redacted]

[Redacted]

[Redacted]

[Redacted]

[Redacted]

[Redacted]

[Redacted]

[Redacted]

[Redacted]

[Redacted]

[Redacted]

[Redacted]

[Redacted]

[Redacted]

[Redacted]

[Redacted]

[Redacted]

[Redacted]

[Redacted]

[Redacted]

[Redacted]

[Redacted]

[Redacted]

[Redacted]

[Redacted]

[Redacted]

[Redacted]

## Tables



[REDACTED]

[REDACTED]

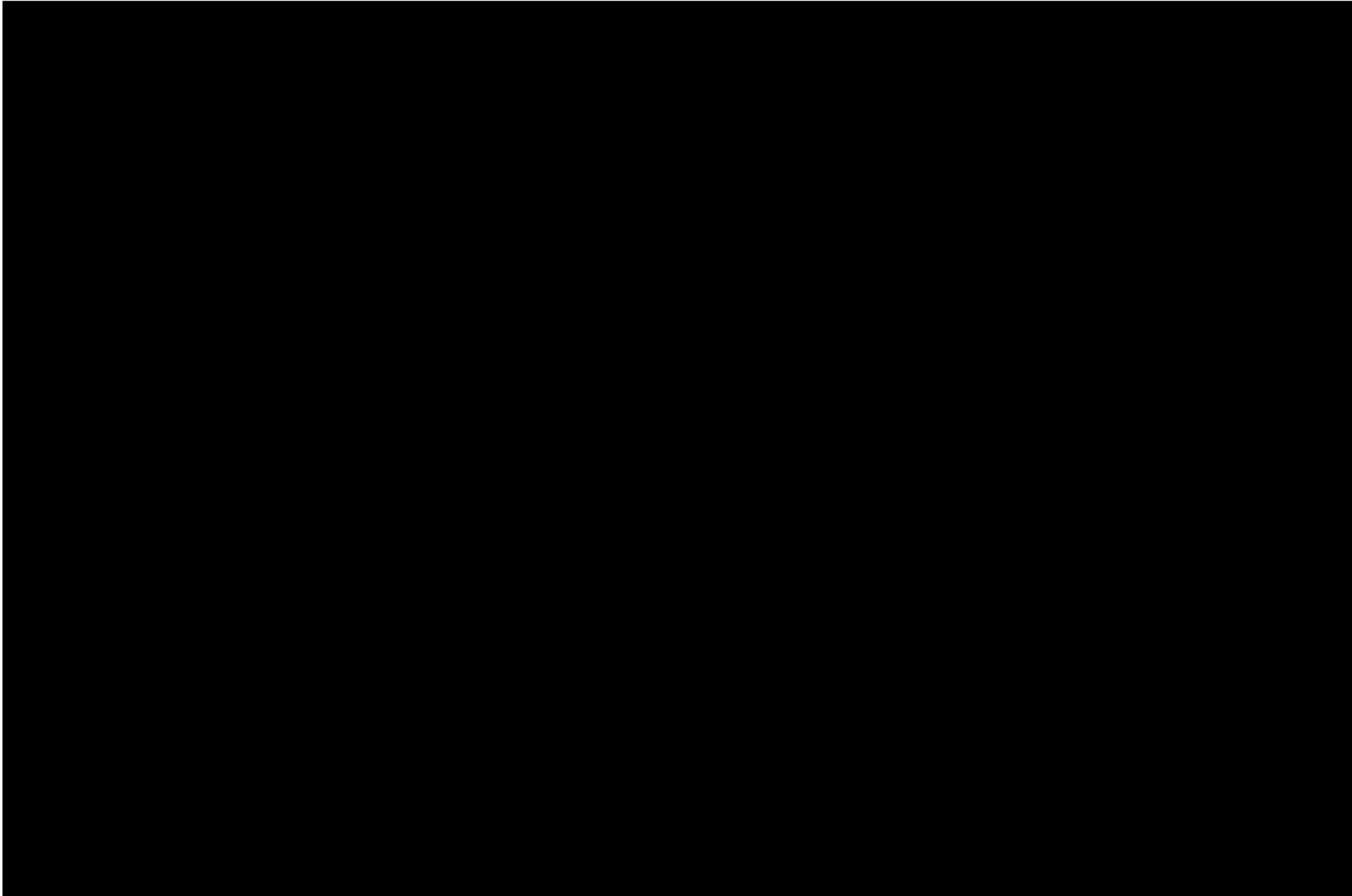
[REDACTED]

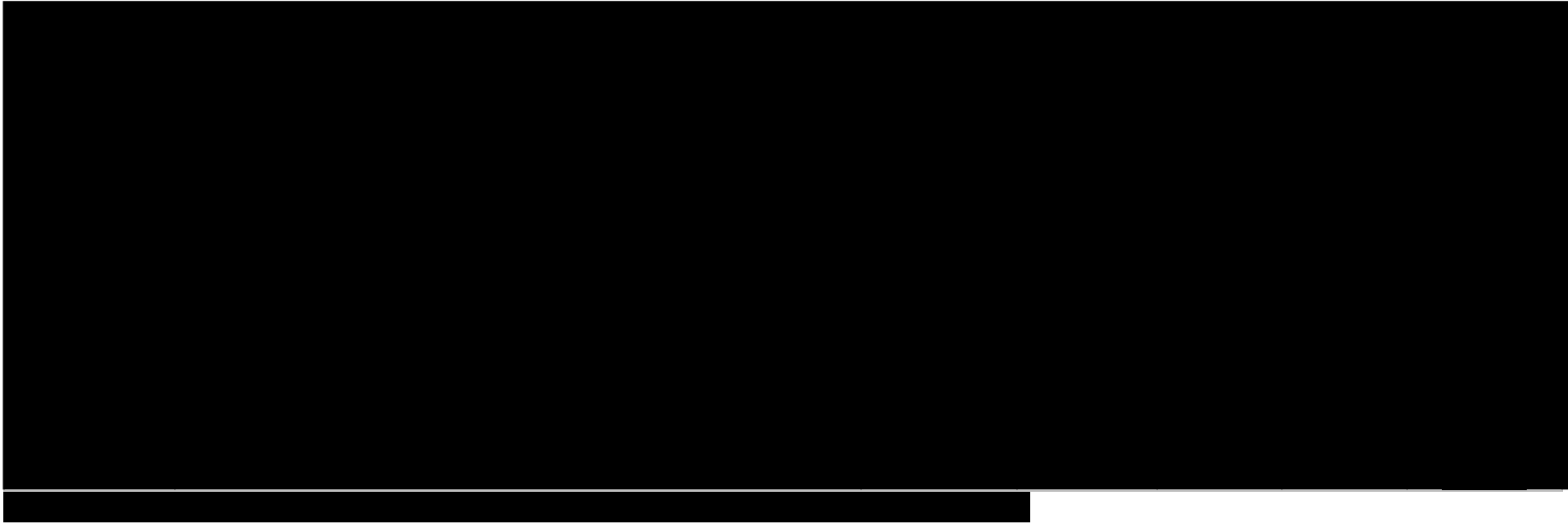
[REDACTED]

[REDACTED]

[REDACTED]

[REDACTED]





## 6. References

- [1] J.W. Costerton, P.S. Stewart, E.P. Greenberg, Bacterial biofilms: a common cause of persistent infections, *Science*, 284 (1999) 1318-1322.
- [2] X.Z. Li, B. Hauer, B. Rosche, Single-species microbial biofilm screening for industrial applications, *Appl Microbiol Biotechnol*, 76 (2007) 1255-1262.
- [3] F.H. Yildiz, K.L. Visick, *Vibrio* biofilms: so much the same yet so different, *Trends Microbiol*, 17 (2009) 109-118.
- [4] I. Doghri, S. Rodrigues, A. Bazire, A. Dufour, D. Akbar, V. Sopena, S. Sablé, I. Lanneluc, Marine bacteria from the French Atlantic coast displaying high forming-biofilm abilities and different biofilm 3D architectures, *BMC Microbiol*, 15 (2015) 231.
- [5] J.W. Lee, J.H. Nam, Y.H. Kim, K.H. Lee, D.H. Lee, Bacterial communities in the initial stage of marine biofilm formation on artificial surfaces, *J Microbiol*, 46 (2008) 174-182.
- [6] M. Salta, J.A. Wharton, Y. Blache, K.R. Stokes, J.F. Briand, Marine biofilms on artificial surfaces: structure and dynamics, *Environ Microbiol*, 15 (2013) 2879-2893.
- [7] K.A. Lema, F. Constancias, S.A. Rice, M.G. Hadfield, High bacterial diversity in nearshore and oceanic biofilms and their influence on larval settlement by *Hydroides elegans* (Polychaeta), *Environ Microbiol*, (2019).
- [8] K.K. Jefferson, What drives bacteria to produce a biofilm?, *FEMS Microbiol Lett*, 236 (2004) 163-173.
- [9] H. Dang, C.R. Lovell, Bacterial primary colonization and early succession on surfaces in marine waters as determined by amplified rRNA gene restriction analysis and sequence analysis of 16S rRNA genes, *Appl Environ Microbiol*, 66 (2000) 467-475.
- [10] E. Karatan, P. Watnick, Signals, regulatory networks, and materials that build and break bacterial biofilms, *Microbiol Mol Biol Rev*, 73 (2009) 310-347.
- [11] H.C. Flemming, J. Wingender, Relevance of microbial extracellular polymeric substances (EPSs)--Part II: Technical aspects, *Water Sci Technol*, 43 (2001) 9-16.
- [12] C.C.C.R. de Carvalho, Marine Biofilms: A Successful Microbial Strategy With Economic Implications, *Frontiers in Marine Science*, 5 (2018).
- [13] M. Grzegorzczak, S. Pogorzelski, A. Pospiech, K. Boniewicz-Szmyt, Monitoring of Marine Biofilm Formation Dynamics at Submerged Solid Surfaces With Multitechnique Sensors, *Frontiers in Marine Science*, 5 (2018).
- [14] K.A. Dafforn, J.A. Lewis, E.L. Johnston, Antifouling strategies: history and regulation, ecological impacts and mitigation, *Mar Pollut Bull*, 62 (2011) 453-465.
- [15] Y.K. Demirel, M. Khorasanchi, O. Turan, A. Incecik, On the importance of antifouling coatings regarding ship resistance and powering, 3rd International Conference on Technologies, Operations, Logistics and Modelling for Low Carbon ShippingGBR, pp. 13.
- [16] V.B. Damodaran, N.S. Murthy, Bio-inspired strategies for designing antifouling biomaterials, *Biomater Res*, 20 (2016) 18.
- [17] C. Magin, S. Cooper, A. Brennan, Non-toxic antifouling strategies, *Materials Today*, 13 (2010) 36-44.
- [18] J. Xuan, Y. Yu, T. Qing, L. Guo, L. Shi, Next-generation sequencing in the clinic: promises and challenges, *Cancer Lett*, 340 (2013) 284-295.
- [19] S. Goodwin, J.D. McPherson, W.R. McCombie, Coming of age: ten years of next-generation sequencing technologies, *Nat Rev Genet*, 17 (2016) 333-351.

- [20] S. Behjati, P.S. Tarpey, What is next generation sequencing?, *Arch Dis Child Educ Pract Ed*, 98 (2013) 236-238.
- [21] S. Rampadarath, K. Bandhoa, D. Puchooa, R. Jeewon, S. Bal, Early bacterial biofilm colonizers in the coastal waters of Mauritius, *Electronic Journal of Biotechnology*, 29 (2017) 13-21.
- [22] Y. Sun, Y. Lang, Z. Yan, L. Wang, Z. Zhang, High-throughput sequencing analysis of marine pioneer surface-biofilm bacteria communities on different PDMS-based coatings, *Colloids Surf B Biointerfaces*, 185 (2020) 110538.
- [23] J.T. Antunes, A.G.G. Sousa, J. Azevedo, A. Rego, P.N. Leão, V. Vasconcelos, Distinct Temporal Succession of Bacterial Communities in Early Marine Biofilms in a Portuguese Atlantic Port, *Front Microbiol*, 11 (2020) 1938.
- [24] P.Y. Qian, A. Cheng, R. Wang, R. Zhang, Marine biofilms: diversity, interactions and biofouling, *Nat Rev Microbiol*, 20 (2022) 671-684.
- [25] S. Sunagawa et al. Structure and function of the global ocean microbiome. *Science*, 348 (2015), 1261359
- [26] D. FAITH, CONSERVATION EVALUATION AND PHYLOGENETIC DIVERSITY, *Biological Conservation*, 61 (1992) 1-10.
- [27] X. Zhu, J. Wang, C. Reyes-Gibby, S. Shete, R. Elston, Processing and Analyzing Human Microbiome Data, *Statistical Human Genetics: Methods and Protocols*, 2nd Edition, 1666 (2017) 649-677.
- [28] C. Lozupone, R. Knight, UniFrac: a new phylogenetic method for comparing microbial communities, *Appl Environ Microbiol*, 71 (2005) 8228-8235.
- [29] M. Hamady, C. Lozupone, R. Knight, Fast UniFrac: facilitating high-throughput phylogenetic analyses of microbial communities including analysis of pyrosequencing and PhyloChip data, *ISME J*, 4 (2010) 17-27.
- [30] M.G. Langille, J. Zaneveld, J.G. Caporaso, D. McDonald, D. Knights, J.A. Reyes, J.C. Clemente, D.E. Burkpile, R.L. Vega Thurber, R. Knight, R.G. Beiko, C. Huttenhower, Predictive functional profiling of microbial communities using 16S rRNA marker gene sequences, *Nat Biotechnol*, 31 (2013) 814-821.
- [31] G. Douglas, V. Maffei, J. Zaneveld, S. Yurgel, J. Brown, C. Taylor, C. Huttenhower, M. Langille, PICRUSt2 for prediction of metagenome functions, *Nature Biotechnology*, 38 (2020) 685-688.
- [32] M. Kanehisa, S. Goto, S. Kawashima, Y. Okuno, M. Hattori, The KEGG resource for deciphering the genome, *Nucleic Acids Res*, 32 (2004) D277-280.
- [33] T. Vissers, A.T. Brown, N. Koumakis, A. Dawson, M. Hermes, J. Schwarz-Linek, A.B. Schofield, J.M. French, V. Koutsos, J. Arlt, V.A. Martinez, W.C.K. Poon, Bacteria as living patchy colloids: Phenotypic heterogeneity in surface adhesion, *Sci Adv*, 4 (2018) eaao1170.
- [34] J.C. Conrad, Physics of bacterial near-surface motility using flagella and type IV pili: implications for biofilm formation, *Res Microbiol*, 163 (2012) 619-629.
- [35] J.C. Conrad, M.L. Gibiansky, F. Jin, V.D. Gordon, D.A. Motto, M.A. Mathewson, W.G. Stopka, D.C. Zelasko, J.D. Shrout, G.C. Wong, Flagella and pili-mediated near-surface single-cell motility mechanisms in *P. aeruginosa*, *Biophys J*, 100 (2011) 1608-1616.
- [36] L.L. Burrows, *Pseudomonas aeruginosa* twitching motility: type IV pili in action, *Annu Rev Microbiol*, 66 (2012) 493-520.
- [37] A.J.T.M. Mathijssen, N. Figueroa-Morales, G. Junot, É. Clément, A. Lindner, A. Zöttl, Oscillatory surface rheotaxis of swimming *E. coli* bacteria, *Nat Commun*, 10 (2019) 3434.
- [38] C. Beloin, A. Houry, M. Froment, J.M. Ghigo, N. Henry, A short-time scale colloidal system reveals early bacterial adhesion dynamics, *PLoS Biol*, 6 (2008) e167.

- [39] E. Gardin, S. Zanna, A. Seyeux, D. Mercier, A. Allion-Maurer, P. Marcus, Early stage of marine biofilm formation on duplex stainless steel, *Biointerphases*, 15 (2020) 041014.
- [40] A.J. Paula, G. Hwang, H. Koo, Dynamics of bacterial population growth in biofilms resemble spatial and structural aspects of urbanization, *Nat Commun*, 11 (2020) 1354.
- [41] K. Doiron, L. Beaulieu, R. St-Louis, K. Lemarchand, Reduction of bacterial biofilm formation using marine natural antimicrobial peptides, *Colloids Surf B Biointerfaces*, 167 (2018) 524-530.
- [42] N. Rabin, Y. Zheng, C. Opoku-Temeng, Y. Du, E. Bonsu, H.O. Sintim, Biofilm formation mechanisms and targets for developing antibiofilm agents, *Future Med Chem*, 7 (2015) 493-512.
- [43] R.D. Acemel, F. Govantes, A. Cuetos, Computer simulation study of early bacterial biofilm development, *Sci Rep*, 8 (2018) 5340.
- [44] G. Melaugh, J. Hutchison, K.N. Kragh, Y. Irie, A. Roberts, T. Bjarnsholt, S.P. Diggle, V.D. Gordon, R.J. Allen, Shaping the Growth Behaviour of Biofilms Initiated from Bacterial Aggregates, *PLoS One*, 11 (2016) e0149683.
- [45] O.E. Petrova, K. Sauer, Escaping the biofilm in more than one way: desorption, detachment or dispersion, *Curr Opin Microbiol*, 30 (2016) 67-78.
- [46] C. Solano, M. Echeverz, I. Lasa, Biofilm dispersion and quorum sensing, *Curr Opin Microbiol*, 18 (2014) 96-104.
- [47] V. Ray, K. Visick, LuxU connects quorum sensing to biofilm formation in *Vibrio fischeri*, *Molecular Microbiology*, 86 (2012) 954-970.
- [48] J. Li, X. Zhao, Effects of quorum sensing on the biofilm formation and viable but non-culturable state, *Food Research International*, 137 (2020).
- [49] Y. Liu, H. Hu, F. Luo, Roles of autoinducer-2 mediated quorum sensing in wastewater treatment, *Water Science and Technology*, 84 (2021) 793-809.
- [50] S.M. Hunt, E.M. Werner, B. Huang, M.A. Hamilton, P.S. Stewart, Hypothesis for the role of nutrient starvation in biofilm detachment, *Appl Environ Microbiol*, 70 (2004) 7418-7425.
- [51] E. Paluch, J. Rewak-Soroczyńska, I. Jędrusik, E. Mazurkiewicz, K. Jermakow, Prevention of biofilm formation by quorum quenching, *Appl Microbiol Biotechnol*, 104 (2020) 1871-1881.
- [52] M.K. Kim, F. Ingremeau, A. Zhao, B.L. Bassler, H.A. Stone, Local and global consequences of flow on bacterial quorum sensing, *Nat Microbiol*, 1 (2016) 15005.
- [53] P. Thomen, J. Robert, A. Monmeyran, A. Bitbol, C. Douarche, N. Henry, Bacterial biofilm under flow: First a physical struggle to stay, then a matter of breathing, *Plos One*, 12 (2017).
- [54] C. Beloin, A. Roux, J. Ghigo, T. Romeo, *Escherichia coli* biofilms, *Bacterial Biofilms*, 322 (2008) 249-289.
- [55] R. Colin, K. Drescher, V. Sourjik, Chemotactic behaviour of *Escherichia coli* at high cell density. *Nat Commun*, 10 (2019) 5329
- [56] A. Monmeyran, W. Benyoussef, P. Thomen, N. Dahmane, A. Baliarda, M. Jules, S. Aymerich, N. Henry, Four species of bacteria deterministically assemble to form a stable biofilm in a millifluidic channel, *NPJ Biofilms Microbiomes*, 7 (2021) 64.
- [57] M. Shigematsu, Y. Meno, H. Misumi, K. Amako, The measurement of swimming velocity of *Vibrio cholerae* and *Pseudomonas aeruginosa* using the video tracking methods. *Microbiol Immunol*, 39 (1995) 741-4.
- [58] E. Guyon, J. P. Hulin, L. Petit, *Hydrodynamique physique*, Paris, EDP Sciences (CNRS editions), 2001.
- [59] H. Lee, S. Balachandar, Drag and lift forces on a spherical particle moving on a wall in a shear flow at finite Re. *Journal of Fluid Mechanics*, 657 (2010) 89-125



- [60] K.P. Rumbaugh, K. Sauer, Biofilm dispersion, *Nat Rev Microbiol*, 18 (2020) 571-586.
- [61] K. Sauer, P. Stoodley, D.M. Goeres, L. Hall-Stoodley, M. Burmølle, P.S. Stewart, T. Bjarnsholt, The biofilm life cycle: expanding the conceptual model of biofilm formation, *Nat Rev Microbiol*, 20 (2022) 608-620.
- [62] J.B. Kaplan, Biofilm dispersal: mechanisms, clinical implications, and potential therapeutic uses, *J Dent Res*, 89 (2010) 205-218.
- [63] A. Maravic, M. Skocibusic, S. Cvjetan, I. Samanic, Z. Fredotovic, J. Puizina, Prevalence and diversity of extended-spectrum-beta-lactamase-producing Enterobacteriaceae from marine beach waters, *Marine Pollution Bulletin*, 90 (2015) 60-67.
- [64] J. Schindelin, I. Arganda-Carreras, E. Frise, V. Kaynig, M. Longair, T. Pietzsch, S. Preibisch, C. Rueden, S. Saalfeld, B. Schmid, J.Y. Tinevez, D.J. White, V. Hartenstein, K. Eliceiri, P. Tomancak, A. Cardona, Fiji: an open-source platform for biological-image analysis, *Nat Methods*, 9 (2012) 676-682.
- [65] J. Caporaso, J. Kuczynski, J. Stombaugh, K. Bittinger, F. Bushman, E. Costello, N. Fierer, A. Pena, J. Goodrich, J. Gordon, G. Huttley, S. Kelley, D. Knights, J. Koenig, R. Ley, C. Lozupone, D. McDonald, B. Muegge, M. Pirrung, J. Reeder, J. Sevinsky, P. Tumbaugh, W. Walters, J. Widmann, T. Yatsunenko, J. Zaneveld, R. Knight, QIIME allows analysis of high-throughput community sequencing data, *Nature Methods*, 7 (2010) 335-336.
- [66] C. Quast, E. Pruesse, P. Yilmaz, J. Gerken, T. Schweer, P. Yarza, J. Peplies, F. Glockner, The SILVA ribosomal RNA gene database project: improved data processing and web-based tools, *Nucleic Acids Research*, 41 (2013) D590-D596.
- [67] C. Lozupone, M. Hamady, S. Kelley, R. Knight, Quantitative and qualitative beta diversity measures lead to different insights into factors that structure microbial communities, *Applied and Environmental Microbiology*, 73 (2007) 1576-1585.
- [68] A. Ramette, Multivariate analyses in microbial ecology, *FEMS Microbiol Ecol*, 62 (2007) 142-160.
- [69] C.P. McNally, A. Eng, C. Noecker, W.C. Gagne-Maynard, E. Borenstein, BURRITO: An Interactive Multi-Omic Tool for Visualizing Taxa-Function Relationships in Microbiome Data, *Front Microbiol*, 9 (2018) 365.
- [70] C. Schneider, W. Rasband, K. Eliceiri, NIH Image to ImageJ: 25 years of image analysis, *Nature Methods*, 9 (2012) 671-675.
- [71] D. Julkowska, M. Obuchowski, I.B. Holland, S.J. S ror, Comparative analysis of the development of swarming communities of *Bacillus subtilis* 168 and a natural wild type: critical effects of surfactin and the composition of the medium, *J Bacteriol*, 187 (2005) 65-76.
- [72] F. Le Roux, A. Goubet, F. Thompson, N. Faury, M. Gay, J. Swings, D. Saulnier, *Vibrio gigantis* sp nov., isolated from the haemolymph of cultured oysters (*Crassostrea gigas*), *International Journal of Systematic and Evolutionary Microbiology*, 55 (2005) 2251-2255.
- [73] K. Kim, K. Won, E. Lee, M. Cho, S. Jung, M. Kim, Detection of *Vibrio* and ten *Vibrio* species in cage-cultured fish by multiplex polymerase chain reaction using house-keeping genes, *Aquaculture*, 506 (2019) 417-423.
- [74] H. Sohn, J. Kim, C. Jin, J. Lee, Identification of *Vibrio* species isolated from cultured olive flounder (*Paralichthys olivaceus*) in Jeju Island, South Korea, *Fisheries and Aquatic Sciences*, 22 (2019) 14.
- [75] I. Borre, E. Sonnenschein, Draft Genome Sequences of Nine Environmental Bacterial Isolates Colonizing Plastic, *Microbiology Resource Announcements*, 10 (2021).
- [76] S.C. Chew, L. Yang, Biofilms, in: P.M.F. Benjamin Caballero, Fidel Toldr , (Ed.) *Encyclopedia of Food and Health*, Academic Press 2016, pp. 407-415.

- [77] J.A. Freeman, B.N. Lilley, B.L. Bassler, A genetic analysis of the functions of LuxN: a two-component hybrid sensor kinase that regulates quorum sensing in *Vibrio harveyi*, *Mol Microbiol*, 35 (2000) 139-149.
- [78] M. Liu, X. Zhu, C. Zhang, Z. Zhao, LuxQ-LuxU-LuxO pathway regulates biofilm formation by *Vibrio parahaemolyticus*, *Microbiological Research*, 250 (2021).
- [79] J. Zhu, M.B. Miller, R.E. Vance, M. Dziejman, B.L. Bassler, J.J. Mekalanos, Quorum-sensing regulators control virulence gene expression in *Vibrio cholerae*, *Proc Natl Acad Sci U S A*, 99 (2002) 3129-3134.
- [80] B.L. Bassler, M. Wright, M.R. Silverman, Multiple signalling systems controlling expression of luminescence in *Vibrio harveyi*: sequence and function of genes encoding a second sensory pathway, *Mol Microbiol*, 13 (1994) 273-286.
- [81] M.B. Miller, K. Skorupski, D.H. Lenz, R.K. Taylor, B.L. Bassler, Parallel quorum sensing systems converge to regulate virulence in *Vibrio cholerae*, *Cell*, 110 (2002) 303-314.
- [82] B.K. Hammer, B.L. Bassler, Quorum sensing controls biofilm formation in *Vibrio cholerae*, *Mol Microbiol*, 50 (2003) 101-104.
- [83] L. Xu, H. Li, C. Vuong, V. Vadyvaloo, J. Wang, Y. Yao, M. Otto, Q. Gao, Role of the luxS quorum-sensing system in biofilm formation and virulence of *Staphylococcus epidermidis*, *Infect Immun*, 74 (2006) 488-496.
- [84] N.L. Lyell, A.K. Dunn, J.L. Bose, E.V. Stabb, Bright mutants of *Vibrio fischeri* ES114 reveal conditions and regulators that control bioluminescence and expression of the lux operon, *J Bacteriol*, 192 (2010) 5103-5114.
- [85] D. Kolibachuk, E.P. Greenberg, The *Vibrio fischeri* luminescence gene activator LuxR is a membrane-associated protein, *J Bacteriol*, 175 (1993) 7307-7312.
- [86] L. Tanet, C. Tamburini, C. Baumas, M. Garel, G. Simon, L. Casalot, Bacterial Bioluminescence: Light Emission in, *Front Microbiol*, 10 (2019) 365.
- [87] B.O. Emerenini, B.A. Hense, C. Kuttler, H.J. Eberl, A Mathematical Model of Quorum Sensing Induced Biofilm Detachment, *PLoS One*, 10 (2015) e0132385.
- [88] J. Janda, A. Newton, C. Bopp, Vibriosis, *Clinics in Laboratory Medicine*, 35 (2015) 273-+.
- [89] S. Gomez, L. Bureau, K. John, E.N. Chêne, D. Débarre, S. Lecuyer, Substrate stiffness impacts early biofilm formation by modulating, *Elife*, 12 (2023).
- [90] A.J. Silva, J.A. Benitez, *Vibrio cholerae* Biofilms and Cholera Pathogenesis, *PLoS Negl Trop Dis*, 10 (2016) e0004330.
- [91] D. Jenkins, M.G. Richard, G.T. Daigger, Manual on the causes and control of activated sludge bulking, foaming, and other solids separation problems, CRC Press 2003.
- [92] A.M. Martins, J.J. Heijnen, M.C. van Loosdrecht, Effect of dissolved oxygen concentration on sludge settleability, *Appl Microbiol Biotechnol*, 62 (2003) 586-593.
- [93] Lesson 8: Filamentous Bacteria., Mountain Empire Community College, ENV 108.
- [94] S Yilmaz, S Karataş, TM Steinum, M Gürkan, DK Yilmaz, HMR Abdel-Latif. Isolation, Identification, and Pathogenicity of *Vibrio gigantis* Retrieved from European Seabass (*Dicentrarchus labrax*) Farmed in Türkiye. *Animals (Basel)*, 13 (2023) 3580.